BREAKUP CHARACTERISTICS OF A LIQUID JET IN SUBSONIC CROSSFLOW

A Thesis

Presented to

The Academic Faculty

by

Yogish Gopala

In Partial Fulfillment
of the Requirements for the Degree
Doctor of Philosophy in the
School of Aerospace Engineering

Georgia Institute of Technology
August 2012

BREAKUP CHARACTERISTICS OF LIQUID JET IN SUBSONIC CROSSFLOW

Approved by:

Dr. Ben T. Zinn, Advisor
School of Aerospace Engineering
Georgia Institute of Technology

Dr. Jerry Seitzman
School of Aerospace Engineering
Georgia Institute of Technology

Dr. Suresh Menon
School of Aerospace Engineering
Georgia Institute of Technology

Dr. Caroline L. Genzale
School of Mechanical Engineering
Georgia Institute of Technology

Dr. Eugene Lubarsky
School of Aerospace Engineering
Georgia Institute of Technology

Date Approved: April 20 2012

DEDICATION

For my family who offered me unconditional love and support throughout the course of this thesis

ACKNOWLEDGEMENTS

I would like to express my deepest gratitude to my advisor, Dr. Ben T. Zinn for his invaluable guidance and mentoring throughout this research work. I would also like to thank Dr. Suresh Menon, Dr. Jerry Seitzman, Dr. Eugene Lubarsky and Dr. Caroline Genzale for their many helpful comments and for taking an active part in my thesis committee. I would also like to thank Dr. Oleksandr Bibik and Dmitriy Shcherbik for their help with setting up and running the experiments.

I would like to thank Orcun Kozaka, Jonathan Riechel, Modou Mar, Peng Zhang and Jessica Baird for working with me on the spray project. Thanks to Karthik Periagaram, Sai Kumar Thumuluru, Yash Kochar and Arun Radhakrishnan for all the discussions on various topics during my graduate school life. I would also like to thank the following in the Aerospace Combustion Lab for their help and discussions: Adithya, Amy, Ben, Caleb, Chiluwata, Dong, Jacqueline, James, Jayprakash, John Crane, John Cutright, Matt, Mohan, Muruganandam, Nori, Priya, Rajesh, Ravikiran, Santosh S., Santosh H., Shai, Shashvat, Shreekrishna, Thao, Venkat and all the other students and staff in the combustion lab.

I would like to thank my friends: Kiruthika, Nandita, Prasad, Smitha, Vinay, Priyanka, Ashna, Nagesh, Deepthi, Komal, Manoj, Krishna, Kaaranji, Pooja, Rakshita, Nischint, Neelakantan, Archana, Akbar, Sandeep, Sravani for making my stay in Atlanta memorable. I thank my dance partners Peng Meng, Shannon, Danjue, Amy, Neha and Leihong for helping me learn various forms of ballroom dance and salsa. I thank my

friends Nithyanand, Rukma, Kandarp, Arjun, Sachin, Shyam and Vinay who kept in touch with me and kept me motivated.

I thank Dr. Satyanarayana R. Chakravarthy, Dr. Sujith R. I. and Dr. Panchapakesan N. R. for getting me started with research during my undergraduate studies and encouraging me to pursue graduate studies.

I would like to thank Drs. Christian Vandervort, Fei Han, Kapil Singh, Preetham and Qingguo Zhang for providing me internship opportunities at General Electric Global Research Center. The things I got to learn about the work culture in industries were invaluable.

The financial support of GE Aviation through the University Strategic Alliance program is greatly acknowledged. I would also like to thank Drs. Hukam Mongia, Tim Held, Zhongtao Dai, Michael Foust, Michael Benjamin and Nayan Patel for their creative contributions.

Finally, I would like to thank my family for their love and support, which encouraged me at every step in my life. This thesis would not have been possible without the emotional support and sacrifices of my parents, K N Gopala Rao and B R Usha. This thesis is dedicated to them.

TABLE OF CONTENTS

LIST OF TABLES

LIST OF FIGURES

LIST OF SYMBOLS AND ABBREVIATIONS

d	Droplet diameter
σ	Surface tension
ρ	Density
U,u	Velocity
q	Liquid to air momentum-flux ratio, $\rho_l U_l^2 / \rho_a U_a^2$
μ	Viscosity
Re	Reynolds number, ρ lu/μ
We	aerodynamic Weber number, $\rho_a U_a^2 D / \sigma_l$
We_l	Liquid Weber number, $\rho_l U_l^2 D / \sigma_l$
D	Diameter of the orifice
L	Length of the injector orifice
t_b	Time from jet exit to column breakup
Z_b	Z location of jet column breakup
X_b	X location of jet column breakup
t*	$\sqrt{\frac{\rho_l}{\rho_a}}\frac{d}{U_a}$
C_d	Discharge Coefficient, $C_d = \frac{\dot{m}_l}{A\sqrt{2\rho_l \Delta P}}$
$\dot{m}$	Flow Rate
ΔP	Pressure drop across the injector

A Area of the orifice

X, x Co-ordinate in the direction of fuel injection starting at the center of the orifice

Z, z Co-ordinate in the direction of air flow starting at the center of the orifice

Y Co-ordinate perpendicular to X and Z forming a left handed system

CBP Column Breakup Point

AMD Arithmetic Mean Diameter, $\sum D_i n_i / \sum n_i$

SMD Sauter Mean Diameter, the diameter of a drop having the same volume/surface area ratio as the entire spray.

LJLGT Liquid Jet Light Guiding Technique, a diagnostic technique developed

CVP Counter-Rotating Vortex Pair

Subscripts

a : air

l : liquid

SUMMARY

This thesis describes an experimental investigation of the breakup processes involved in the formation of a spray created by a liquid jet injected into a gaseous crossflow. This work is motivated by the utilization of this method to inject fuel in combustors and afterburners of airplane engines. This study aims to develop a better understanding of the spray breakup processes and to provide better experimental inputs to improve the fidelity of numerical models.

A review of the literature in this field identified the fundamental physical processes involved in the breakup of the spray and the dependence of spray properties on operating conditions. The time taken for the liquid column to break up into ligaments and droplets, the primary breakup time and the effect of injector geometry on the spray formation processes and spray properties as the key research areas in which research done so far has been inadequate.

Determination of the location where the liquid column broke up was made difficult by the presence of a large number of droplets surrounding it. This study utilizes the liquid jet light guiding technique that enables accurate measurements of this location for a wide range of operating conditions. Prior to this study, the primary breakup time was thought to be a function the density ratio of the liquid and the gas, the diameter of the orifice and the air velocity. This study found that the time to breakup of the liquid column depends on the Reynolds number of the liquid jet. This suggests that the breakup of a turbulent liquid jet is influenced by both the aerodynamic breakup processes and the turbulent breakup processes. Observations of the phenomenon of the liquid jet splitting

up into two or more jets were made at some operating conditions with the aid of the new visualization technique.

Finally, this thesis investigates the effect of injector geometry on spray characteristics. One injector was a round edged orifice with a length to diameter ratio of 1 and a discharge coefficient of 0.95 at the operating conditions of interest. The other injector was a sharp edged orifice with a length to diameter ratio of 10 and a discharge coefficient of 0.74 at the operating conditions of interest. It was shown that the sharp edged orifice was likely to develop cavitation bubbles beyond a flow Reynolds number of 8,000. It was found that a sharp transition in the injector can lead to the liquid column disintegrating sooner. The classical Rayleigh Taylor instabilities that are usually seen with a smooth transition in the injector were not seen in the presence of a sharp transition. The droplets produced with such an injector are larger in size and the spray penetrated deeper into the crossflow.

CHAPTER I

INTRODUCTION AND LITERATURE REVIEW

1.1 BACKGROUND

This thesis describes an experimental investigation of the characteristics and the breakup processes involved in the formation of a spray created by transverse injection of a liquid jet into a gaseous crossflow. This form of liquid injection finds applications in various aerospace propulsion systems such as ramjets, lean premixed prevaporized combustors and afterburners. The quality of the spray directly influences the performance of the combustor. Consequently, it is important to understand the fundamental physical processes that control the spray formation and use this knowledge to improve the fidelity of models and correlations that describe spray formation processes and contribute to combustion systems design.

Figure 1-1 shows an image of spray created by injecting a liquid jet perpendicularly into a crossflow, highlighting the spray characteristics of interest. The spray region can be considered to comprise of a dense near field and a sparse far field. Generally, in the near field, the liquid issuing out of the orifice forms a liquid column that breaks up into ligaments and eventually into droplets. The process of liquid column breaking up into ligaments is called primary breakup and the process of ligaments or larger droplets breaking up into smaller droplets is called secondary breakup. The location where the liquid column breaks up into ligaments is known as the column

breakup point (CBP). The location of the CBP is used as an input for numerical models of sprays in the form of primary breakup time, defined as X_b/u_l. One of the prime engineering concerns in design of combustors is the placement of fuel. It is generally described by spray penetration trajectories that contains information on how far the fuel travels into the airstream and lateral spread trajectories that describes how wide the spray spreads. Knowledge of droplet sizes and velocities is also important since they govern the residence time of the fuel droplets. There has been considerable interest in determining the above described spray characteristics and their dependence upon combustor operating conditions. Another area of interest is the effect of the injector geometry on the fuel internal flow and consequently, the spray properties. For example, the presence of a sharp edge in the injector can lead to flow separation and higher turbulence level of the liquid issuing out of the orifice compared to a smooth transition.

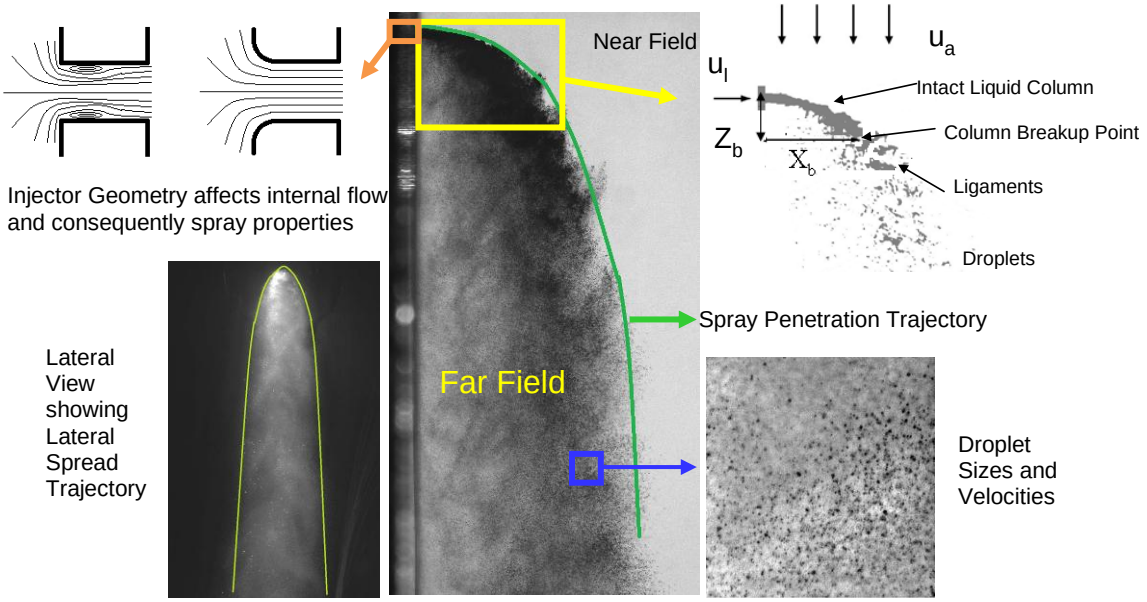

Figure 1-1. Typical image of a liquid jet in crossflow showing spray characteristics of interest partly adopted from [26]

1.2 LITERATURE REVIEW

There exists substantial literature exploring the characteristics of sprays created by jets in crossflows and the processes governing the formation of the sprays. A large number of these studies can be found in [1,2,3,4]. This section focuses on recent literature dealing with the spray properties and breakup processes relevant to this thesis. The topics covered in this section include the breakup regimes, spray characteristics of interest, an overview of numerical models and finally the effect of injector geometry on spray characteristics.

1.2.1 Breakup Regimes

Spray formation studies have identified two modes of liquid jet breakup in a crossflow, i.e., the column breakup and the shear (or surface) breakup [5,6]. During column breakup, hydrodynamic instabilities develop and distort the liquid jet column [7,8]. Such instabilities produce waves or disturbances that increase in magnitude as they propagate downstream along the liquid jet. These disturbances grow, distort and form ligaments that break off the liquid column and subsequently disintegrate into droplets. In the shear breakup mechanism, aerodynamic forces exerted by the flow on the surface of the liquid jet, ligaments and large droplets strip off small droplets from them. The domination of one mechanism over the other strongly depends on a non-dimensional parameter known as the Weber number, *We* [6,9,10,11,12,13]. *We* is the ratio of the aerodynamic drag force ($\rho_a u^2$) that tends to break up a liquid mass (i.e., liquid column or droplet) to the capillary force (σ / d) that tend to hold the liquid mass together; i.e.,

$We = \rho_a u^2 d / \sigma$. Another important parameter that affects the spray formation process is the momentum flux ratio, *q*, which is the ratio of the liquid jet momentum flux, to the air momentum flux, i.e., $q = \rho_l u_l^2 / \rho_a u_a^2$. Figure 1-2 shows a map of breakup regimes based on *We* and *q*. It has been shown that the column breakup mechanism dominates the spray formation at low *We* and low *q* numbers and that shear breakup mechanism dominates at high *We* (i.e., *We*>200) [6,14,15,16].

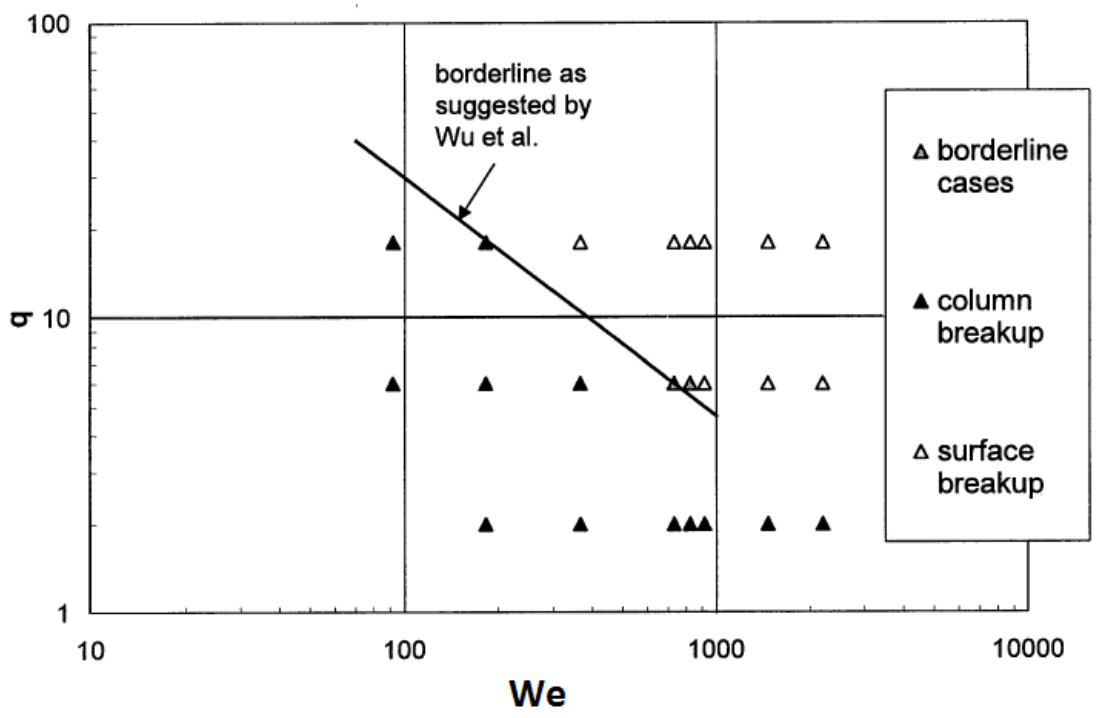

Figure 1-2. Mapping of the breakup regimes as a function of *We* and *q* (adopted from Becker and Hassa [14])

1.2.2 Spray Characteristics: Spray Penetration

Data describing spray penetration trajectory is needed for combustor design as it determines the distribution of the fuel in the combustor, for example it plays a role in

preventing fuel impingement on the combustor walls. Spray penetration trajectory measurements in the past have relied on image analysis of sprays obtained from shadowgraphy [5,6,14,17,18,19] and Mie scattering, [20,21] and the analysis of droplet counts obtained using PDPA [22, 23]. There is a general agreement that spray penetration is dependent mainly on momentum flux ratio, *q* and the nozzle diameter, d. Spray trajectories have been described using correlations. Three popular forms of equations that have been used in the past for this purpose are the power equation (Equation 1-1) [6,20,23,24,25], the logarithmic equation (Equation 1-2) [14,15] and the multizone equation (Equation 1-3) [21]. Here x and z refer to the coordinates in the direction of liquid injection and air flow, respectively. While the power and logarithmic equations provide good representations of the penetration trajectory in the near field, the multizone equation takes into account the different regions of the spray and can describe the entire region with one single equation [21].

$$\frac{x}{d} = a_1 q^{a_2} \left(\frac{z}{d} \right)^{a_3} \qquad \text{Equation 1-1}$$

$$\frac{x}{d} = a_1 q^{a_2} \log\left(1 + a_3 \frac{z}{d} \right) \qquad \text{Equation 1-2}$$

$$\frac{x}{d} = a_1 q^{a_2} \left(1 - e^{a_3 z/d} \right) \left(1 + a_4 e^{a_5 z/d} \right) \left(1 + a_6 e^{a_7 z/d} \right) \qquad \text{Equation 1-3}$$

However, the correlations suggested by different researchers differ from each other quantitatively by a large margin. An example comparing the trajectory correlations for *q*=20 is shown in Figure 1-3. It can be seen that the penetration distance varies by up to 70% between different correlations.

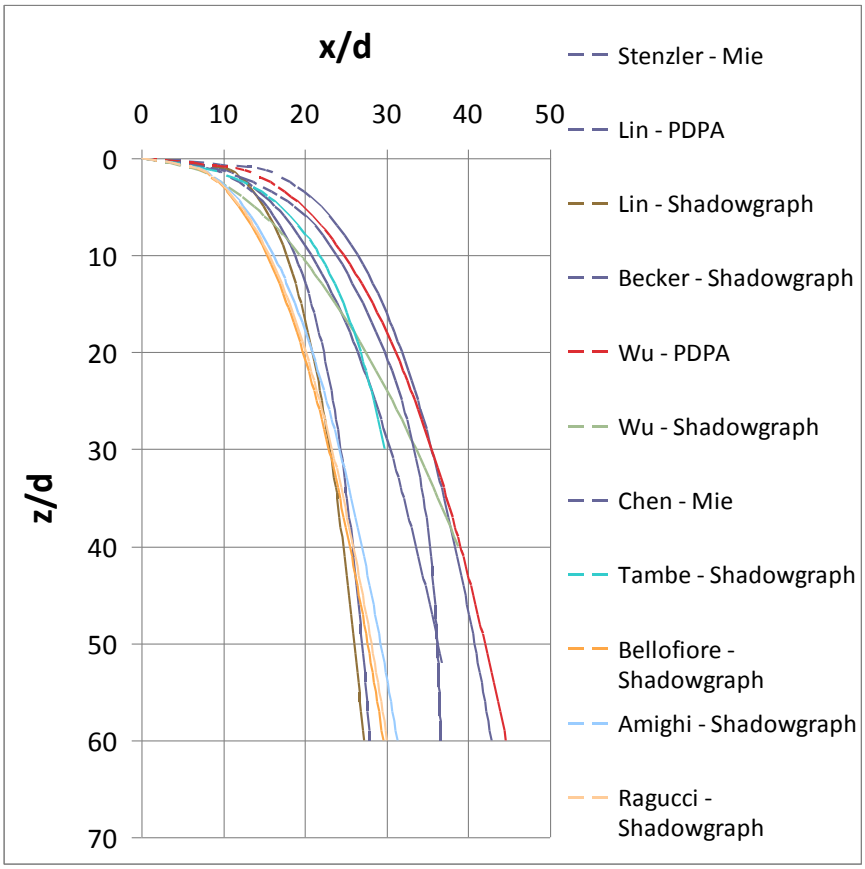

Figure 1-3. Penetration trajectories for q=20 plotted using correlations provided by several researchers [5,6,14,15,17,18,19,20,21,22,23]

These correlations differ because of other factors, not included in the correlations, that change the spray behavior or because of the way the spray penetration was measured. The possible causes for a change in spray penetration measured at the same q are

1. Use of injectors with different geometry that change the internal flow and affect spray properties [26]
2. The effect of non-uniformities in airflow, particularly the boundary layer. For example, Chelko [27] showed that the penetration data of a spray from an injector mounted flush with the orifice plate does not match with the data of the same nozzle extending 2 in. into the airflow and thus avoiding

the injection of the liquid in the wall boundary layer.

3. Different operating conditions. Though the main factor influencing the spray penetration is the momentum ratio, if the breakup regime changes, with change in *We*, the spray penetration could be different [28].

Even if the spray penetrations of two sprays match closely, the methodology used to measure the penetration trajectories can lead to discrepancy in the results obtained. The main causes for this include

1. Different measurement techniques. Trajectories measured using PDPA show higher spray penetration than those obtained by analyzing spray images because the PDPA technique is very sensitive to the presence of droplets and can detect droplets that are typically not seen in spray images [13].

2. Inconsistencies in the definition of spray boundary. Spray trajectories evaluated using spray images often use an arbitrary threshold value of luminance/brightness to define the spray boundary, which could influence the trajectories obtained.

One of the objectives of this work is to develop a methodology to experimentally determine the spray boundary in a manner that is less sensitive to the value of the threshold used and agrees reasonably well with other methods of measurement of spray penetration. As part of this thesis, spray penetration trajectories determined using the developed methodology for different injector geometries are compared to get an insight into the effect of injector geometry on spray penetration.

1.2.3 Spray Characteristics: Primary Breakup Time

Computations of the liquid jet in crossflow employ models for the jet breakup time scales and obtain downstream spray properties. One of the most popular models used for the primary jet breakup comes from early work on the aerodynamic breakup of liquid droplets in supersonic flows, including that of Ranger and Nichollas [29]. They carried out experiments to find the time required for individual droplets dropped into a supersonic crossflow to breakup to form a mist. They found this time (t_b) was proportional to the droplet diameter (d), inversely proportional to the relative velocity between the droplet and the airflow (u_a), and proportional to the square root of liquid-to-air density ratio ($(\rho_l / \rho_a)^{1/2}$). Based on the images taken, they found that the constant of proportionality (t_b/t^*), defined by equation (1-4) to be 5. Another conclusion of their study was that the effect of the shock wave on the aerodynamic breakup of the droplets was minimal. The main function of the shock wave was to produce the high speed convective flow that was responsible for the disintegration of droplets. This prompted subsequent researchers to use this characteristic time (t*) for droplets in subsonic flows and liquid jets in subsonic crossflows.

$$\frac{t_b}{t^*} = \frac{t_b}{(\rho_l / \rho_a)^{1/2} d \ / u_a} = 5 \qquad \text{Equation 1-4}$$

Wu *et al.* [6] analyzed spray images obtained at *We* in the range of 71 – 200 to locate the column breakup location. An example of such an image is shown in Figure 1-4. This image was captured at *We*=71 and *q*=7.7. It can be seen that the liquid jet disintegrates to form large ligaments and bag like structures that subsequently break up into smaller droplets. However, the location of the jet breakup was not definite but

subject to human judgment. They reported that the column breaks up at an average location of about eight diameters downstream of the orifice in the direction of airflow regardless of the operating conditions. They defined t_b as the time required for a liquid particle to travel from the orifice to the CBP, i.e., X_b/u_l, with the assumption that the liquid maintains a constant velocity, u_l until it reaches the CBP. Adopting the non-dimensional form for primary breakup time described in equation 1-4, they reported an average t_b/t^* value of 3.44. Sallam *et al*. [30] measured the location of column breakup point at *We* range of 0.5-260. Their studies yielded a different value of t_b/t^*=2.5. Their observations also showed that the column breaks up at eight diameters downstream of the orifice. Lee *et al*.[31] measured the location of the CBP of a turbulent liquid jet and reported a value of t_b/t^*=1.6.

Figure 1-4. Spray image at *We*=71, q=7.7; Adopted from Wu et al. (1997)

The time scale for the primary breakup was adopted from the time scale for the breakup of a droplet in supersonic flow. The physics of the primary breakup of the liquid jet is significantly different from the breakup of a droplet. The variation in the primary breakup time scale for a liquid jet in crossflow by different researchers indicates that the physics is not completely captured and there is a possibility that some scaling parameter

is missing in the equation. Birouk *et al*.[32,33] measured the location of the CBP for different liquids and found that the breakup distance depends on the momentum ratio and the viscosity of the liquid. They found that the primary breakup occurred farther from the orifice for liquids with higher viscosity.

One of the biggest challenges in studying the primary breakup in the shear breakup regime is optical access to the liquid column. At such conditions, the liquid column is surrounded by a high density of droplets as seen in Figure 1-5. This makes it impossible to locate the CBP visually from spray images. Thus, there is a need for an alternate technique that would enable us to locate the CBP accurately in the shear breakup regime and is independent of human judgment.

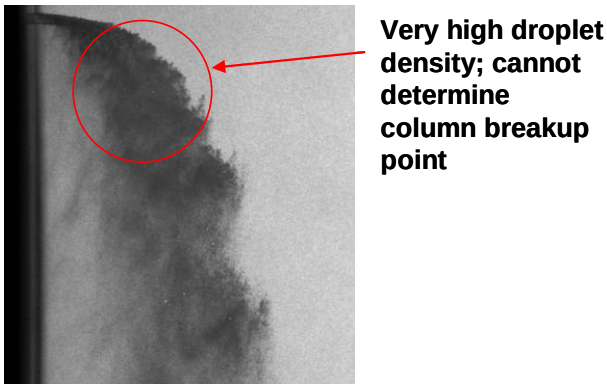

Figure 1-5. Spray image at *We*=1000, *q*=20, which lies in the shear breakup regime

1.2.4 Modeling approaches of a liquid jet in crossflow

Models of liquid jet in crossflow are used in the design and development of combustors. They are useful tools to calculate the effects of design modifications on such spray characteristics as spray penetration, droplet size distribution, spatial distribution of liquid mass and droplet velocities and thus, serve as a quick and inexpensive means to arrive at a configuration with desired spray characteristics. In order to calculate the spray

characteristics, models incorporate important processes involved in the formation of a spray such as the primary breakup of the liquid column, secondary breakup of large droplets, shredding of droplets from the liquid jet due to shear forces, aerodynamic drag on the liquid jet and droplets and changes in droplet drag due to distortion. The models available in the literature [34,35,36,37,38,39,40] differ from one another in the number of spray formation processes incorporated into the model and the experimental correlations used to model the parameters. A brief overview of one of these models by Madabushi [37] that incorporates all the processes of spray formation listed above is given here to familiarize the reader with the experimental parameters required for such modeling.

A schematic showing the aspects of Madabushi's model is shown in Figure 1-6. A Lagrangian approach is used to describe the droplet motion. The liquid jet is represented by a series of spherical droplets issuing out of an orifice. The diameter of these droplets is set equal to the orifice diameter, and the droplet velocity is set equal to the jet exit velocity. Empirical values for effective drag coefficient and primary breakup time are used to calculate the trajectory of the liquid jet prior to the CBP. Beyond the CBP, the drag coefficient is increased from the drag coefficient of a column to that of a disk to simulate the effect of deformation of droplets. Secondary breakup occurs if the ligaments or droplets have a local *We* larger than 12, the critical *We* below which breakup does not occur [41]. The time for secondary breakup is modeled using a breakup time for droplet disintegration in airflow measured by Pilch *et al*. [41]. Empirical correlations are used to model the Sauter mean diameter and volumetric distribution of the droplets after secondary breakup. The shear breakup mechanism that removes small droplets from the surfaces of larger droplets is modeled with the wave model by Reitz [42]. This wave

model involves solving the linear stability equation for Kelvin-Helmholtz type instability to obtain the most unstable wave. To summarize, this model employs a combination of analytical solutions of the equations of hydrodynamic instabilities and experimentally obtained parameters like drag coefficient, primary breakup time and droplet size distribution. One of the objectives of the present work is to experimentally determining the primary breakup time, which is not currently available for the shear breakup regime due to an inability to resolve these physics using conventional imaging and diagnostic techniques.

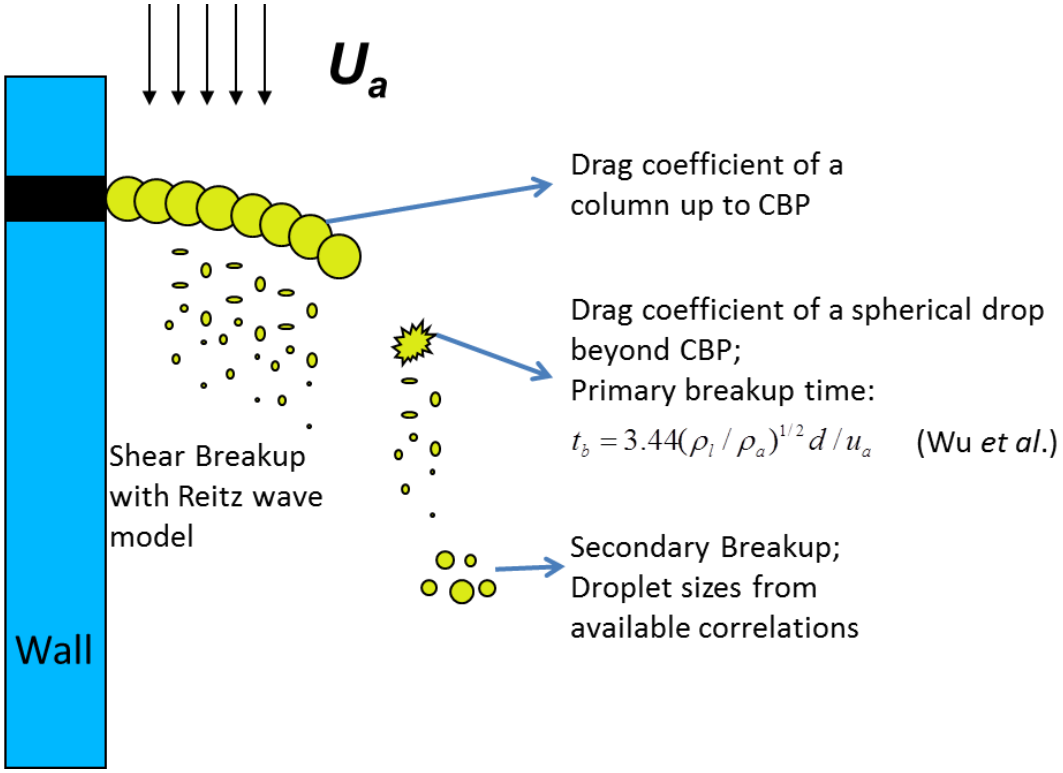

Figure 1-6. Schematic of Madabushi's model for spray formation

Pai *et al*. [43] and Hermann *et al*. [44] performed detailed simulations of a liquid jet in crossflow. Accurate measurements of the location of the CBP can serve as validation data for such simulations in the future.

Figure 1-7. Detailed simulation of a jet in crossflow by Pai *et al.*[43]. It shows the column breaks up at 2-3 diameters downstream of the orifice

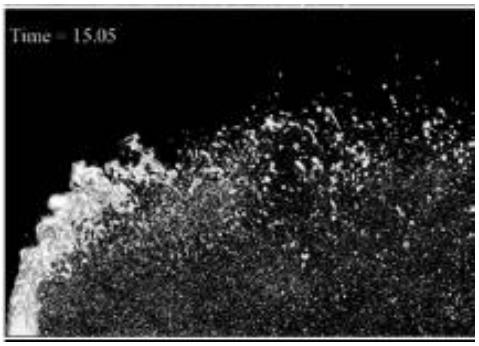

Figure 1-8. Detailed simulation of a jet in crossflow by Hermann [44]. It shows the column breaks up at ~3 diameters downstream of the orifice

1.2.5 Primary Breakup of Turbulent Jets in Quiescent Medium

Section 1.2.1 discussed the effect of aerodynamic forces that lead to the breakup of the liquid jet. Studies in the past have identified the liquid jet turbulence at the jet exit as an important parameter that affects the properties of the spray created. [45,46,47,48,49,50,51,52,53]. These studies were carried out on a liquid jet injected into quiescent medium and are briefly reviewed here. Figure 1-9 shows the schematic of a turbulent liquid jet injected into a quiescent medium. Generally, the spray region consists

of a dense spray region and dilute spray region as shown. The dense region consists of a liquid core surrounded by droplets that separated from the liquid column after issuing out of the orifice. The jet spreads reducing the droplet density and forms the dilute spray region where the interaction between droplets is not very high. Similar to the atomization of a liquid jet in crossflow, the atomization of the turbulent jet consists of two processes, the primary breakup and the secondary breakup processes. Primary breakup process includes formation ligaments and droplets along the surface of the liquid core. The secondary breakup process describes the subsequent breakup of shed droplets and ligaments.

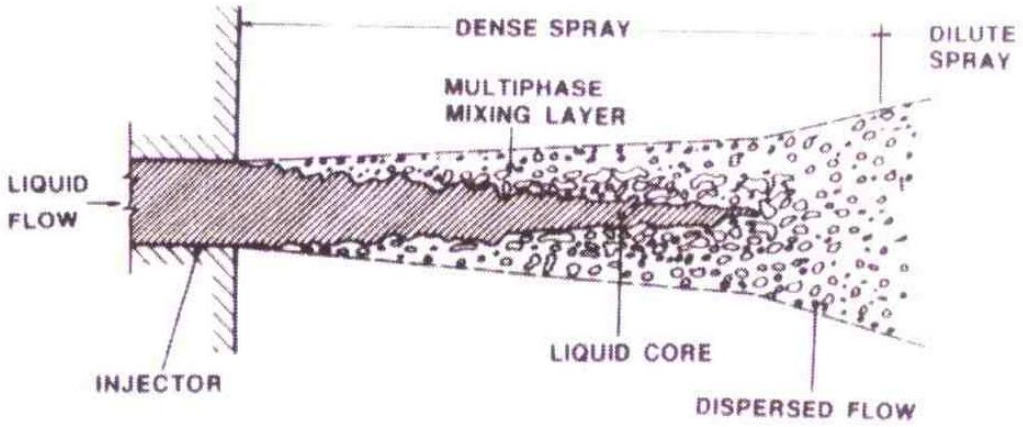

Figure 1-9. Schematic of a turbulent liquid jet atomizing in quiescent medium; Adopted from Faeth *et al*.[50]

Juhasz *et al*. [45] and Lee *et al*. [46] showed that the rate of mixing between the liquid and surrounding gas differed for a spray created by a laminar and a turbulent liquid jet. Grant *et al*. [48] and Phinney [49] showed that the onset of breakup on the surface of the liquid column and the jet stability was affected by turbulence of the jet. They also found that the breakup length of the liquid core decreases with increase in Reynolds number of the liquid jet beyond a critical value of 3000. This was confirmed by the results obtained by Chehroudi et al. [54]. Ruff *et al*. [55,56,57] and Tseng *et al*. [58]

performed experiments with relatively large liquid jets (9.5mm and 19.1mm in diameter). They found that in general, the drop sizes after primary breakup were larger for turbulent jets than non-turbulent jets. The droplet sizes for the turbulent jets were found to approach the dimensions of the spatial integral scales in the liquid for turbulent primary breakup. Wu *et al*. [59] linked the surface tension energy required to form a droplet to the kinetic energy of a corresponding liquid eddy relative to its surroundings within the inertial region of the turbulence spectrum. This showed a close correspondence between the liquid turbulent properties and primary breakup. They also concluded that the aerodynamic forces on the protruding turbulence induced ligaments assists the kinetic energy of the turbulent eddy in overcoming the surface tension energy and enhances atomization [60] as shown in Figure 1-10.

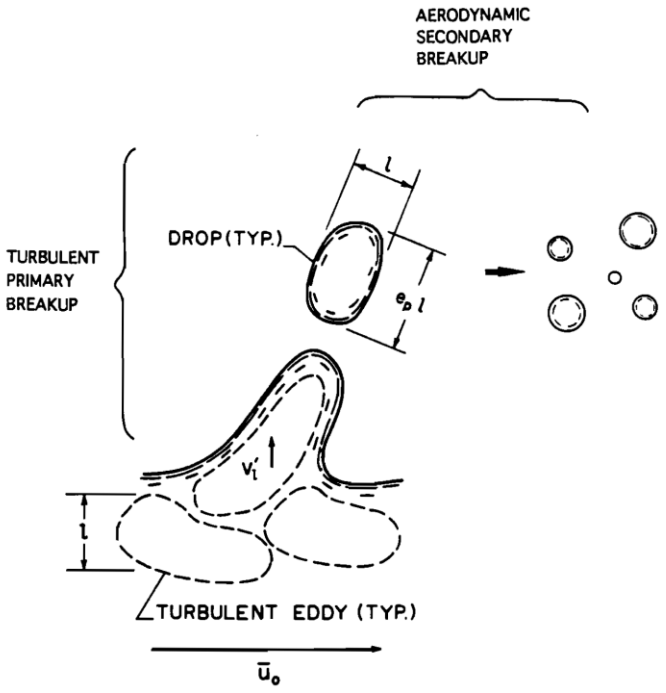

Figure 1-10. Turbulent eddy forming ligament on the surface of the liquid column. The eddy can separate from the liquid column if it overcomes the surface tension energy. The protrusion of the eddy into still air creates aerodynamic forces that assist the atomization

1.2.6 Effect of Injector Geometry

The injector geometry affects the internal flow of the orifice and thus can influence the spray properties. The design parameters of a standard cylindrical injector (also referred to as plain orifice) that affect the internal flow are the length to diameter ratio (L/d ratio) and the “smoothness” of the transition from the line supplying the liquid to the orifice [63]. L/d ratio affects the exit velocity profile of the jet. For a flow to be fully developed, high L/d ratios are required [61]. A smooth transition results in streamlines following the walls of the orifice and consequently, a smooth flow (see Figure 1-11). If the transition is sharp, streamlines are disrupted and the turbulence generated in the flow is higher compared to a smooth transition. Sharp edged orifices can also lead to formation of cavitation bubbles in the orifice that lead to higher turbulence as well. For example, Tamaki *et al.* [62,63] and showed that the occurrence of cavitation or hydraulic flip inside the nozzle significantly influences the breakup of the liquid jet into droplets. Cavitation is the formation and then implosion of cavities in liquid, i.e. small liquid-free zones ("bubbles"), which are the consequence of forces acting upon the liquid. It usually occurs when a liquid is subjected to rapid changes of pressure that cause the formation of cavities or low pressure regions. In injectors, cavitation is usually observed when the liquid encounters a sharp turn causing flow to separate and consequently, a decrease in local pressure below the vapor pressure of the liquid, which results in liquid evaporation (see Figure 1-12). During hydraulic flip, a flow making a sharp turn, gets detached from the walls of the injector and does not reattach itself (see Figure 1-13). This phenomenon is commonly found in injectors with low L/d ratios.

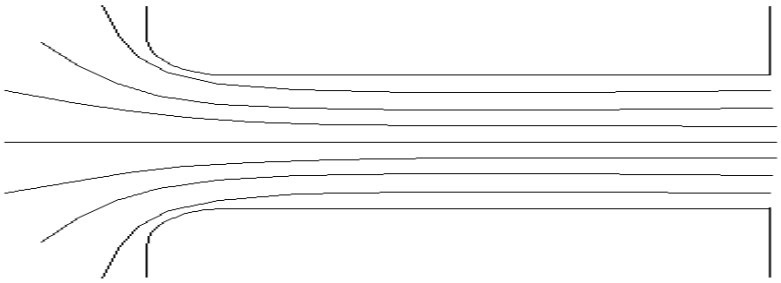

Figure 1-11. A contoured injector keeps the streamlines parallel to each other resulting in a smooth flow

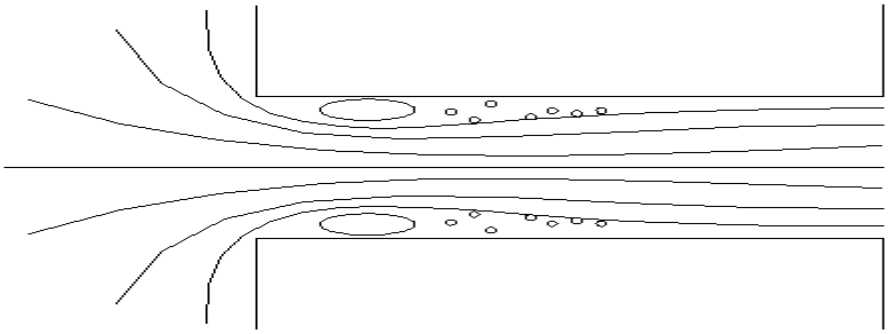

Figure 1-12. An injector with cavitation bubbles. A sharp turn leads to flow separation and a drop in pressure. If the pressure is lower than the vapor pressure of the liquid, the liquid vaporizes and forms cavitation bubbles.

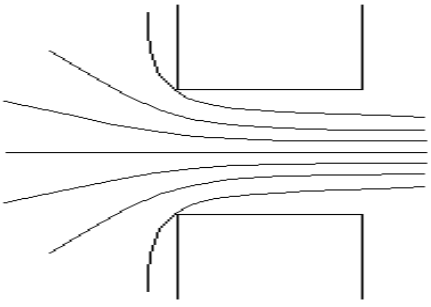

Figure 1-13. Injector with hydraulic flip. The detached flow on a sharp turn does not reattach before exiting the injector.

Cavitation in diesel sprays has received a lot of attention in literature. Schmidt and Corradini [64] have reviewed the work carried out in this field. It has been well

established that cavitation in a diesel injector affects the spray formed significantly. In the presence of cavitation, the spray angle increases and the breakup length shortens [65,66,67]. The two phase flow in the orifice increases the turbulence of the liquid jet, thus accelerating its breakup into droplets [68,69]. Nurick [70] developed a one dimensional model that serves as a useful tool to understand the orifice flow and estimate the occurrence of cavitation. The cavitation parameter, K is defined as

$$K = \frac{P_1 - P_v}{P_1 - P_2}$$ **Equation 1-5**

where, P_1 is the pressure at the inlet of the injector, P_2 is the pressure at the exit and P_v is the vapor pressure of the liquid. The theory states that cavitation is observed when the cavitation parameter goes below a critical value of 2. This parameter is different from the cavitation number often used in literature and defined as

$$CN = \frac{P_1 - P_2}{P_2 - P_v}$$ **Equation 1-6**

This model has been validated with data collected by various researchers [69,67,71,72,73,74,66] who used transparent injectors to detect cavitation. The results obtained are shown in Figure 1-14. The experimental results were consistent but not conclusive with this model.

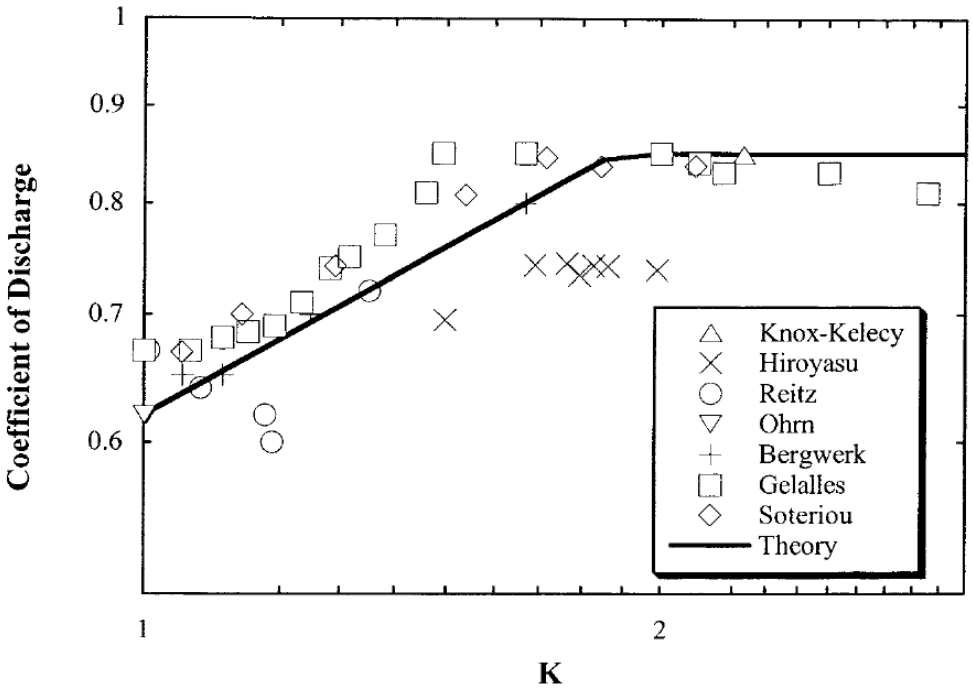

Figure 1-14. Nurick's one dimensional model [64] with validation data.

Ahn *et al*. [26] investigated the effects of orifice internal flow on the properties of a spray created by a water jet in crossflow at atmospheric conditions. They used three transparent injectors: a round edged injector with an L/d ratio of 20 and two sharp edged injectors, one with an L/d ratio of 20 and the other with an L/d ratio of 5. Investigation of the injectors revealed that while the round edged injector did not undergo cavitation or hydraulic flip, the sharp edged injector with L/d ratio of 20 produced a cavitated flow when the pressure drop across the injector was over 3.5 bar. The third injector produced a flipped flow beyond a pressure drop of 3 bar. Figure 1-15 shows the characteristics of these injectors. It shows that the onset of cavitation is characterized by a drop in the value of discharge coefficient. This happens because the cavitation bubbles increases the velocity in the injector and leads to greater pressure loss.

They measured spray penetration in flows from these injectors. They found that

while spray trajectories followed the correlations obtained by Wu *et al*. [6] in the absence of cavitation and hydraulic flip, the presence of these phenomena resulted in reduced penetration between the observed trajectories and the ones reported by Wu *et al.* [6]. Consequently, they concluded that the design of the injector has a significant effect on the spray characteristics. However, the effect of the injector geometry on other characteristics of the spray, such as droplet sizes, droplet velocities and CBP, remain largely unexplored. To fill this gap, this thesis will investigate the differences between the properties of sprays created by two injectors having different geometries and the processes responsible for these differences. The two injectors used in this study are similar to the ones used by Ahn *et al*. [26]. One is a sharp edged orifice with an L/d ratio of 10 and the other is a round edged orifice with L/s ratio of 1.

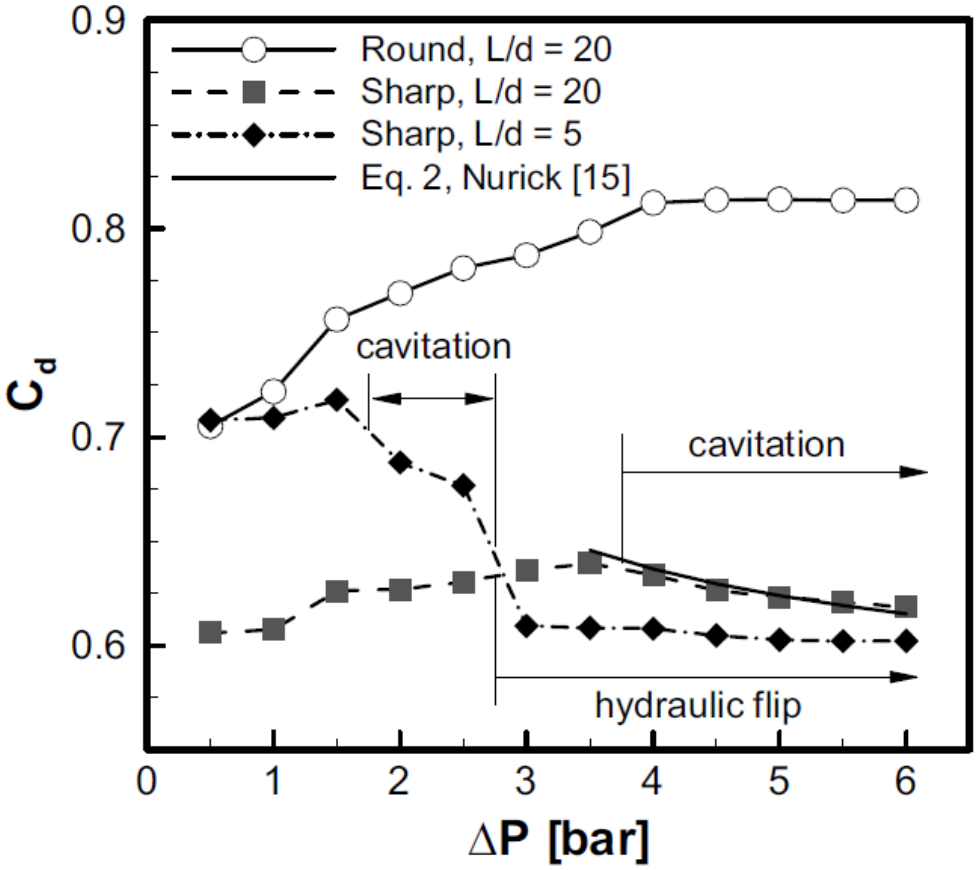

Figure 1-15. Characteristics of the injectors used by Ahn *et al.* [26]

1.3 OVERVIEW OF PRESENT WORK

As can be seen from the previously cited work, there have been several advances in understanding the spray formation processes and in being able to predict the spray characteristics. Breakup regimes have been identified and fundamental processes such as the primary breakup, secondary breakup and shear breakup involved in the formation of sprays have been elucidated. Correlations have been developed for spray properties such as penetration trajectories, lateral spread trajectories, droplet sizes, primary breakup times, secondary breakup times and droplet velocities that link them to flow parameters. This knowledge has helped in design of combustors and development of spray models.

However, knowledge of some of the critical parameters is not adequate and there is a need for better experimental data.

One such parameter is the primary breakup time scale in the shear breakup regime. In this study, the liquid jet light guiding technique (LJLGT), was used to make it possible to locate the CBP and determine the primary breakup time scale in the shear breakup regime. Additionally, this method provides a new way of visualizing sprays and is able to detect the phenomenon of the liquid jet splitting into two or more jets. This method was also used in combination with Particle Image Velocimetry to measure the velocities of the features on the surface of the liquid jet column. These measurements provide insight into the velocity field on the surface of the intact liquid jet. It also helps in assessment of the commonly used assumption of constant velocity of the liquid jet up to the CBP.

Spray penetration trajectories have been well investigated by several researchers as well. However, there are dozens of correlations available and they do not often agree with each other within reasonable limits. This thesis identifies the causes behind the discrepancies observed between the various trajectory equations and arrives at a better way to describe the spray penetration. This approach employed a spatial probability distribution of finding droplets at a given location and describes the fluctuating spray better than a single trajectory equation.

Another area of interest is the effect of injector geometry on spray characteristics. The change in injector geometry affects the flow inside the orifice. This change can lead to a significant change in the breakup mechanisms associated with the primary breakup of the liquid jet. This, in turn, affects the properties of the created spray. The studies so

far have investigated the effect of injector geometry on a liquid jet in the absence of a crossflow. Limited studies of a liquid jet in crossflow with different injectors have shown that the injector geometry plays an important role in determining the spray characteristics. This thesis investigates sprays created by using two different injectors and answers the questions as to how and why the sprays created by different injectors are different. The characteristics investigated as part of this thesis are spray penetration trajectories, the location of the CBP, the structures formed on the liquid jet column, the phenomenon of jet splitting, droplet sizes and velocities.

In view of the above discussion, this thesis consists of five chapters. This chapter covered the introduction and literature review followed by setting of goals for this thesis. The second chapter covers the experimental efforts describing the experimental setup and the diagnostic techniques used in this study. The third chapter covers the results obtained on the primary breakup processes using the LJLGT. The fourth chapter focuses on identifying the effect of injector geometry on spray characteristics. Finally, the fifth chapter presents the conclusions of this research and recommendations for future work.

CHAPTER II

EXPERIMENTAL EFFORTS

This chapter describes the experimental efforts carried out for this PhD research at the Georgia Tech Combustion Laboratory. Section 2.1 describes the experimental setup used in this study covering the air circuit, the liquid circuit and the instrumentation to measure the flow properties. Section 2.2 focuses on the diagnostic techniques used to measure the spray properties. It includes brief descriptions of such conventional diagnostic techniques as Laser Doppler Velocimetry, Phase Doppler Particle Analyzer and Back Illumination. Detailed descriptions are provided for the diagnostic techniques and methods developed as part of this study.

2.1 EXPERIMENTAL SETUP

2.1.1 Air Circuit

The experimental work was carried out in a high pressure and high temperature experimental setup. Figure 2-1 shows a detailed schematic of the experimental setup used. The plenum chamber was connected to a test section by an air supply channel. The test section containing the injector was housed in a pressure vessel, which was connected to an exhaust system. The plenum chamber was 152.4 mm (6 in) in diameter and 457.2 mm (18 in) long. Air entered the plenum through a metal pipe having a symmetric distribution of 60 orifices, each 3.2 mm (1/8 in) in diameter. The chamber was thermally insulated to minimize heat losses. The 304.8 mm (12 in) long air supply channel had a square cross-section measuring 61.7 mm (2.43 in) on each side. It was equipped with a

bell-mouth air intake, which was submerged 25.4 mm (1 in) into the plenum chamber to smooth the air flow. Two aerodynamically shaped plates were attached to the walls at the downstream end of this channel, thus creating the test section. The test section was contained in a pressure vessel with four glass windows providing optical access to the spray. The injector was fixed on the centerline of one of the aerodynamic plates, which shall be referred to in this work as the orifice plate. Two 3.2 mm (1/8 in) thick quartz windows, measuring 76.2 mm (3 in) × 32 mm (1.26 in), were installed in slots cut in the aerodynamically shaped plates (see Figure 2-2). The design of the test section confined the air flow in the spray region and provided optical access to the spray. The dimensions of the test section are 30 mm × 46 mm (from plate to plate and from window to window, respectively).

The assembly consisting of the plenum chamber, the supply channel and the test section was connected to the pressure vessel on a swivel support that allowed free rotation of the test section about its axis. This helped to optimally orient the spray with respect to the optical diagnostic systems.

The RMS velocity fluctuations of the incoming air were found to be around 4% of the mean air velocity for the range of test conditions considered in this study and the boundary layer on the plate with the injection orifice was about 3mm wide. It was determined that the characteristics of the incoming air flow at a plane that was perpendicular to the direction of the airflow and located 5mm upstream of the orifice, were not affected by the spray. Consequently, data measured in this plane can be used as boundary conditions for CFD codes. The flow was found to be uniform and stable in the region of interest. The measured velocity profiles are shown in Appendix A.

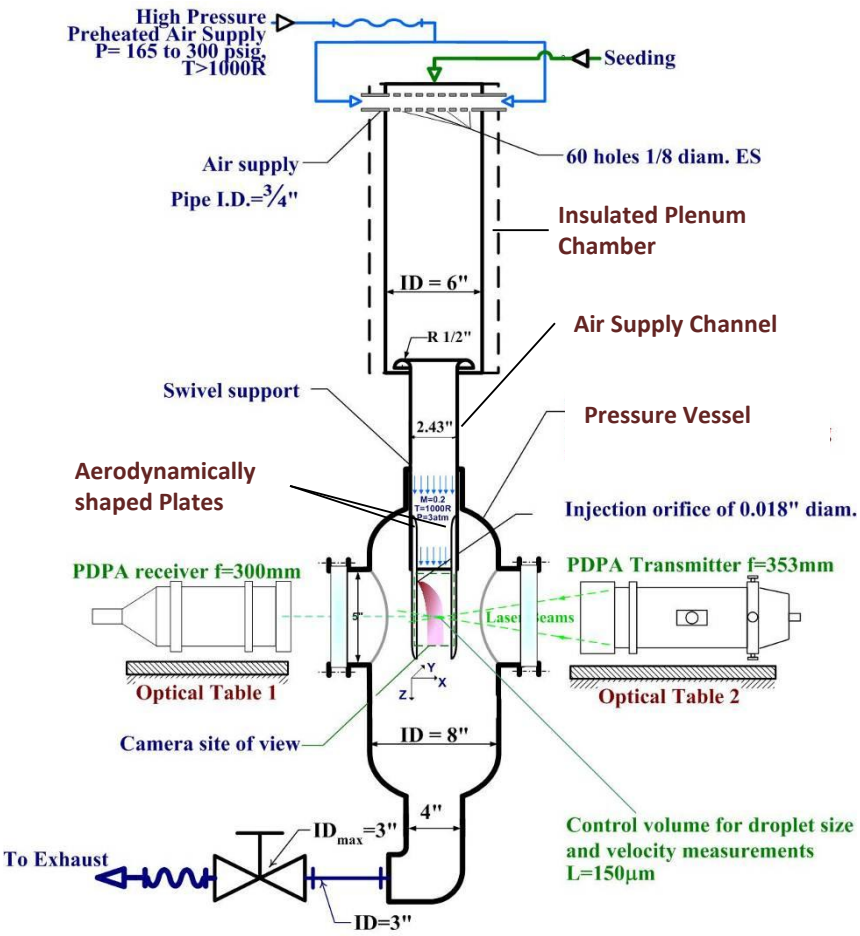

Figure 2-1. Schematic of the experimental test facility used in this study

Figure 2-2. A photograph of the test tection

The pressure vessel was 203.2 mm (8 in) in diameter and 914.4 mm (36 in) long. It had four windows for optical access. Three of the windows were placed at an angle of 90°, 150° and 240° relative to the main window as shown in Figure 2-3. The Phase Doppler Particle Analyzer (PDPA), when operated in the Forward Scattering Mode (FSM) to measure droplets' diameters and two components of droplets' velocities, needed an angle of 150° or 240° between its transmitter and receiver for optimal performance. The third component of the velocity was measured using the window oriented at 90° to the primary window.

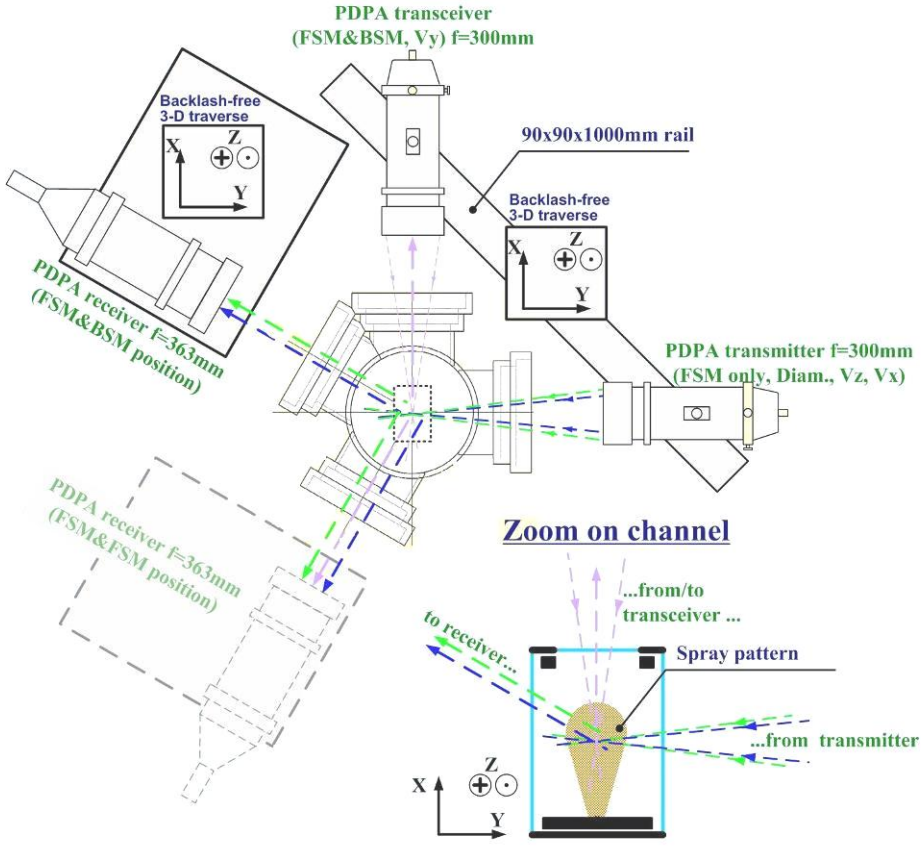

Figure 2-3. Top view of the pressure vessel showing the orientation of its windows

Preheated air was supplied to the test rig from a high pressure blow down facility (P_{max}=720psi, T_{max}=555K), which automatically maintained constant pressure and

temperature (as set on the panel) at the inlet of the plenum chamber. The high pressure air was stored in 14 high-pressure cylinders at 2500 psia (17.24 Mpa). The air passed through a natural gas heater where it was heated to a desired temperature. The pipes leading to the test cell were insulated to minimize heat losses. The pipes were also electrically heated to prevent cooling of the air. The air velocity and pressure in the test section were controlled by varying the air supply pressure and controlling the throttle valve in the exhaust line where the air flow was choked. The exhaust system included an afterburner, which was used to burn the Jet A before letting the exhaust flow out of the building.

2.1.2 Liquid Circuit

Two liquids were used in this study, Jet A and water. The values of the surface tension of these two liquids differ significantly from each other, and thus the range of operating *We* was widened by their use. Experiments with water involved short operating durations and a simple system with a one gallon high pressure reservoir pressurized by a nitrogen cylinder that was used to force water into the injector. The mass flow rate of the liquid was measured with an FTB-9504 turbine flow meter equipped with OMEGA FLSC-62 transmitter. Since experiments with Jet A involved complete spray characterization using PDPA, capabilities for longer duration tests were required. A schematic of the Jet A supply system is shown in Figure 2-7. An outdoor 60 gallon tank was used to store and supply Jet A. The fuel tank was pressurized to about 60 psig with a nitrogen cylinder. This pressure was sufficient to produce a mass flow rate of up to 3g/s. When higher flow rate was required, an air-powered MAXIMATOR fuel pump LSF15-2

was used to provide the required pressure head. A bladder type accumulator with a volume of one gallon was attached to the pump discharge line to absorb the hydraulic shocks created by the pump. The flow rate was controlled by a valve that was actuated from a dial on the instrumentation panel. The fuel flow rate was measured with the same turbine flow meter that used in the water tests.

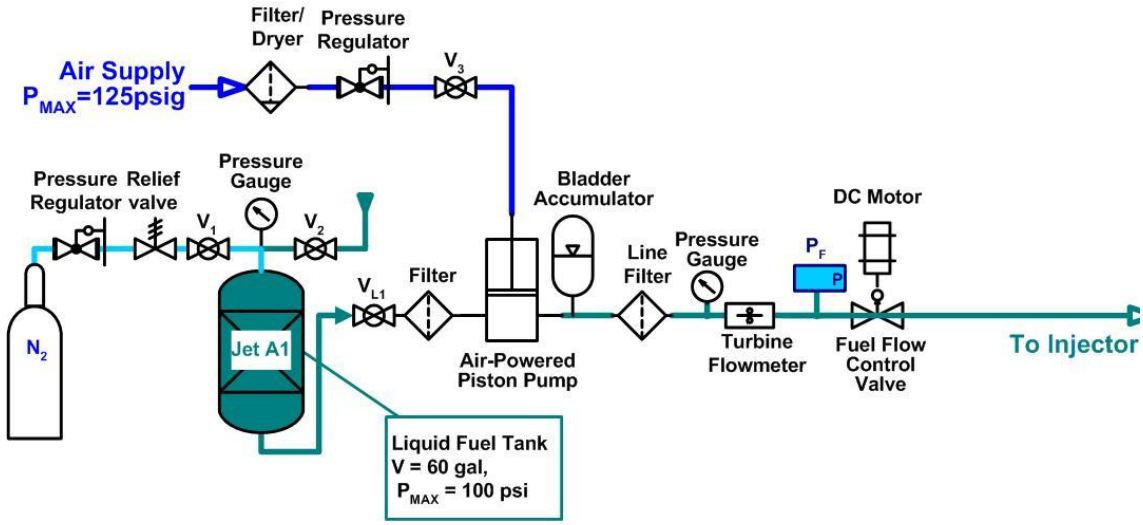

Figure 2-4. Schematic of the Jet A supply system

Two different injectors were used in this study, both having a diameter of 0.47 mm (0.018 in). One was a round-edged orifice with a length to diameter (L/d) ratio of 1 (see Figure 2-5). This injector provided a smooth flow and has a discharge coefficient, C_d of 0.95. The other injector was a sharp-edged orifice with an L/d ratio of 10 shown in Figure 2-6. The jet from this injector was more turbulent because of the higher L/d ratio and the sharp area transition. The pressure drop across this injector was higher than that of the first injector, resulting in a lower value of C_d=0.74.

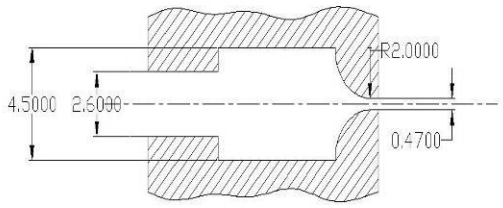

Figure 2-5. Schematic of the Round Edged Orifice

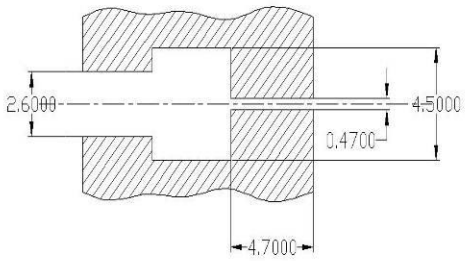

Figure 2-6. Schematic of the Sharp Edged Orifice

2.1.3 Instrumentation

Figure 2-7 shows a schematic of the instrumentation that was used to monitor the operating conditions of the test. The velocity of the air flow was monitored using a combination of static and total pressure probes installed in the air supply channel about 150 mm upstream of the injector. Static pressure in the test section was measured at a wall pressure port using an Omega PX303-100G5V transducer with a range of 0–100 psig. The total pressure probe was located in the middle of the air supply channel at the same height as the static pressure probe. A differential pressure sensor, Datametrics Inc. Barocel Model 511.16 (7.5 psi), measured the differential pressure between these two probes. Temperatures of the air and liquid were measured using K-type thermocouples, 1/16" in diameter each. Air temperature was measured at the center of the air supply channel cross-section 1.4" (35.56 mm) upstream of the injector. Temperature of the liquid was measured just before it entered the injector. The pressure of the liquid was measured using an OMEGA P303-1K5v (1000psig) transducer just upstream of the injector.

All signal cables were connected to a BNC-2090 National Instruments board. The signals ran from the board into the computer and were measured, displayed, and saved. A National Instruments PCI-6071E data acquisition card was used in the computer to

receive all the measured data. The LABVIEW program used the measured voltages of the pressure, the temperature and the fuel flow rate and using them, calculated the values of the following flow properties: free stream Mach number, velocity of air, mass flow rate of air, density of air, fuel velocity, Weber Number and momentum ratio. The velocity of the liquid jet is obtained by dividing the mass flow rate of the liquid by the geometric area of the orifice.

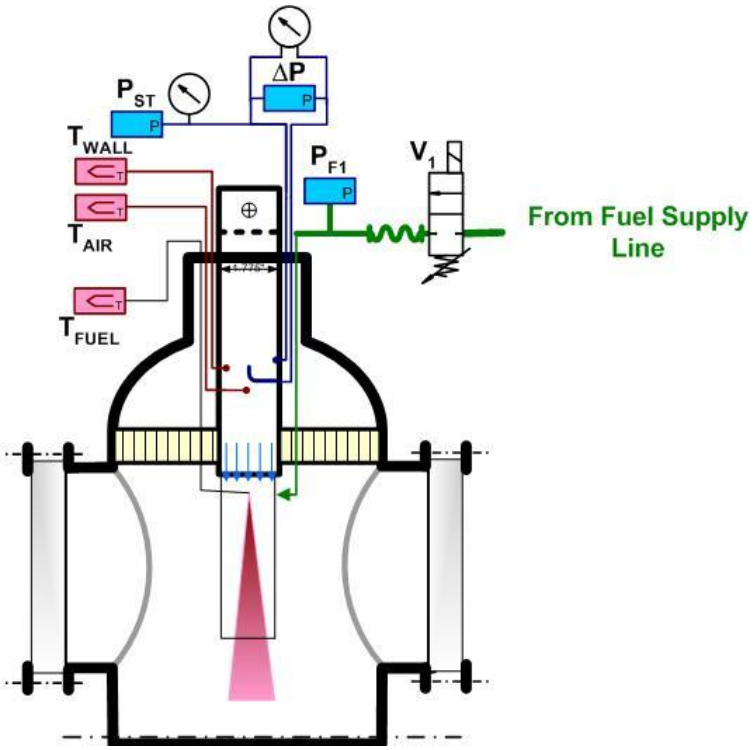

Figure 2-7. Schematic showing the instrumentation of test facility

2.1.4 Coordinate system

The coordinate system used to describe the experimental results has its origin at the orifice. The three mutually orthogonal directions (*X*, *Y*, & Z) are aligned as shown in Figure 2-8. The positive X-axis points in the direction of fuel injection, the Z-axis points in the direction of incoming air flow and the positive Y-axis is on the plate having the

orifice forming a left handed coordinate system. X-scans refer to the measurement of velocity components while moving in the X-direction

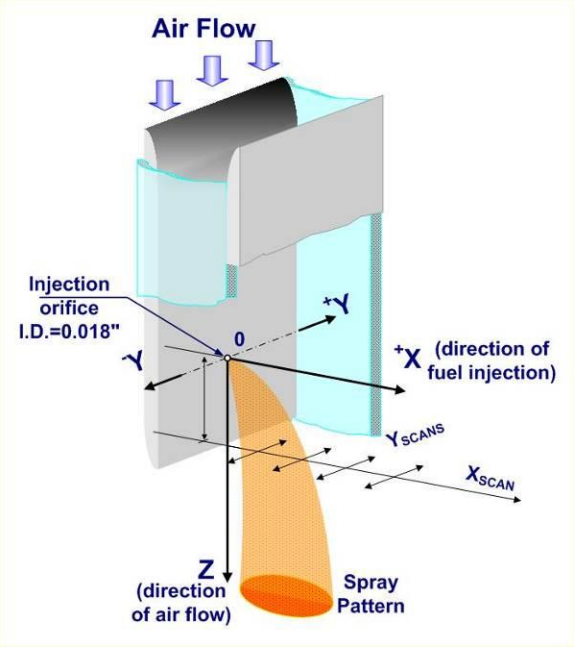

Figure 2-8. Convention for the coordinate system followed in this study

2.2 DIAGNOSTIC TECHNIQUES AND APPROACHES

The following diagnostic techniques were used to experimentally investigate the spray properties.

- A Phase Doppler Particle Analyzer (PDPA) was used to measure the droplet sizes and the droplet velocities. The same system was used in Laser Doppler Velocimetry (LDV) mode to measure the mean and the RMS velocity components of the incoming airflow.
- A Micro LDV system was employed to measure the velocity profile within the wall boundary layer on the plate that housed the orifice.
- The Liquid Jet Light Guiding Technique (LJLGT) that was developed as part of this study to locate the CBP.
- The LJLGT integrated with aspects of Particle Image Velocimetry (PIV) that enabled measurements of the velocity field on the surface of the liquid column.
- A Back Illumination technique to capture spray images that were used to analyze the structure of the spray and obtain the penetration trajectories.

2.2.1 The Laser Doppler Velocimetry (LDV) and Phase Doppler Particle Analyzer (PDPA) system

A TSI three component PDPA was used to measure the sizes and velocities of liquid droplets. A detailed description of the system is given elsewhere [75]. The data obtained was analyzed using the software Flowsizer to obtain the mean velocity, the root mean square (RMS) velocity, the Arithmetic Mean Diameter (AMD) and the Sauter Mean Diameter (SMD) of the droplets. This system was used in the LDV mode as well,

to measure air flow velocities. For this purpose, the air was seeded with alumina particles by bleeding part of the air into a cylindrical chamber containing finely powdered alumina before it entered the plenum chamber.

2.2.2 Micro LDV

The LDV system described above was modified to increase its resolution to enable velocity measurements in the wall boundary layer. The LDV system utilizes two intersecting beams of laser that create an interference fringe pattern. When a particle moves through this pattern, it creates a Doppler burst, the frequency of which is proportional to the velocity of the particle. The spatial resolution of LDV measurements is, thus dependent on the dimensions of the control volume of the intersecting laser beams. The control volume of the interrogation window of the LDV system used in this study is an ellipsoid with the largest dimension of about 240 μm. To characterize the boundary layer in the near wall region, a higher resolution is required. Thus, the LDV system was modified by increasing its resolution to enable velocity measurements in the boundary layer. There are two approaches to increase the resolution of LDV systems. One approach is to reduce the dimensions of the control volume by either reducing the thickness of the laser beams or by changing the angle between them. This reduces the dimensions of the control volume used for interrogation. The second approach is to optically magnify the existing control volume and collect Doppler bursts from a fraction of this volume. The latter approach was followed in this study. A long distance microscope, the QUESTAR QM1 (see Figure 2-9) was used to optically magnify the control volume of the intersecting laser beams and Doppler bursts were collected from a cylindrical region of radius of 12.5 μm and depth of about 5 μm. This enhanced the

spatial resolution of velocity measurements by about 20 fold. However, the higher spatial resolution required reduction in the median size of seeding particles to 1 µm compared to 5 µm that were used during normal LDV system operations. At the same time, since the control volume was diminished in size, the number of particles passing through it decreased and thus, Doppler bursts were acquired for a longer duration than during normal operation of the LDV system.

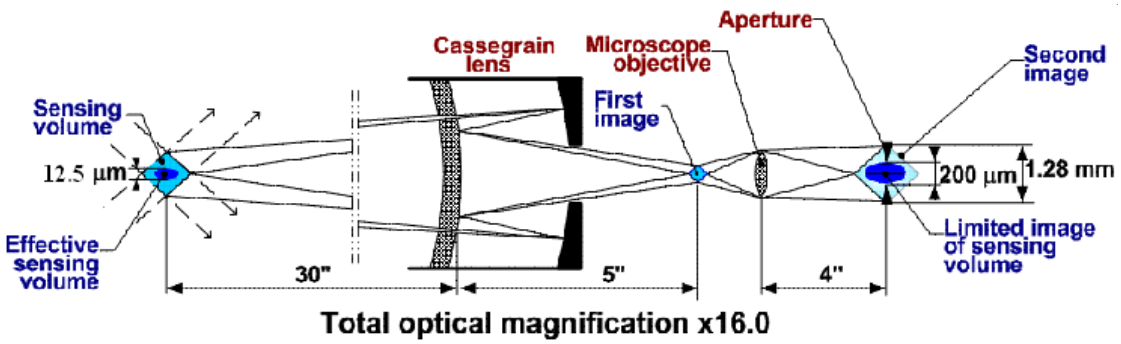

Figure 2-9. Schematic of the developed Micro-LDV Setup that was used to measure air velocity profiles in the wall boundary layer

2.2.3 Liquid Jet Light Guiding Technique

The LJLGT utilizes the well-known optical phenomenon of total internal reflection. When light crosses an interface between materials having different refractive indices, the light beam is partially refracted at the boundary surface and partially reflected. However, if the angle of incidence is greater (i.e., the ray is closer to being parallel to the boundary) than the critical angle (i.e., the angle of incidence at which the refracted light travels along the boundary), then the light does not cross the interface is totally reflected back internally. This only occurs where light travels from a medium with a higher refractive index to one with a lower refractive index. For example, it occurs when passing from glass to air, but not when passing from air to glass. This phenomenon

is used in optical fibers (flexible transparent fiber made of glass) that function as waveguides or “light pipes” between the two ends of the fiber. Light entering at one end of the fiber is reflected internally many times and is propagated to the other end without significant loss of light intensity.

The LJLGT takes advantage of this property to better visualize the liquid jet column of the spray. The liquid column is used as a waveguide for laser light. The light propagates through the column up to the location of the CBP where it is scattered. This provides means for accurately locating the CBP. This technique also provides very good visibility to the structures on the liquid jet compared to conventional imaging techniques. The principle of guiding of light by total internal reflection was first demonstrated by Daniel Colladon and Jacques Babinet [76] in the early 1840s. Figure 2-10 shows a picture from one of their demonstrations. It can be seen that the light illuminating the liquid jet from the back of the orifice follows the liquid jet through its parabolic path. If the angle of incidence (i.e., the angle between the incident ray of light and the normal to the surface) is greater than the critical angle, the ray will not exit the liquid column at all. The critical angle for total internal reflection for the interface between Jet A and air is 43°. For water and air interface, the critical angle is 48°. An analysis of the penetration trajectories of the investigated sprays showed that a ray of light coming out of the orifice never encountered an angle of incidence smaller than the critical angle. This ensured that the light was completely contained in the liquid column after the first reflection. This argument is valid for a liquid column with a very smooth surface. However, the surfaces of liquid columns encountered at conditions relevant to this study are often uneven. In such cases, the uneven surfaces could produce light refraction out of the liquid column

and a reduction in intensity of light, resulting in an inaccurate measurement of the CBP location. Thus, caution was exercised while studying jets with uneven surfaces. This section follows with a description of the setup for the diagnostic technique and considerations undertaken to avoid any source of errors in the measurements.

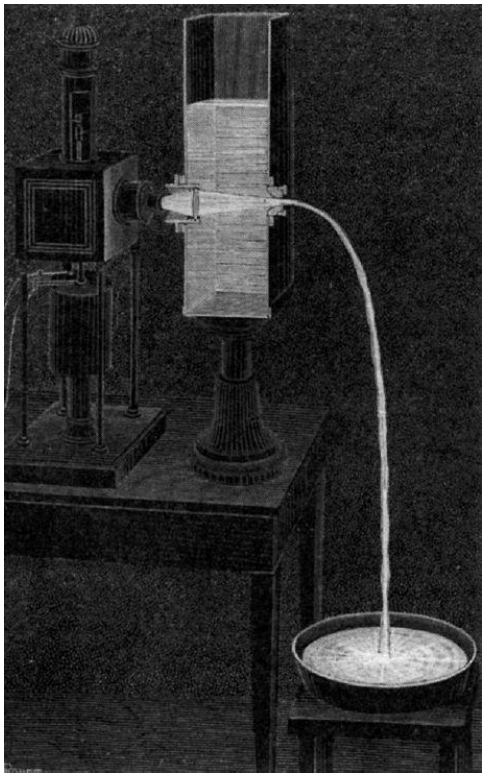

Figure 2-10. Demonstration of the use of liquid column to guide light through it adopted from [76]. This demonstration was a precursor to the development of optical fibres.

Charalompous *et al*. [77] utilized this technique to locate the CBP for a co-axial air blast atomizer in situations where the presence of a dense droplets cloud around the liquid jet column limited optical access to the jet. To overcome this problem, they illuminated a liquid jet column seeded with fluorescent Rhodamine WT dye with a laser beam from the back of the injector. The light was transmitted through the liquid column

up to the CBP before getting scattered. An optical filter was used to cut off scattered laser light and capture only the fluorescent image of the liquid column. The precise location of the CBP was obtained using these images.

The schematic in Figure 2-11 shows the setup developed for LJLGT in this study. Liquid entering the injector issues out of the orifice into the crossflow of air and breaks up into ligaments and droplets. The injector was modified to allow the introduction of an optical fiber coaxial with the direction of liquid injection. The optical fiber was used only in experiments for locating the column breakup. Pulsed laser light was sent through this optical fiber to illuminate the liquid column. When the studied liquid was Jet A, a Metalaser Technology MTS-20 pulsed Copper Vapor laser (λ=510.6nm) with tunable pulse frequency (in the range of 5 kHz – 8 kHz) and a power of about 5mJ per pulse was used for illuminating the liquid jet. When water sprays were studied, a Nd:YAG laser (λ=532nm) with a frequency of 10 Hz and a power of about 50mJ per pulse was used for illumination. Light coming out of the orifice underwent total internal reflection and was guided by the liquid column like in optical fibers. In this study, Pyrromethene 567 ($\lambda_{max\_absorption}$=518nm) and Fluorescein 548 ($\lambda_{max\_absorption}$=512nm) were used to dope the Jet A and water, respectively. Both dyes absorbed the green laser light and emitted fluorescent yellow light. These dyes were chosen because they were soluble in their respective liquids and had good absorption at the wavelengths of the lasers that were available for this study. A Foculus FO531SB CCD camera with resolution 1628×1236 pixels was used to capture images of the spray. The camera and the laser were synchronized so that every image captured was illuminated by light from only one laser pulse with pulse duration of about 13ns.

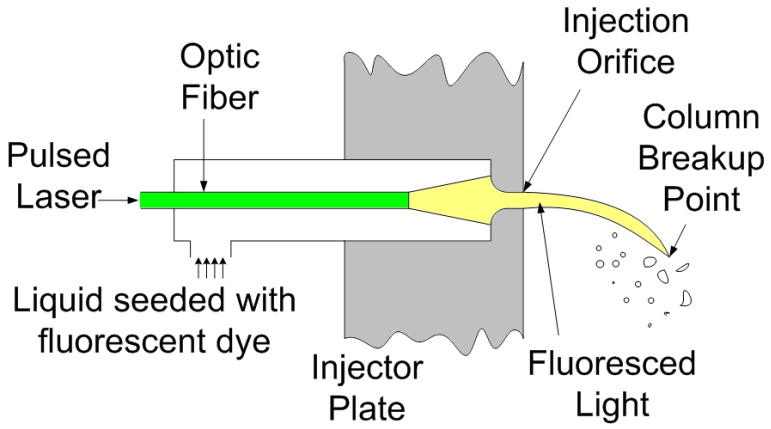

Figure 2-11. A Schematic of the setup used for the Liquid Jet Light Guiding Technique developed as part of this study to locate the Column Breakup Point

Figure 2-12 shows a typical image of the spray obtained using this technique. It is seen that the light is guided through the liquid jet. However, the presence of light scattered from a large number of droplets blocks the view of the CBP. In order to overcome this drawback, a cut-off optical filter was used with the camera that blocked the green laser light scattered from the droplets and only allowed fluorescent yellow light to reach the camera sensor. Since the droplets reflect a significant percentage of the light energy incident on them and have very weak fluorescence signal compared to the liquid column, an image captured using the cut off filter primarily shows the liquid column and can be used to locate the CBP. Figure 2-13(a) shows such an image. The images thus obtained were characterized by a sharp drop in intensity through the entire liquid column in spite of the presence of a very large number of droplets around it. A threshold to the intensity of the image was chosen to locate the boundary of the column. This threshold was used to convert the image into a binary field as shown in Figure 2-13(b). The edge of this binary field was tracked to obtain the complete boundary of the liquid column (see

Figure 2-13(c)). The farthest point on this boundary from the center of the orifice was defined as the CBP in this study. The CBP was thus found for 150 instantaneous images and the mean location was determined. The location of the CBP from each of these images and the mean location are shown in Figure 2-14 over an averaged image.

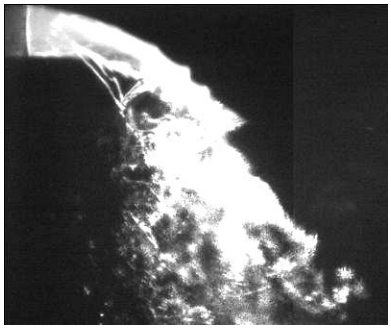

Figure 2-12. Typical image obtained with LJLGT without a cut-off filter

(a) (b) (c)

Figure 2-13. Methodology for locating the CBP a) raw image b) logical image using threshold c) logical image with recognized boundary

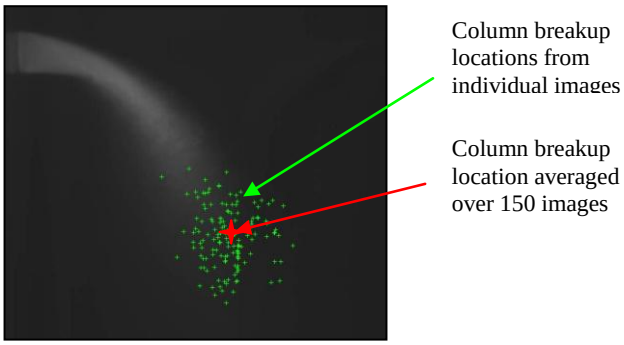

Figure 2-14. Averaged Image with column breakup locations

The intensity of light dropped sharply towards the end of the liquid column ensuring that the drop in light intensity was the column breakup and not loss of light owing to scattering (in which case, the drop in light intensity would be gradual and not abrupt). To check whether the intensity of light was decreasing gradually or abruptly, the value of threshold for the intensity was changed by 5% in either direction and the results for the CBP obtained were compared. It was found that this change in the value of threshold did not significantly change the determined locations of the CBP showing that there exists an abrupt change in the intensity between the liquid column and its surroundings. Another approach was used to verify the credibility of data obtained. The Nd-YAG laser that was used has power settings that can be varied between 10 – 100% of the maximum power (50mJ per pulse). The results for the location of the CBP were compared for three of these power settings (10%, 50% and 100%). It was found that the mean location of the CBP changed by lower than 5% for these power settings and showed that 5mJ/pulse was enough for these experiments. These two approaches conclusively proved that the change in intensity seen in the images using this technique was due to the column breaking up and not the gradual loss of light.

2.2.4 LJLGT integrated with Spatial Correlation Velocimetry (SCV) to measure velocity field on the surface of liquid column

This section discusses the method developed to integrate the LJLGT and SCV techniques to provide an approach for measuring the velocities of the structures on the surface of the liquid jet. The central idea behind the SCV technique is to capture two images of a flow field within a short interval of time. The velocities of the

particles/features are then calculated by cross-correlating these two images. The use of this approach to determine the velocities of structures on the surface of the liquid jet was investigated. SCV is very similar in approach to Particle Image Velocimetry (PIV) [78]. In this study, a LaVision PIV system was utilized to capture the images of the liquid column illuminated by employing the LJLGT and the Flowmaster software was used to determine the correlation velocities. The velocities thus obtained were assumed to be equal to the velocities of liquid mass on the surface of the column. Figure 2-15 shows an example of the velocity vectors on the surface of the liquid column calculated using this method. Ideally, cross-correlation algorithms require bright spots in a dark background. The accuracy of velocity obtained by this method is usually estimated with peak ratio, which is the ratio between the largest and second largest cross correlation coefficients. Generally, measurements with high peak ratios (~10) are considered very accurate. However, the current measurements track naturally formed structures on the liquid jet with no dark background and the peak ratios obtained were not very high. Thus, caution was exercised by setting other stringent requirements for determining the validity of the measured velocity vectors. The minimum peak ratio for a velocity vector to be considered valid was set to 4. Only locations that provided valid velocity vectors in more than one third of all the image pairs acquired (typically 50 out of 150 pairs) were retained. Additionally, the velocities obtained were validated by tracking the flow features by visual inspection. In this method, two images of the jet were taken with a time interval of 10 microseconds between them. An example of the images obtained for this purpose is shown in Figure 2-16. The large number of structures seen in the first image can also be seen in the second image and are a bit displaced. With the knowledge of this

displacement and the time lag between the two images, the velocities of the structures were obtained. The mean velocities obtained using cross-correlation algorithms in PIV were well within 5% of the velocities measured employing PTV.

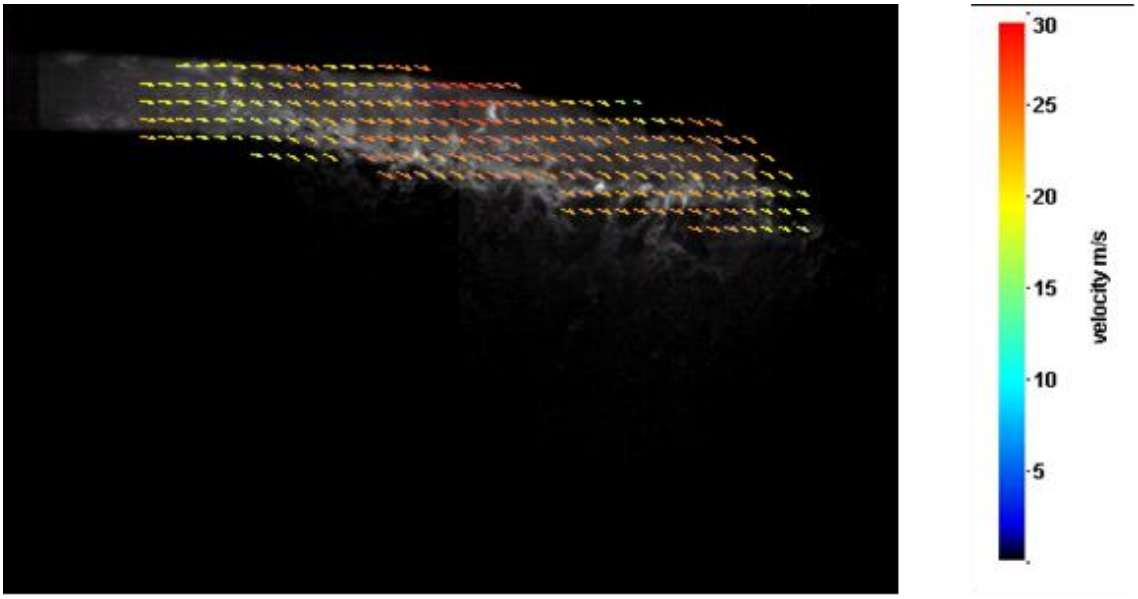

Figure 2-15. Velocity vectors obtained using two images with a time gap of 1 microsecond at *We*=180 and *q*=20

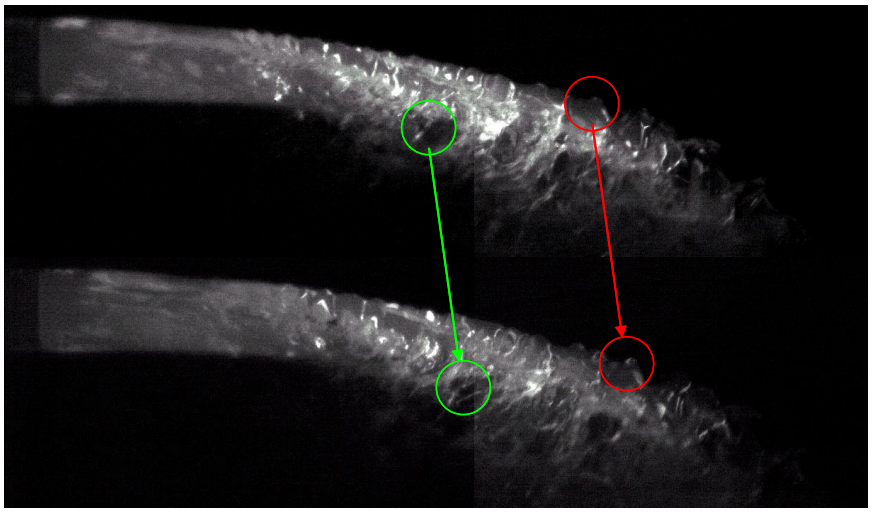

Figure 2-16. Two images of the liquid jet obtained with a time interval of 10 microseconds between them. The structures on the jet were tracked manually and the velocities were calculated to validate the velocities obtained using cross correlation algorithms

2.2.5 Spray Imaging

Figure 2-17 shows the schematic of the facility used for imaging the spray using back illumination. A Metalaser Technology MTS-20 pulsed Copper Vapor laser with pulse repetition rate of 6 kHz and pulse duration of 30ns was used to illuminate a mirror that reflected the light in the direction of the camera. A CCD camera with resolution 1600 X 1200 was used at frame rate of 10Hz. The exposure time of the camera was set to 160 microseconds so that every image was captured within one pulse of the illuminating laser light (time between 2 laser pulses was 166 microseconds), essentially freezing the flow. Generally, spray images were captured at two levels of magnification, macro-imaging and micro-imaging. Macro-imaging covered the entire area of the test section that was optically accessible (i.e., 30mm X 20mm) and micro-imaging usually covered an area of 2mm X 3mm close to the orifice for studying the droplet formation mechanisms. A QUESTAR QM1 photo-visual long distance microscope capable of focusing in a plane 3 μm in thickness was used for this purpose.

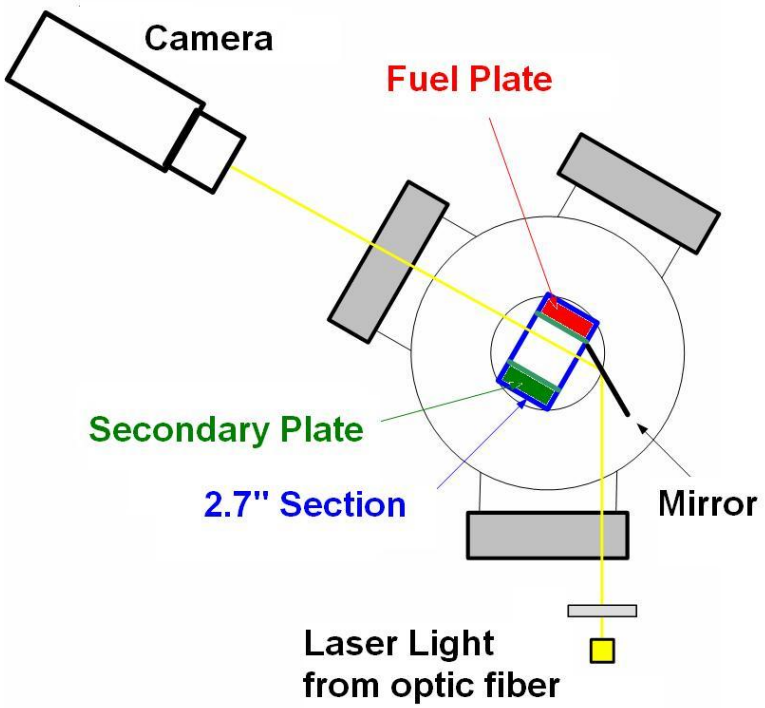

Figure 2-17. A schematic of the Spray Imaging Apparatus to obtain spray images with the back illumination technique

2.2.6 Spray Penetration Trajectories

Figure 2-18 shows the methodology for obtaining the spray penetration trajectory from spray images. The raw images (as seen in Figure 2-18(a)) are first corrected for background noise by subtracting the background image (see Figure 2-18(b)). Figure 2-18(c) shows a typical spray image with the background subtracted. This image is converted into a binary image using a threshold as seen in Figure 2-18(d). In the current study, the value of threshold used was 90% of the peak light intensity.

An observation of the instantaneous images of the spray revealed that the jet penetration trajectory is a time dependent phenomenon. Thus, one trajectory equation cannot describe the spray penetration adequately. In this study, a probability of finding

droplets at a given spatial location was used to describe the spray penetration. In the binary images, the presence of droplets at a given location was denoted by a value of one and the absence of droplets as zero. Over 20,000 such binary images were added up and normalized to obtain the spatial probability of finding droplets at a given location as shown in Figure 2-20. Trajectories that represent the maximum, median and minimum penetrations of the liquid jet were obtained. The outermost edge of the spray represents the line beyond which there were no droplets seen in any of the spray images. On the other hand, the innermost edge of the spray is the line before which droplets were seen in all the spray images. The median penetration was defined as the line beyond which droplets are found in half the number of images.

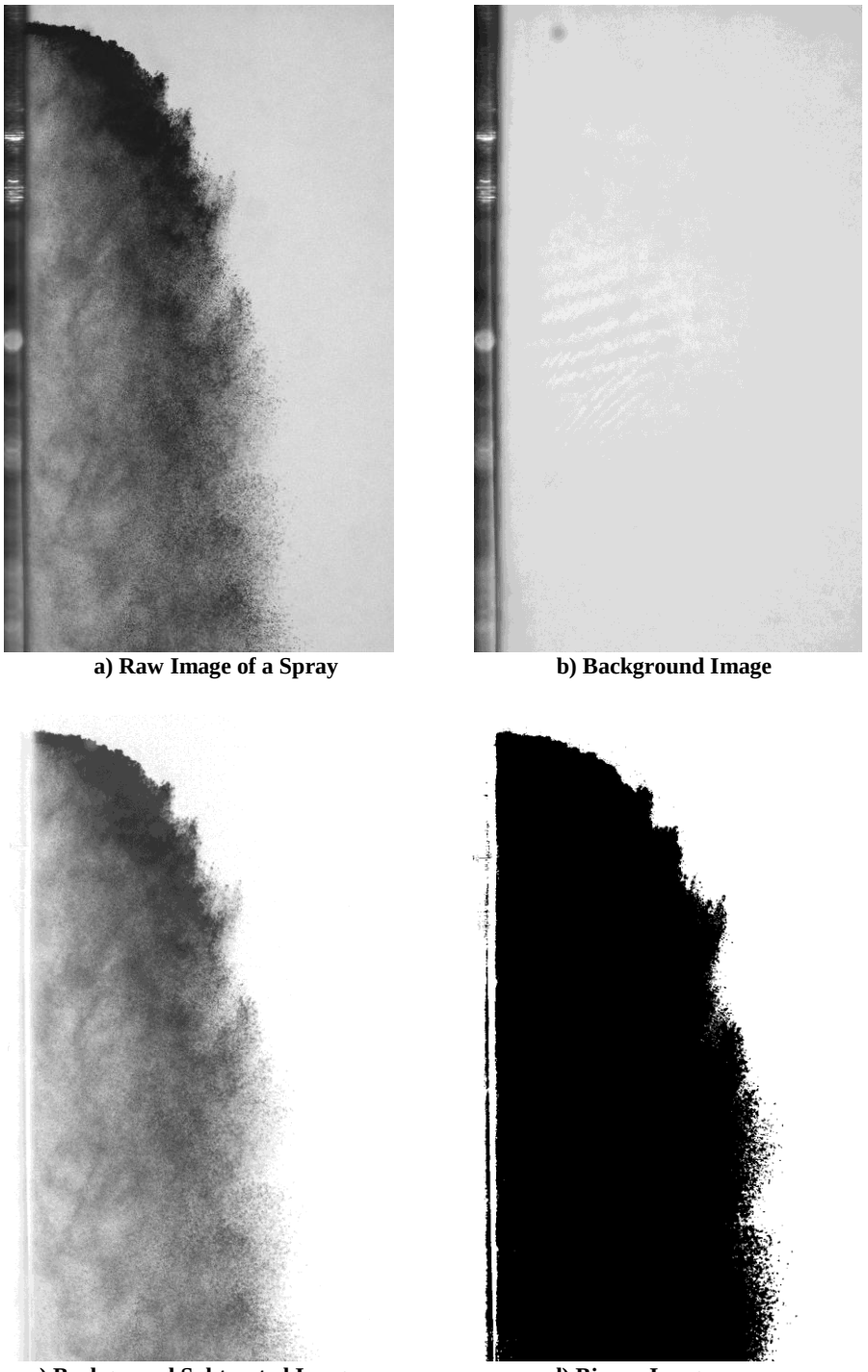

a) Raw Image of a Spray **b) Background Image**

c) Background Subtracted Image **d) Binary Image**

Figure 2-18. Methodology used to process the raw images obtained.

The PDPA technique is very sensitive to the presence of droplets and is capable of detecting droplets in sparsely populated regions of the spray. It was used to measure the

droplet density at three downstream locations (15, 30 and 60 orifice diameters downstream) along the X-direction on the centerline of the spray. The data rate (i.e., the number of droplets detected per second) measured with the PDPA was used as a metric to locate the edge of the spray. The edge of the spray was assumed to be around a region with 10-50% (see Figure 2-19) of the maximum data rate (the maximum data rate was about 50,000 droplets per second). Figure 2-20 shows the innermost edge, the outermost edge and the mean edge plotted along with the spray boundary obtained using the PDPA data that correspond to 10%, 30% and 50% of the data rate. It is seen that the outermost trajectories matched reasonably well with the PDPA data, showing that spray imaging can capture the highest penetration of the spray when this method was employed for obtaining the spray trajectories.

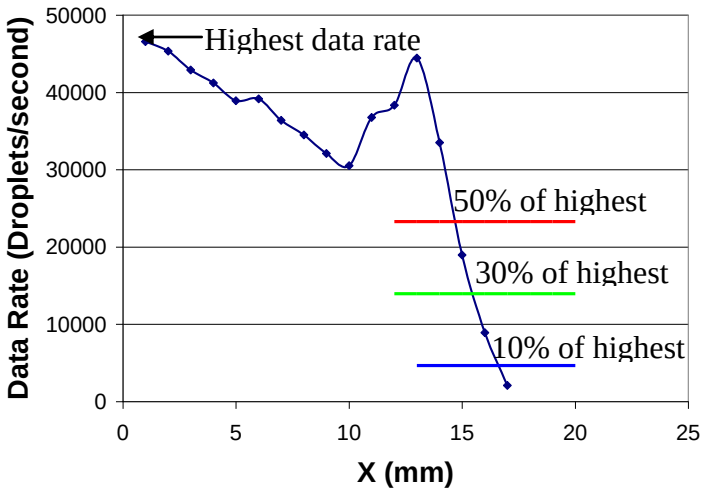

Figure 2-19. The data rate (number of droplets detected per second) along the centerline of the spray at a particular Z/d location. 10% of the highest value of the data rate can be used as a metric to mark the edge of the spray

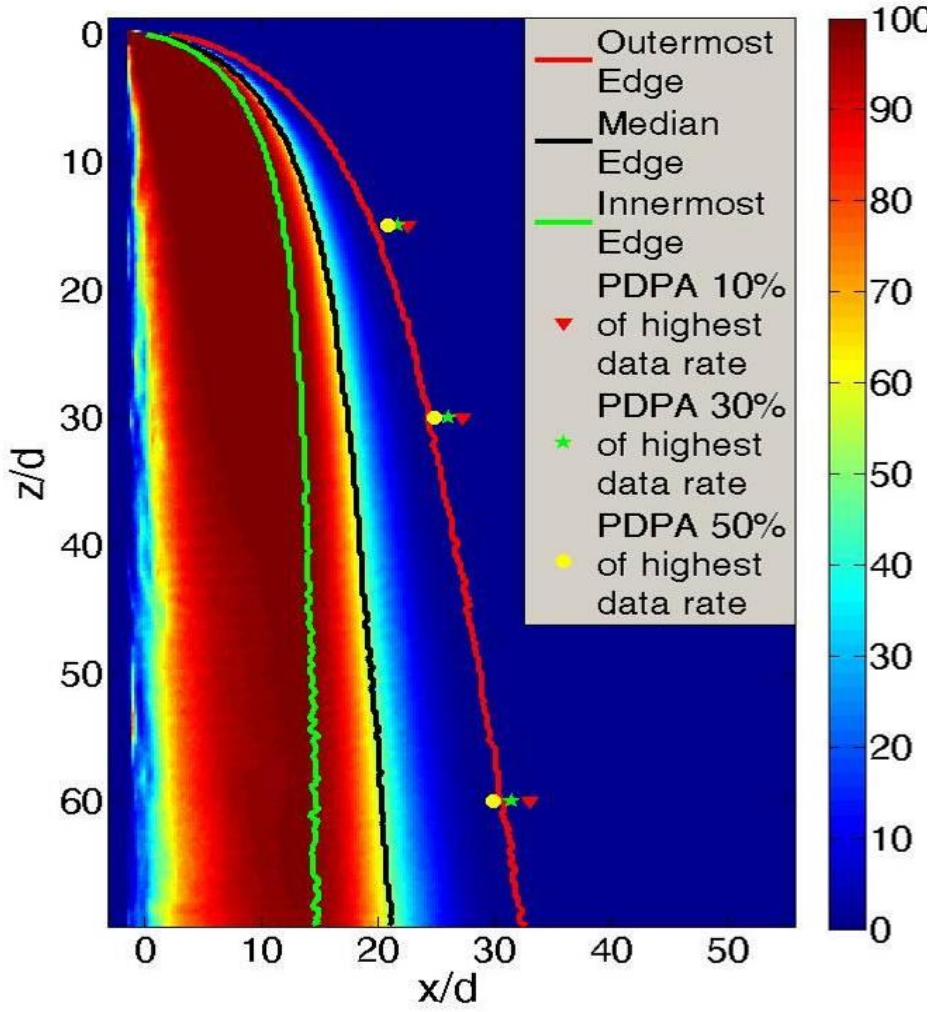

Figure 2-20. Spatial probability distribution of finding droplets in the field of view at *We*=1000 and *q*=20

CHAPTER III

PRIMARY BREAKUP PROCESSES

This chapter describes the experimental investigation of the primary breakup region of the spray. The LJLGT described in section 2.2.3 was employed to locate the column breakup point and is covered in section 3.1. Section 3.2 describes the structure of the liquid column. It includes the description of the velocity field on the surface of the liquid column, which was measured by integrating the LJLGT with PIV. Finally, the phenomenon of jet splitting into two or more jets is reported in section 3.3. The possible mechanisms for this phenomenon are discussed as well.

3.1 Primary Breakup Time Scale

This section discusses the measurements of primary breakup time obtained by locating the CBP using the LJLGT. With an assumption that the velocity of the liquid jet does not change in the direction of liquid injection, the primary breakup time, t_b is defined to be equal to X_b/u_l. First, the results obtained by varying the operating conditions (*We*, *q* and by the use of a different liquids) are presented. Then, the parameters that can have an influence on the location of the CBP are discussed. Finally, the expression for the primary breakup time is provided.

The location of the CBP was measured for various operating conditions. First, the *We* of the flow was varied by changing the velocity of the air. The momentum ratio was

maintained constant (at 20) by varying the liquid mass flow rate. Two liquids, Jet A and water, with significantly different surface tension were used to get a wide range of *We*. The mean coordinates of the CBP are plotted in Figure 3-1. It was observed that the CBP was located at a distance of about 5-7 orifice diameters away from the injector plate in the shear breakup regime (We > 200). In the column breakup regime (We < 200), the value of X_b/d was between 7 and 10. As the *We* increased, the CBP moved closer to the orifice plate. Z_b/d was between 1.5 and 2.5 in the shear breakup regime and between 2.5 and 4.5 in the column breakup regime. The variance of the measured locations of X_b/d was less than 10% of the mean value and the variance of the mean locations of Z_b/d was less than 5%. Again, this distance decreased as the *We* increased. However, this distance was much smaller compared to the previously reported studies by Wu *et al*. [6] and Sallam *et al*. [12] who have reported a Z_b/d value of 8. This discrepancy can be attributed to the different measuring technique. Locating the CBP using shadowgraph images involved some form of human judgment and is likely to have resulted in a bias. Moreover, past studies could not locate the CBP in the shear breakup regime and extrapolated the results from the column breakup regime. The use of LJLGT eliminates the need for human judgment and provides an accurate measurement of the CBP. Computational models use correlations for the time required to attain the primary breakup. This primary breakup time was assumed to be a multiple of the characteristic time t* as defined in Equation 1-4. For example, Madabushi [37] used a t_b/t^* value of 3.44 for computing the spray characteristics as found by experiments carried out by Wu *et al*. [6] The measured values of this parameter using the LGLGT are plotted in Figure 3-2. It shows that this parameter is not a constant and that it decreases with an increase in

We. It is also seen that the value for this parameter is lower than the previously reported values of 3.44 and 2.5.

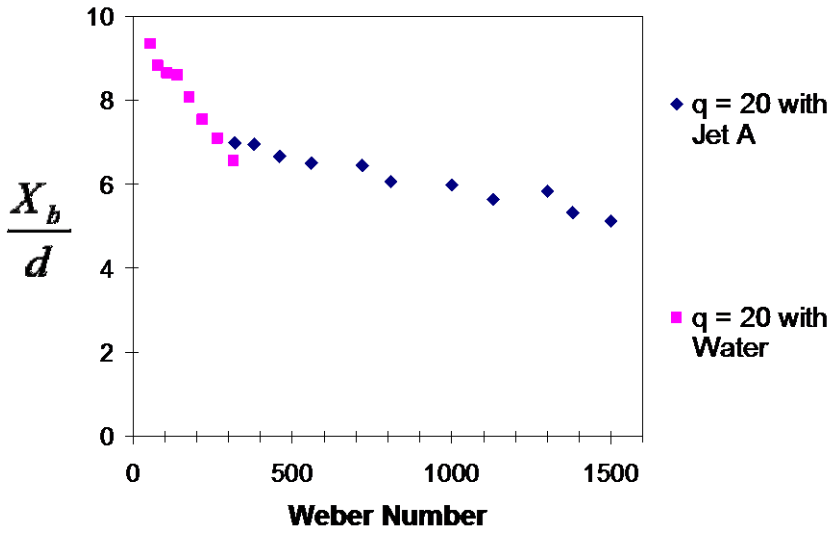

a)

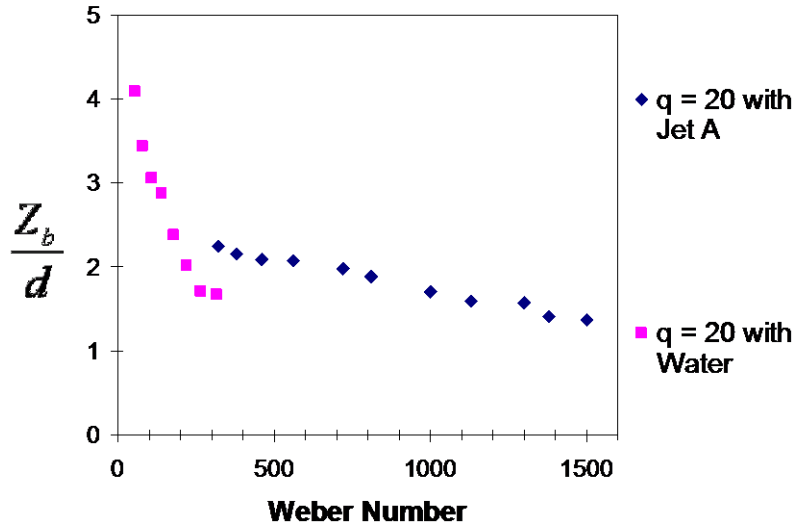

b)

Figure 3-1. The coordinates of the mean location of the column breakup point as different values of We. The q was maintained at a constant value of 20. a) X coordinate (in the direction of liquid injection and b) Z coordinate (in the direction of airflow)

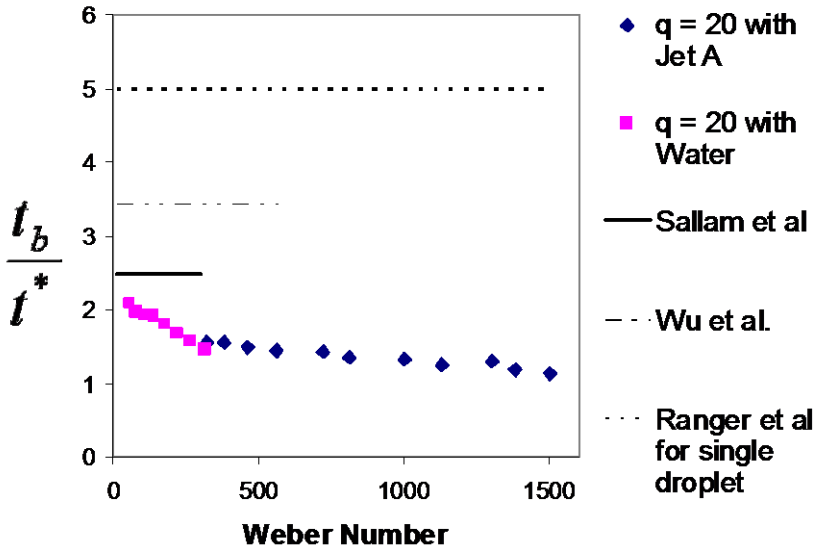

Figure 3-2. Primary breakup time scale (t_b/t^*) variation with Weber number at q=20

Next, the jet exit velocity of the liquid jet was varied keeping the air velocity constant. The CBP locations were measured at operating conditions corresponding to three different values of *We* (1000, 265 and 143). Figure 3-3 shows the coordinates of the CBP at different values of *q*. Comparing the operating conditions with the breakup regime shown in Figure 1-2, it is seen that in the column breakup regime, the value of X_b/d increases with increase in *q*, roughly following the correlation by Wu *et al*. [6], but saturates when it enters the shear breakup regime. In the shear breakup regime, the results obtained for different values of *We* do not vary significantly from each other as observed previously. The highest value of Z_b/d recorded in this set of measurements is about 5 at We=143 and *q*=2.5. t_b/t^*, plotted in Figure 3-4 reveals that this parameter was highly dependent on *q*, which, in turn, depends on the velocity of the liquid jet.

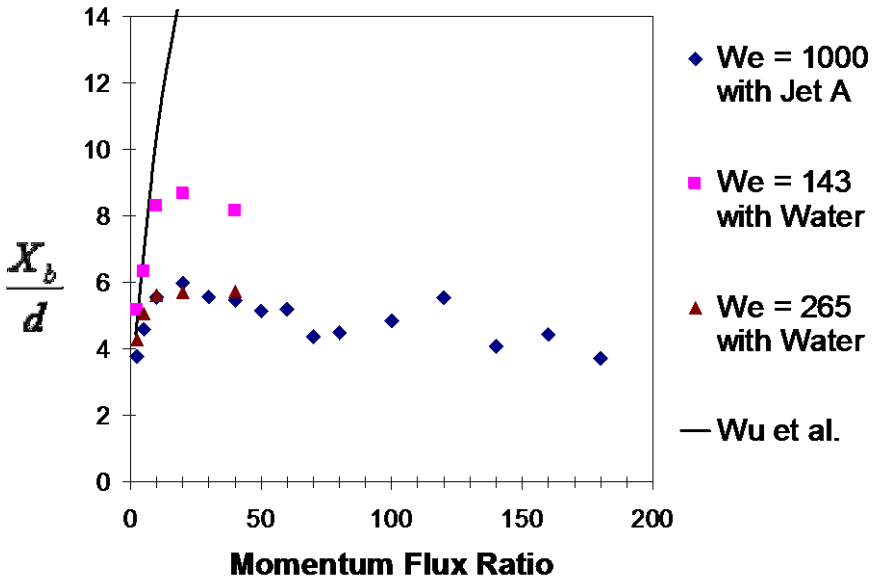

a)

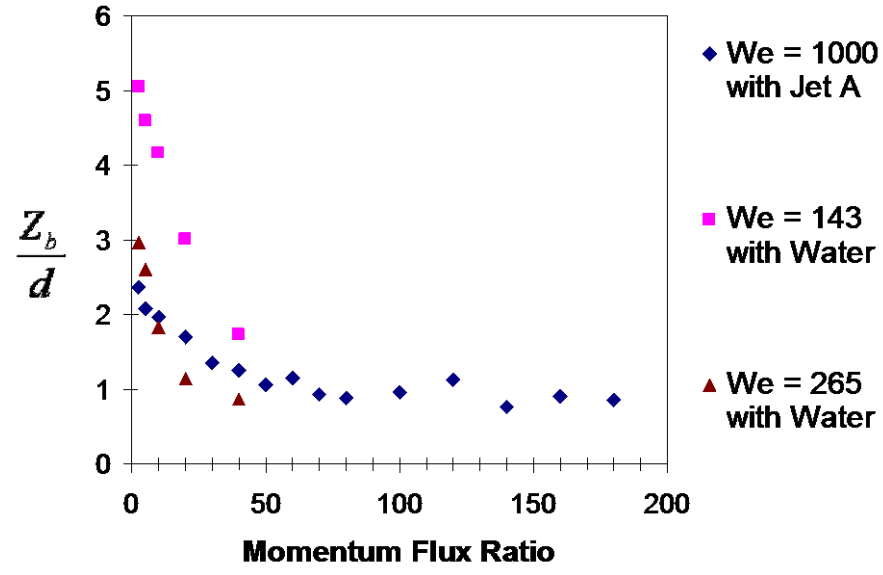

b)

Figure 3-3. The coordinates of the mean location of the column breakup point as different values of *q*. The *We* was maintained at a constant value of 1000. a) X coordinate (in the direction of liquid injection and b) Z coordinate (in the direction of airflow)

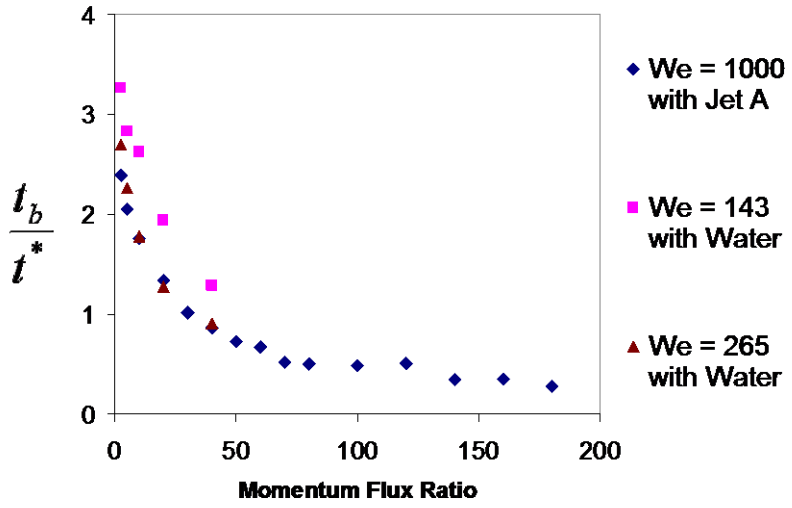

Figure 3-4. Primary breakup time scale (t_b/t^*) variation with momentum ratio

To summarize the observations, the primary breakup location depends on the operating conditions. Neither the Z_b/d nor the t_b/t^* value is a constant as has been reported in the past. The momentum ratio, in particular has a significant effect on the location of the CBP. It was also seen that the behavior of the primary breakup properties was different for the column breakup and the shear breakup regimes. The measured values of X_b/d, Z_b/d and t_b/t^* with the LJLGT were also smaller in value compared to past studies. The next step in this study is to identify the parameter that is most relevant to describe the primary breakup time.

The literature review in Sections 1.2.1 and 1.2.5 showed that the two main mechanisms involved in the primary breakup are the aerodynamic breakup, driven by the interaction between the liquid column and the crossflow and the turbulent breakup, driven by the liquid jet turbulence. A vast majority of the studies in the past on liquid jet in crossflow were carried out with non-turbulent liquid jets and the latter mechanism has received little attention. An increase in *We*, velocity of the liquid jet and the turbulence

level of the air enhance the primary breakup of the liquid jet by the aerodynamic mechanism. *We,* affects the location of the CBP by two mechanisms. An increase in *We* increases the aerodynamic force and/or decreases the surface tension force, both of which result in faster breakup of the liquid column. Increase in *We* also increases the role played by the shear breakup mechanism in the atomization process, leading to more droplets being stripped off from the surface of the liquid jet. This reduces the thickness of the liquid jet and assists in its breakup. Increase in the velocity of the liquid jet increases the shear between the liquid jet and the air and quickens the primary breakup. This effect was seen in Figure 3-4, where the liquid velocity was varied to change the momentum ratio and the breakup time decreased. Investigation of the effect of variations in the turbulence level of the air is beyond the scope of this study. The turbulent breakup is enhanced by increase in Reynolds number of the liquid jet [49,50,54,58], and/or increase in the liquid Weber number (We_l) [79]. The liquid Weber number is the ratio of the inertia of the liquid to the surface tension forces. At higher jet exit velocities, the turbulence of the jet is higher. In this case, turbulent eddies break off of the liquid column if they possess enough kinetic energy to overcome the capillary forces. They also form protruding ligaments which leads to increased friction with the air and eventually results in the disintegration of the liquid jet [59].

The thickness of boundary layer on the orifice plate also has an effect on column breakup. The lower velocity in the wall boundary layer delays the development and growth of disturbances on the surface of the liquid jet leading to longer breakup times. It should also be noted that flows with low q are slow and exhibit lower penetration and, thus, have greater residence time in the boundary layer, which further delays the column

breakup.

This exercise looks for additional parameter that governs the value of t_b/t^*. The primary breakup time was obtained for several values of airflow velocities in the range of 66–140 m/s and liquid jet velocities in the range of 19–40 m/s. The use of two liquids at two different crossflow air temperatures allowed the study of the effect of liquid surface tension and viscosity. These data were plotted against the momentum ratio, the *We*, the liquid Weber number, We_l, the velocity of the liquid jet and the Reynolds number of the liquid jet. They are shown in Figure 3-5 to Figure 3-9. This study showed that the best fit for all the data was obtained when the non-dimensional time for column breakup was plotted as a function of the liquid jet Reynolds number (Re_l) and is shown in Figure 3-9. This correlation is described by Equation 3-1 and has been shown to be valid in the Re_l range of 2,700 – 45,000.

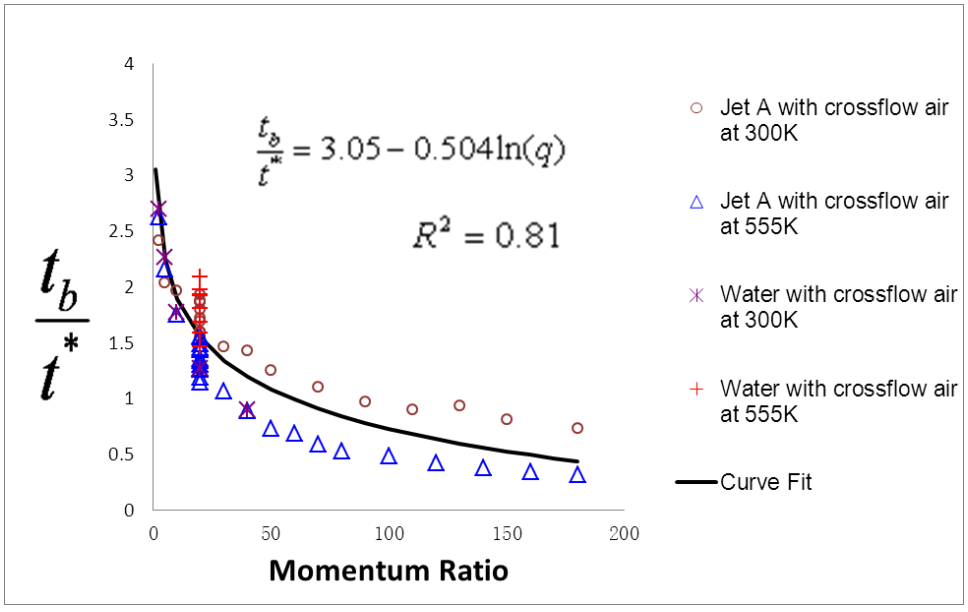

Figure 3-5. Non-dimensional primary breakup time as a function of momentum ratio, *q*

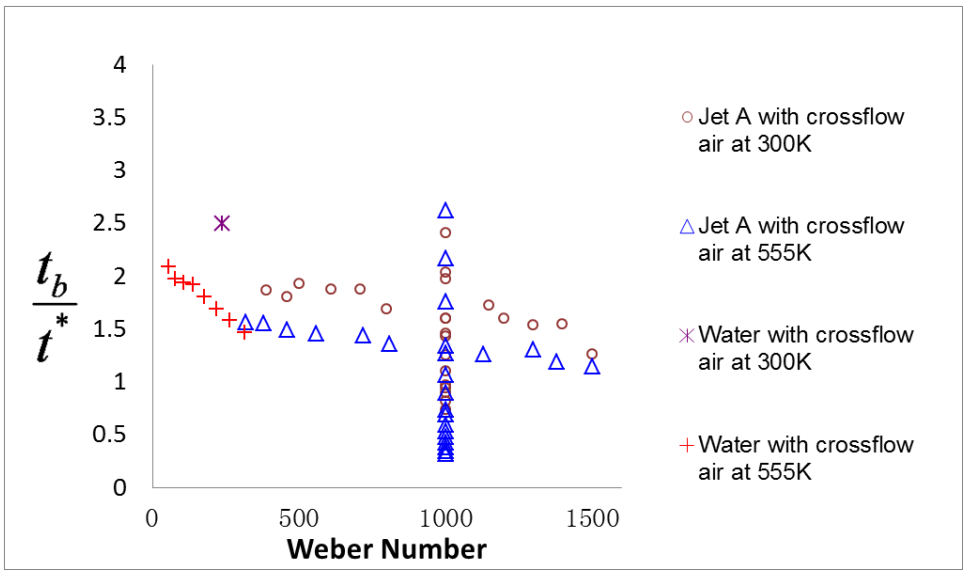

Figure 3-6. Non-dimensional primary breakup time as a function of Weber mnumber, *We*

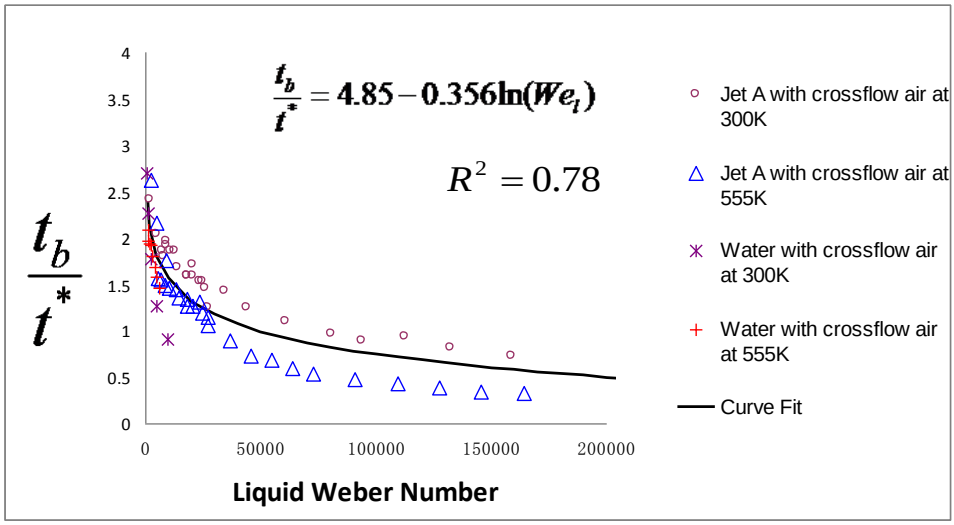

Figure 3-7. Non-dimensional primary breakup time as a function of Liquid Weber number, We_l

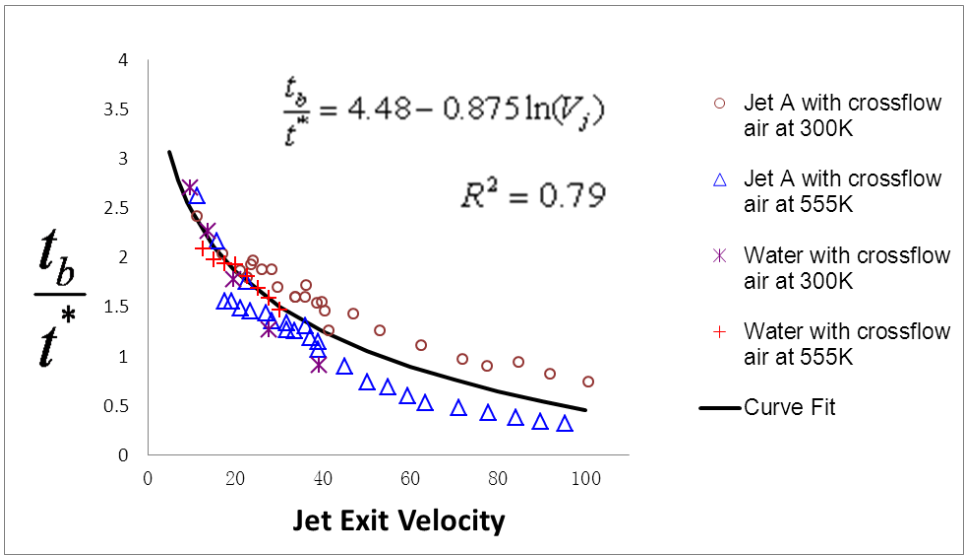

Figure 3-8. Non-dimensional primary breakup time as a function of jet exit velocity

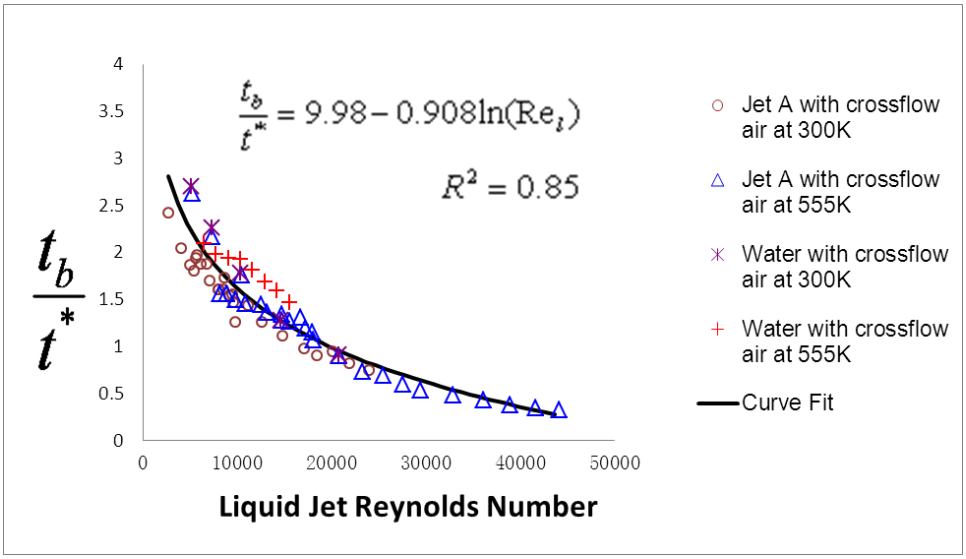

Figure 3-9. Non-dimensional primary breakup time as a function of liquid jet Reynolds number

$$\frac{t_b}{t^*} = 9.98 - 0.908\ln(\mathrm{Re}_l) \qquad \textbf{(Equation 3-1)}$$

This suggests that the primary breakup time scale is not a constant but depends on the liquid jet properties. This study indicates that the liquid jet Reynolds number is the parameter that governs it. The process of the breakup of a droplet in an airflow is

dominated by the effect of aerodynamic forces acting on it and was shown to be proportional to the parameter t* as described earlier [29]. The breakup length of a turbulent liquid jet in quiescent medium was found to be a function of liquid jet Reynolds number by Grant *et al*. [48] and Phinney [49]. Their study showed that the primary breakup time for a turbulent liquid jet in crossflow can be expressed as a function of t* and the liquid jet Reynolds number. This result suggests that the mechanism for the breakup of the liquid jet involves both aerodynamic and turbulent breakup. It is consistent with the works of Wu et al. [59] and Lee et al. [31].

The implications of these findings can be listed as follows

1. They provide validation data for detailed simulations of the liquid jet in crossflow.
2. They provide improved primary breakup time scale for the models and improve their fidelity by expanding the range of operating conditions for these models.
3. It gathered evidence that the mechanism of turbulent breakup is important for a jet in crossflow in addition to the aerodynamic breakup mechanisms of column breakup and shear breakup.

3.2 Structure of the liquid jet column

Figure 3-10 shows a typical image of the liquid column obtained using the LJLGT. It shows that the liquid column is smooth close to the orifice. As it interacts with the surrounding airflow, it becomes granulated/coarse downstream. The boundary layer on the wall with lower air velocities added to the delay of the development and growth of these disturbances. Surface waves are seen on the windward side of the liquid jet. The

shear forces exerted by the air flow outside of the wall boundary layer, which had a thickness of about 5-6 diameters of the orifice, sheared droplets from the surface of the liquid column, flattened the column and eventually resulted in its break up. The process of the peeling off of the outer surface of the liquid jet began at about 3-4 diameters from the orifice and reduced the mass of the liquid column.

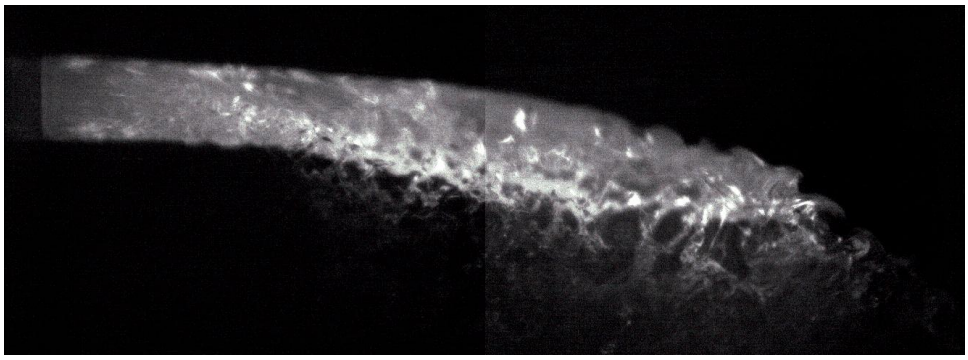

Figure 3-10. A typical image obtained with LJLGT showing spray structures

The velocity field on the surface of the liquid jet was investigated by employing the SCV technique together with the LJLGT to gain a physical insight into the structures formed on the liquid jet. Various regions on the liquid jet surface having different velocities were identified. The measured velocities were compared with the jet exit velocity to assess the accuracy of the assumption of a constant liquid jet velocity in the direction of liquid injection from the orifice exit up to the CBP. For example, consider the velocity measurements at operating conditions of We=177 and q=20. The jet exit velocity for this case was 22.6 m/s as calculated from volumetric flow rate measurements and the geometric area of the orifice. At this operating condition, the velocity vectors of the flow field were obtained using the LJLGT and SCV. The averaged velocities in the X and Z directions are shown in Figure 3-11(a) and Figure 3-11(b), respectively. The velocity vectors represent the direction and magnitude of the total velocity and the color-

map describes the magnitudes of the velocities of the liquid jet surface in the X and Z directions. It was observed that the average velocity in the direction of liquid injection (V_x) on the surface of the liquid jet was smaller than the jet exit velocity of 22.6 m/s. This indicates the presence of a velocity profile on the liquid jet issuing out of the orifice with lower velocities on the outer surface and higher velocities in the core of the jet. However, the region close to the orifice had a very smooth surface and the absence of structures prevented the measurement of the velocities there. The highest measured velocity was found at the center of the liquid jet at about 2-3 mm from the orifice. A close observation of images of the liquid jet column (see Figure 3-10) revealed that droplets were being sheared off from the surface of the liquid jet, thus exposing the core of the jet. This again shows the presence of a non-uniform velocity profile within the liquid jet. Another observation was that the velocities of the ligaments and droplets just downstream of the jet were significantly lower (i.e., ~17m/s) compared to the jet exit velocity. This region contained ligaments and droplets that were stripped from the liquid column and decelerated rapidly in the X direction. Quantitatively, the surface velocities of the liquid jet were found to lie between 80 – 90% of the jet exit velocity. Since hydrodynamic instabilities develop on the surface of the liquid jet, correcting the velocity by 15% is recommended for the computation of the wavelengths of the instabilities. However, after this correction is made, it is likely that the assumption of constant jet velocity up to the CBP is a reasonable one. Analysis of the contour map of the velocities in the direction of airflow (Figure 3-11 (b)), it is seen that there was a rapid increase of velocity in the Z direction (V_z). The velocities vary from 4 m/s on the windward side of the jet to about 12 m/s at Z/d location of 1.

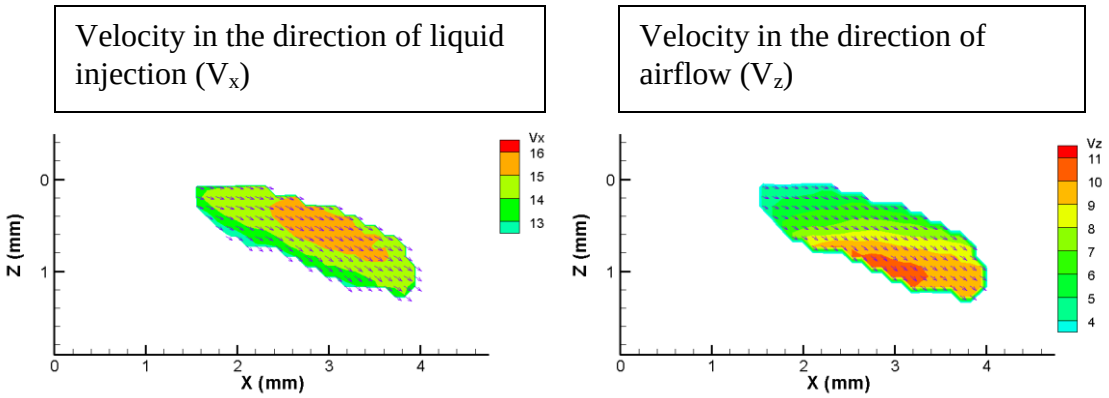

a) *We*=105, Jet exit velocity=17.6 m/s, Crossflow velocity=70 m/s

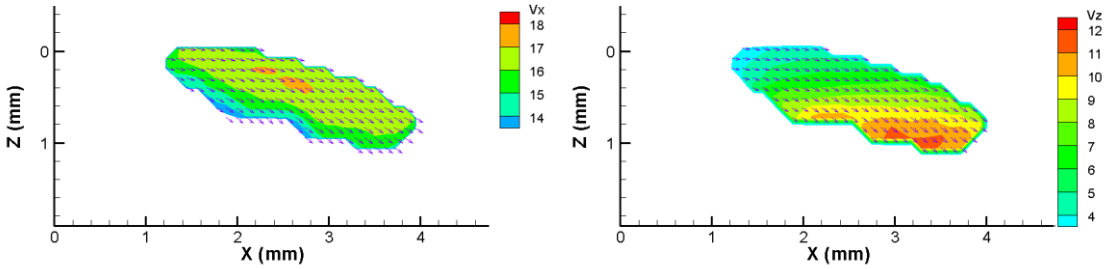

b) *We*=140, Jet exit velocity=20.1 m/s, Crossflow velocity=70 m/s

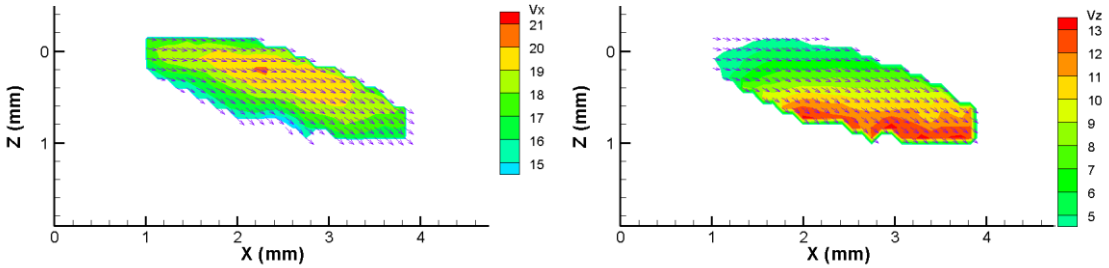

c) *We*=177, Jet exit velocity=22.6 m/s, Crossflow velocity=90 m/s

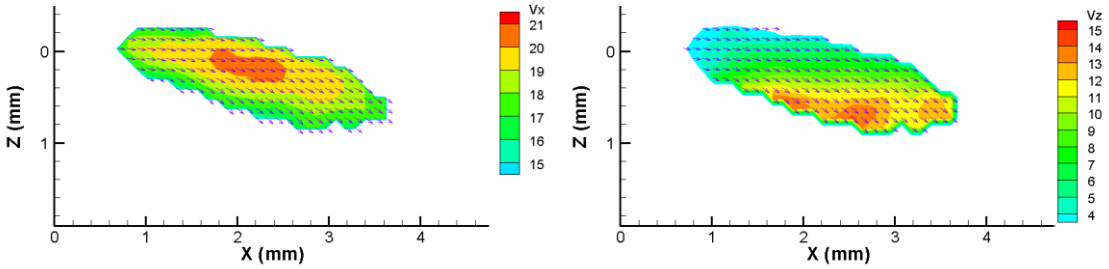

d) *We*=219, Jet exit velocity=25.1 m/s, Crossflow velocity=100 m/s

Figure 3-11. Velocity field on the surface of the intact liquid jet at different operating conditions. The momentum ratio was maintained constant at 20 for different *We*

3.3 The Phenomenon of Jet Splitting

A large number of images of the liquid column obtained using the LJLGT exhibited a phenomenon of jet splitting like the ones shown in Figure 3-12. It is seen that the liquid jet column flattens very close to the orifice and a few diameters downstream splits into two or more streams.

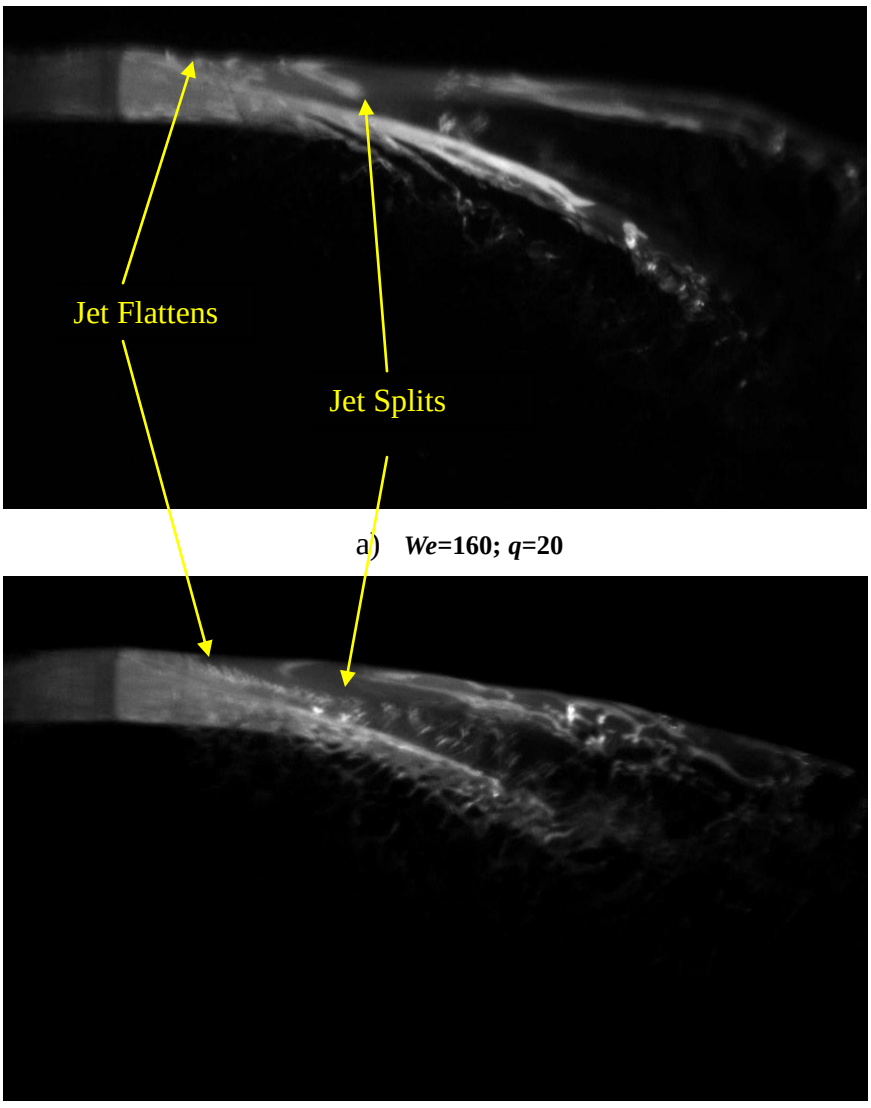

a) ***We*=160; *q*=20**

b) *We*=700; *q*=20

Figure 3-12. Images of liquid jet column exhibiting jet-splitting

The LJLGT enabled the detection of this phenomenon. It is very difficult to spot this phenomenon by analyzing the spray images obtained employing the back illumination technique because of the presence of large number of droplets around the liquid column. Figure 3-13 shows an image of the spray taken at *We*=1500 and *q*=40. A close observation of the image near the orifice reveals the presence of two separated jets. It can be seen that these jets follow different trajectories creating two regions of mass concentration.

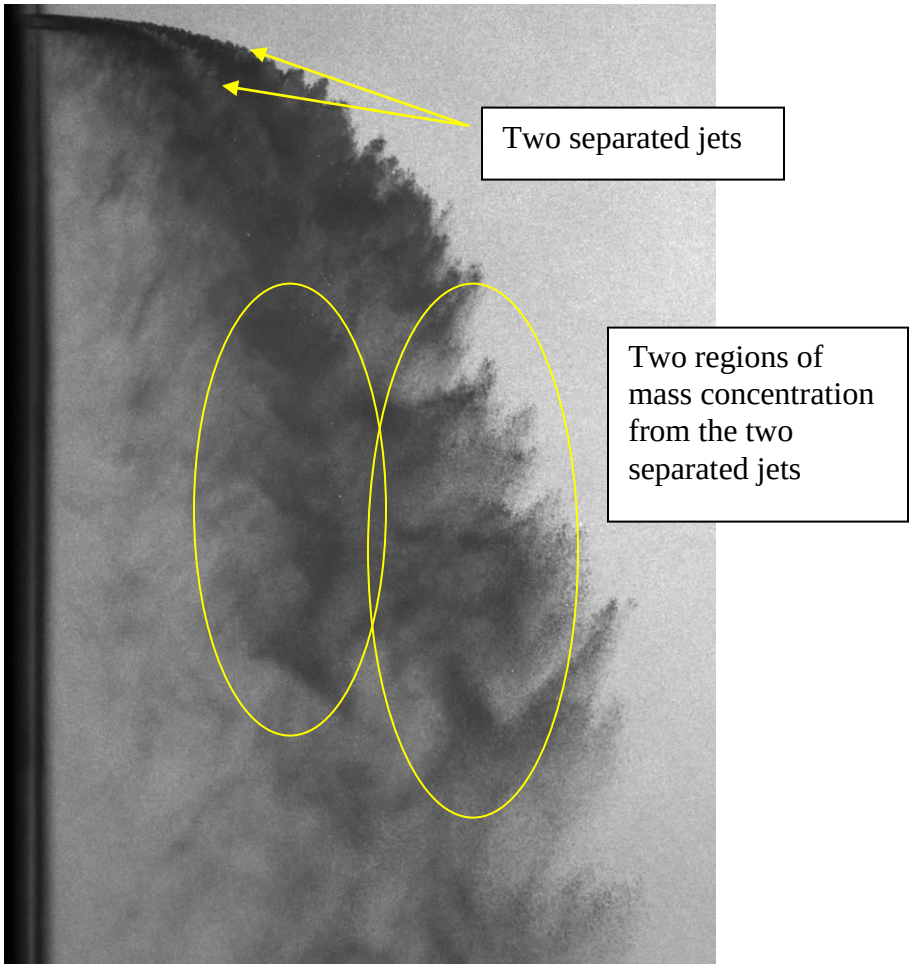

Figure 3-13 Macro-image of a spray showing jet splitting. This spray was created using the round edged orifice at *We*=1500 and *q*=40

It is interesting to note that while jet splitting was observed in experiments with Jet A, images captured in studies with water did not reveal any jet splitting in spite of using the same injector and running the experiment at similar operating conditions. This may suggest a connection between the phenomenon of jet splitting and fluid properties, such as surface tension and viscosity. Jet splitting was observed in about half the images captured at $We<1000$. As the *We* was increased beyond 1000, the occurrence or detection of a split jet became rare. The jet splitting phenomenon was seen only with the round edged orifice. Figure 3-14 shows sample images of the liquid column at different values of *We* for the two injectors.

Salewski and Fuchs [80] carried out a Large Eddy Simulation (LES) of a jet in crossflow. They simulated the liquid column as a series of droplets issuing out the orifice. Their results show the presence of a counter rotating vortex pair (CVP), a commonly observed flow feature in a gaseous jet in gaseous crossflow. This vortex pair created a bifurcation of the mass flux in the downstream of the jet. Figure 3-15 shows the flow features of a gaseous jet in crossflow adopted from Fric and Roshko [81]. The dominant features in this flow are the horseshoe vortices in the wall boundary layer, the shear layer vortices at the upwind boundary of the jet, the wake vortices induced by the flow of crossflowing air around the injected jet and the Counter-rotating Vortex Pair (CVP) in the downstream of the gaseous jet induced by the wake vortices. Sedarsky *et al*. [82] observed the phenomenon of jet splitting in their experiments at low *We* and high values of *q*. They hypothesized that this phenomenon could be because of the CVP.

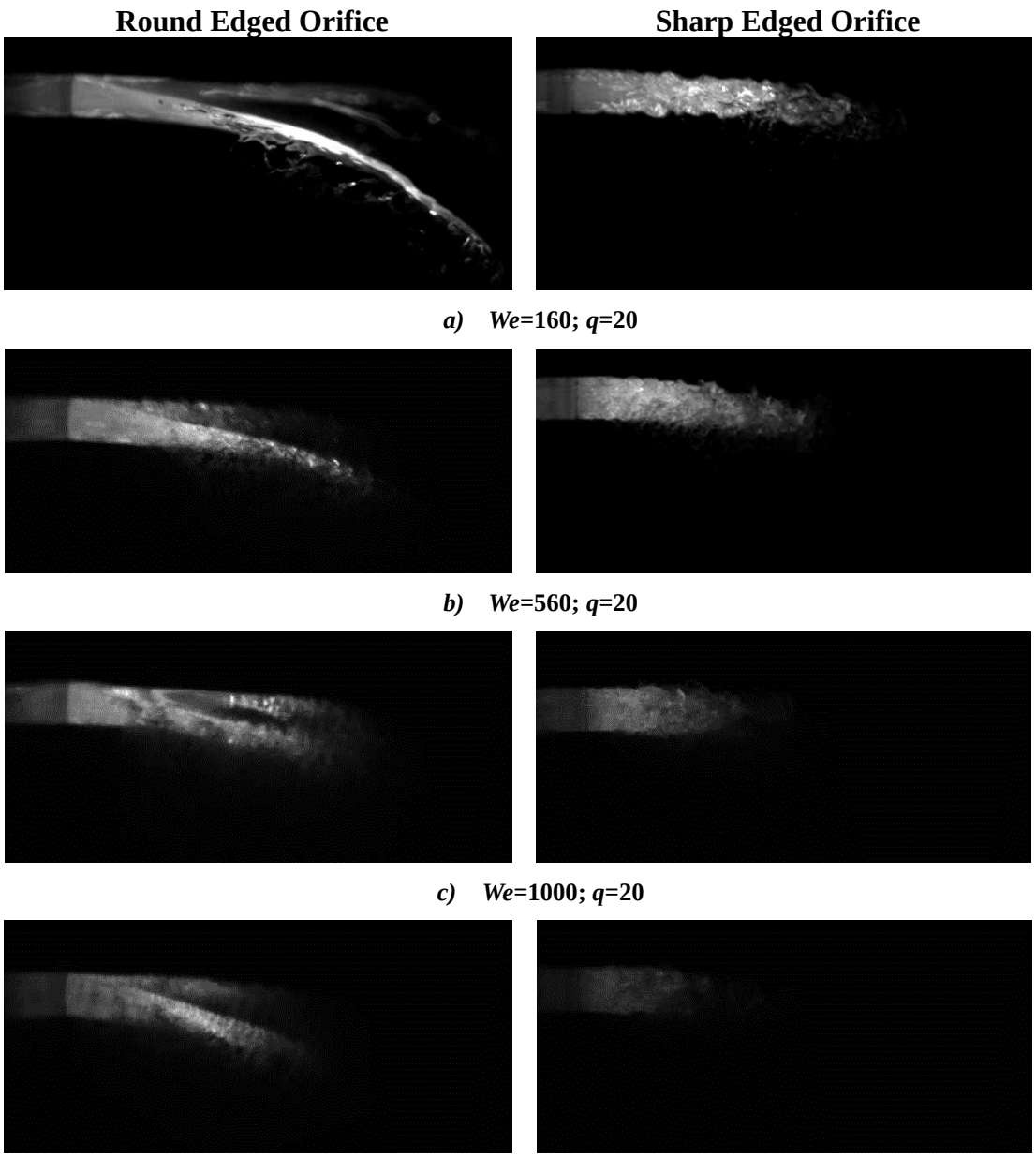

Figure 3-14. Micro-images of the liquid column obtained by employing the LJLGT at different *We* and *q*=20. The round edged orifice exhibits the phenomenon of jet splitting while the sharp edged orifice does not

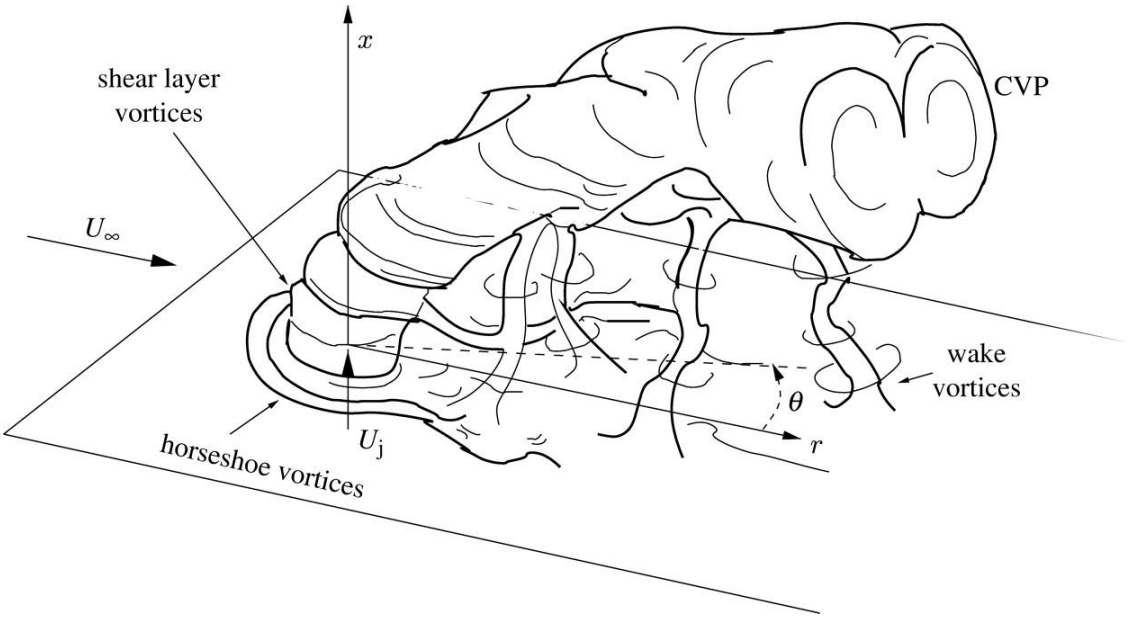

Figure 3-15. Flow features of a gaseous jet in gaseous crossflow adopted from Fric and Roshko [81]

The LJLGT provides a method to clearly visualize the phenomenon of jet splitting. This study stops at providing the experimental evidence of the occurrence of this phenomenon. It did not determine if the presence of CVP was the primary reason for the jet splitting since it was not an objective of this study. The experimental evidence provides motivation for computational studies to investigate the presence of a CVP in the liquid jet and its effects on the structure of the liquid column.

3.4 Summary

This chapter demonstrated the use the LJLGT to accurately measure the primary breakup time scale. Prior to this study, the primary breakup time was believed to be proportional to the ratio of densities between the liquid and the air ($(\rho_l / \rho_a)^{1/2}$), the diameter of the orifice (d), and inversely proportional to the velocity of the airflow (u_a).

The scaling law was arrived at by an experimental investigation of a single droplet in supersonic crossflow and was extended to a liquid jet in crossflow. In the supersonic experiments, the droplets were dropped into the supersonic flow and the parametric study did not include the velocity at which they were dropped. A liquid jet breaking up in a crossflow is different from a droplet breaking in airflow. A droplet in airflow breaks up because of the aerodynamic forces experienced because of its interaction with the surrounding air. The breaking up of a liquid jet in crossflow is caused by two primary factors. One is the effect of aerodynamic forces experienced by the jet because of its interaction with the crossflow and the other is the effect of turbulence of the liquid jet. As described in section 1.2.5, the turbulence of the liquid jet can play a major role in the breakup of a liquid jet in quiescent medium. Studies in the past have accounted for the aerodynamic forces leading to the breakup with the same parameters that affect the breakup of a droplet in airflow. However, the effect of liquid jet turbulence on its breakup was completely ignored and has been partly addressed in this study. The primary breakup time scale was found to be a function of the liquid jet Reynolds number, which relates strongly to the liquid jet turbulence.

Another parameter which can be expected to be of prime importance in governing the breakup of the liquid jet is the surface tension of the liquid, which opposes the aerodynamic force. However, the experimental evidence collected showed a good fit with the liquid jet Reynolds number and not the Weber number of the flow. This study was limited to two liquids at two different temperatures. It cannot be denied that future studies with more number of liquids might find a dependence on the surface tension of the liquid.

The LJLGT also provided a new means of visualizing the liquid jet. This led to

the discovery of the phenomenon of jet splitting. Conventional shadowgraph images were not able to capture this phenomenon. It is hypothesized in this study that the presence of a counter-rotating vortex pair is the reason for the jet to split. The effect of CVPs should be seen several diameters downstream of the liquid jet. However, the possibility of the CVP splitting the jet a few diameters downstream and this disturbance propagating upstream due to the strong aerodynamic forces cannot be ruled out. Since, it is difficult to gather experimental evidence in this small region of two phase flow, future studies of this phenomenon can be expected to rely heavily on computational methods.

CHAPTER IV

EFFECT OF INJECTOR GEOMETRY ON SPRAY FORMATION

4.1 Introduction

This chapter describes the experimental investigation of spray formation processes and spray characteristics such as penetration, location of the CBP, droplet sizes and velocities of sprays created by two injectors having different geometries. As described in Section 2.1.2, one injector was a round edged orifice with an L/D ratio of 1 and a discharge coefficient of 0.95 and the other was a sharp edged orifice with an L/D ratio of 10 and a discharge coefficient of 0.65. Both the injectors had the same diameter of 0.47mm. As described in section 1.2.6, a higher L/D ratio provides longer duration for the flow to develop and attain a higher velocity at the center of the orifice. A smooth transition between the injector plenum and the orifice results in a streamlined flow in the orifice (see Figure 1-11). In contrast, a sharp transition distorts the streamlines and creates a strong component of the radial velocity, which plays a role in the disintegration of the jet issuing out of the orifice. The sharp transition can also lead to flow separation inside the orifice and result in cavitation or hydraulic flip of the flow (see Figure 1-12 and Figure 1-13).

Figure 4-1 shows the discharge coefficient of the injector as a function of the pressure drop across the orifice. It was obtained by measuring the flow rate of the liquid

through the injector, $\dot{m}$, at different pressure drop, ΔP, across the orifice and was calculated as

$$C_D = \frac{\dot{m}}{2\sqrt{2\rho_l \Delta P}} \qquad \textbf{Equation 4-1}$$

The injector characteristics shown was compared to the characteristics of the injectors used by Ahn *et al*. [26] (see Figure 1-15). The discharge coefficient drops to about 0.7 at a pressure drop of about 5 bar across the injector. This indicates a possibility of cavitation in the orifice flow. Figure 4-2 compares the cavitation parameter to the one dimensional cavitation model by Nurick [70]. It shows that the cavitation parameter is below the critical value of 2. However, the critical value for the flow under study could be different. These two graphs show that there is a possibility of cavitation in the orifice internal flow. It should be noted that this indirect evidence of the occurrence of cavitation is suggestive but not conclusive. It could not be confirmed due to the absence of optical access to the internal flow of the orifice.

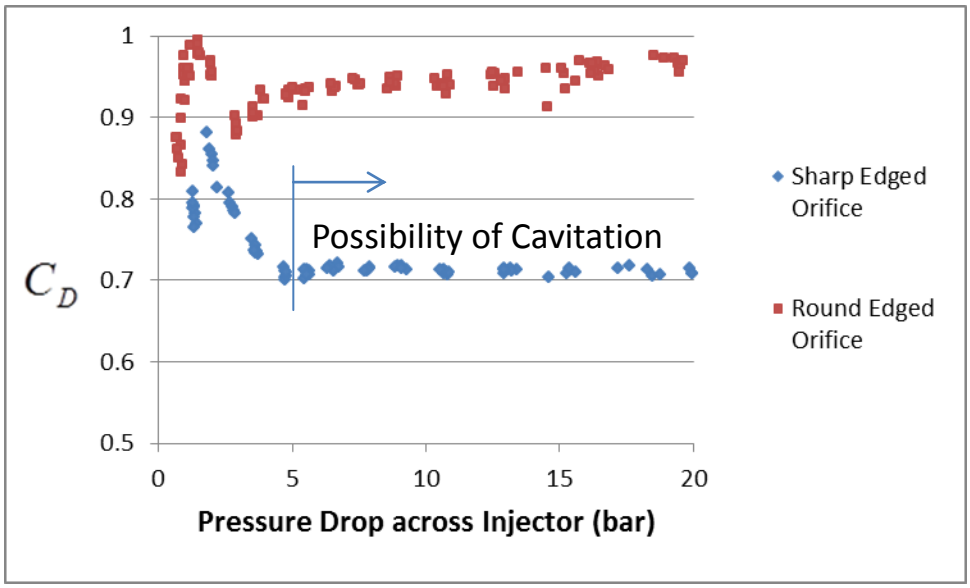

Figure 4-1. Discharge coefficient of the sharp edged and the round edged orifices used in this study

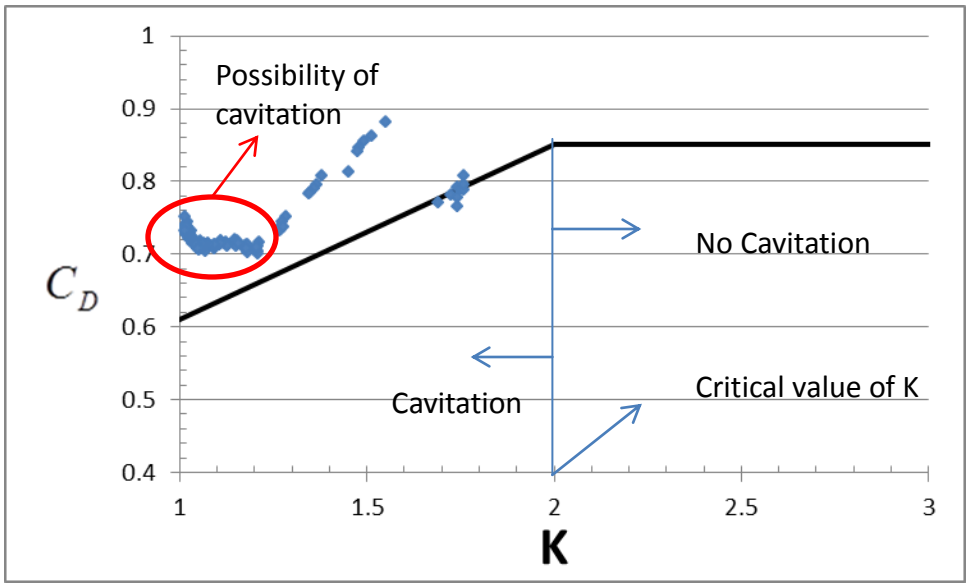

Figure 4-2. Comparison of the characteristics of the sharp edged orifice with Nurick's model [70]

This chapter is divided into several sections, each describing a particular spray property. Section 4.2 covers the investigation of spray images of the liquid jets in the absence of crossflow produced by the two injectors to get some insights on the disintegration of the jets from these injectors due to liquid jet turbulence. This section is followed up by images of the liquid column in crossflow to investigate the structures formed on them. The subsequent sections cover the differences between sprays created by the two injectors with respect to the following spray properties: the location of the CBP, droplet sizes, droplet velocities and spray penetration trajectories. For every spray property measured, the flow rate of the liquid is kept the same unlike the measurements made by Ahn *et al*. [26], who matched the theoretically evaluated jet exit velocities. Finally, the results are summarized and discussed.

4.2 Liquid jet without crossflow

This section presents the images obtained of a liquid jet with no crossflow for the two injectors. Images were obtained for three cases (1-3) in the order of increasing mass flow rate of the liquid (Jet A). These flow rates are representative of the operating conditions of other experiments reported in this thesis, which are tabulated in Table 4-1.

Table 4-1. Operating Conditions for the spray images with no crossflow

Case Number	Mass Flow Rate (g/s)	Jet Exit Velocity (m/s)	Liquid Jet Reynolds Number
1	3	23.3	7033
2	5	38.7	11742
3	7	54.2	16421

Figure 4-3 shows the images of the liquid jet produced by a round edged orifice at the operating conditions listed above. It can be seen that for case 1 (Re_l~7000), the liquid jet does not disintegrate and also has a smooth surface throughout the length of column shown (~110 diameters of the orifice). In case 2, with an increase in Re_l to 11,700, the liquid jet forms structures on its surface that grow in size and distort the column. However, the jet does not disintegrate at these conditions in the field of view. With further increase of the Re_l to 16,000, (i.e., case 3) the jet not only distorts but also disintegrates at a distance of about 60 diameters from the orifice.

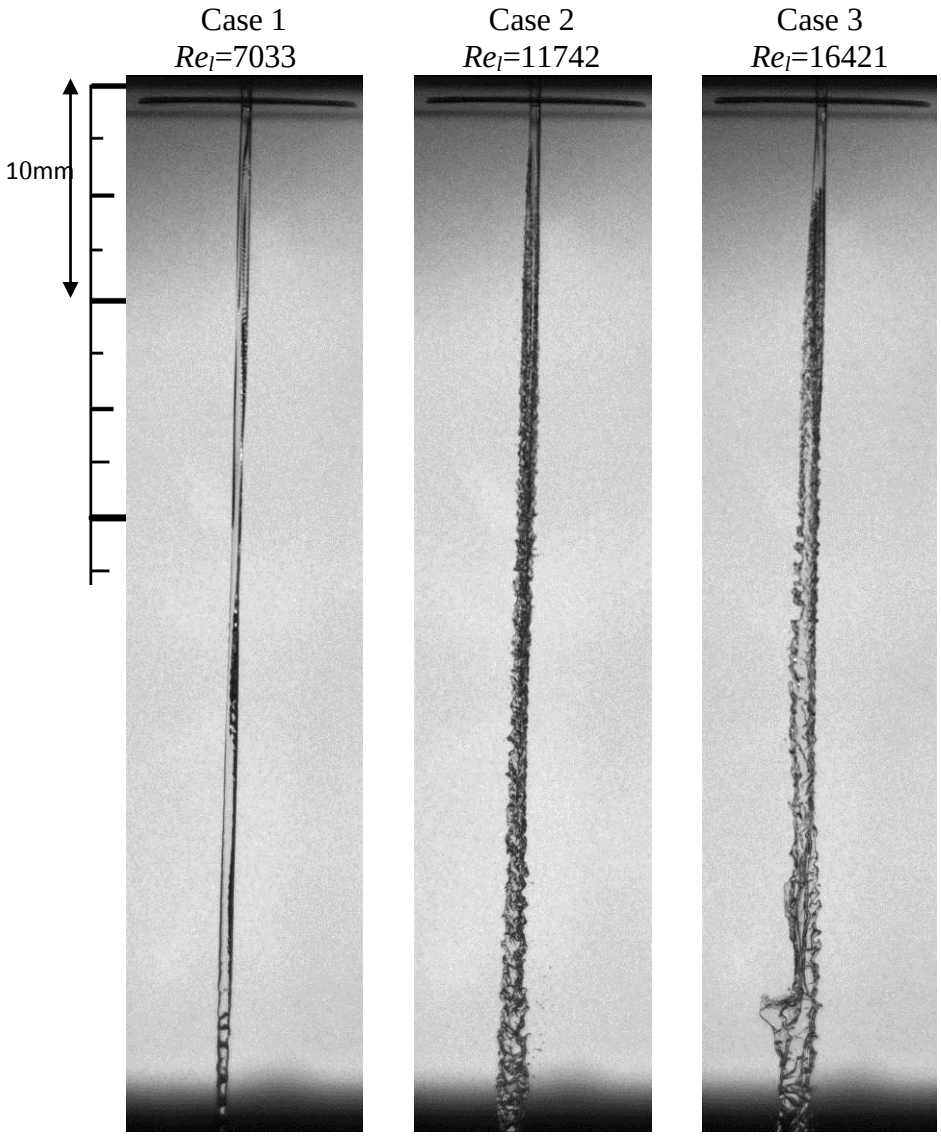

Figure 4-3. Macro-images of the liquid column in the absence of crossflow at various flow rates. These sprays were generated using the Round edged orifice

Images of the jet produced by the sharp edged orifice were acquired at the same operating conditions and are shown in Figure 4-5. In this case, the jet forms irregular structures on its surface within a few jet diameters from the orifice for all three cases. The jet in case 1 appears a highly distorted, although it is not completely disintegrated. The jets in cases 2 and 3 completely disintegrate and form of a large number of ligaments and droplets. The droplets that are formed experience higher drag force compared to larger

liquid elements and decelerate faster. An increase in the mass flow rate (and thus jet exit velocity), results in generation of more droplets.

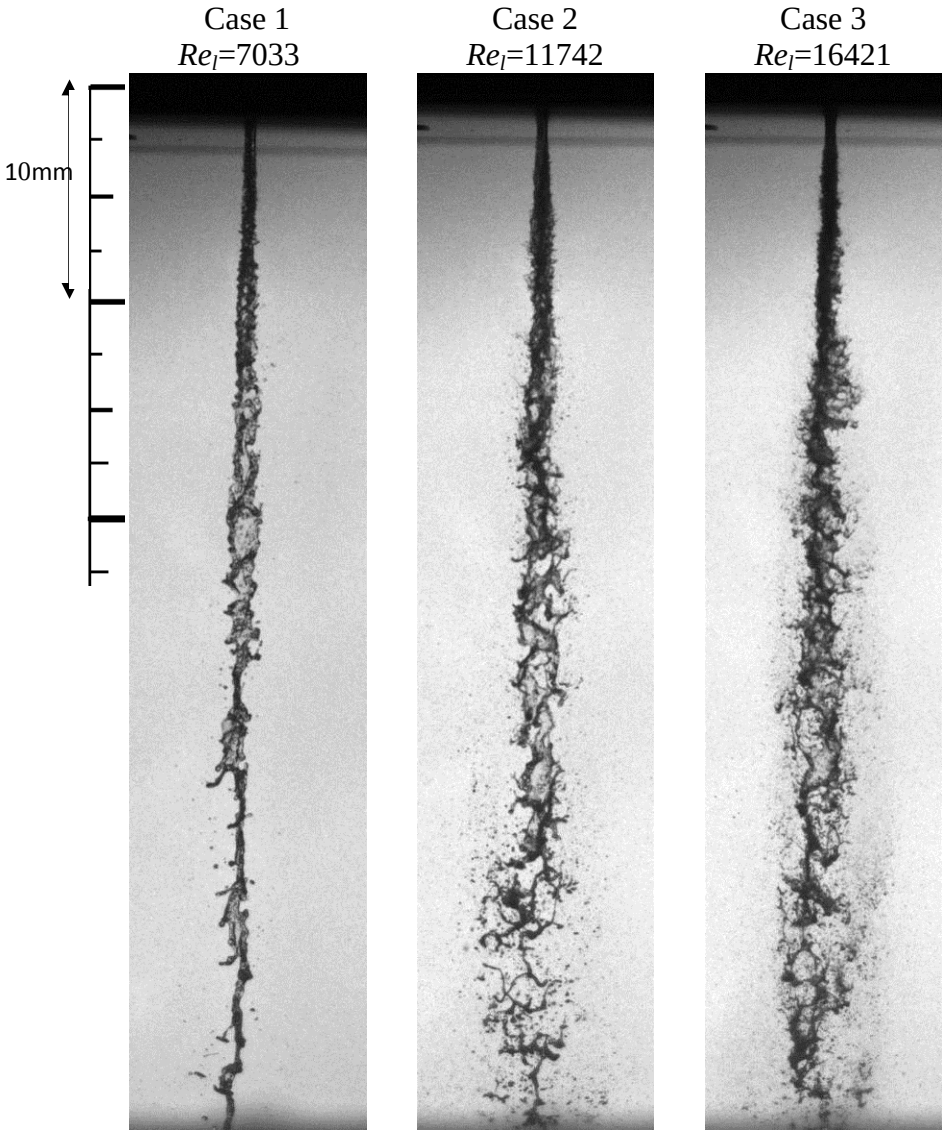

Figure 4-5. Macro-images of the liquid column in the absence of crossflow at various flow rates. These sprays were generated using the Round edged orifice

To observe the flow features of the breakup of the liquid jet, micro-images of the liquid jet were acquired close to the injection orifice and at a distance of about 90 diameters downstream of the orifice for the same operating conditions. Figure 4-6 shows

the micro-images of the jet close to the orifice for the two injectors. It shows that the round edged orifice forms a smooth jet with nearly constant diameter. Surface waves are present on the column. These waves have been linked to the classical Rayleigh-Taylor instabilities in the literature [12]. The sharp edged orifice generates a liquid column with several flow features. The surface becomes rough close to the orifice with several ligaments protruding out of the liquid column. The diameter of the liquid column increases with downstream distance and a dispersed region is formed as described in Section 1.2.5.

Figure 4-7 shows the micro-images of the spray at a distance of 90 diameters downstream of the orifice. It can be seen that the liquid jet generated by the round edged orifice is mostly unperturbed for case 1. However, for case 2, the jet has a larger diameter. For case 3, the jet disintegrates into droplets and large ligaments. On the other hand, the jet from the sharp edged orifice disintegrates completely at this downstream distance. With higher exit velocity of the jet, smaller droplets are formed as a result of this disintegration.

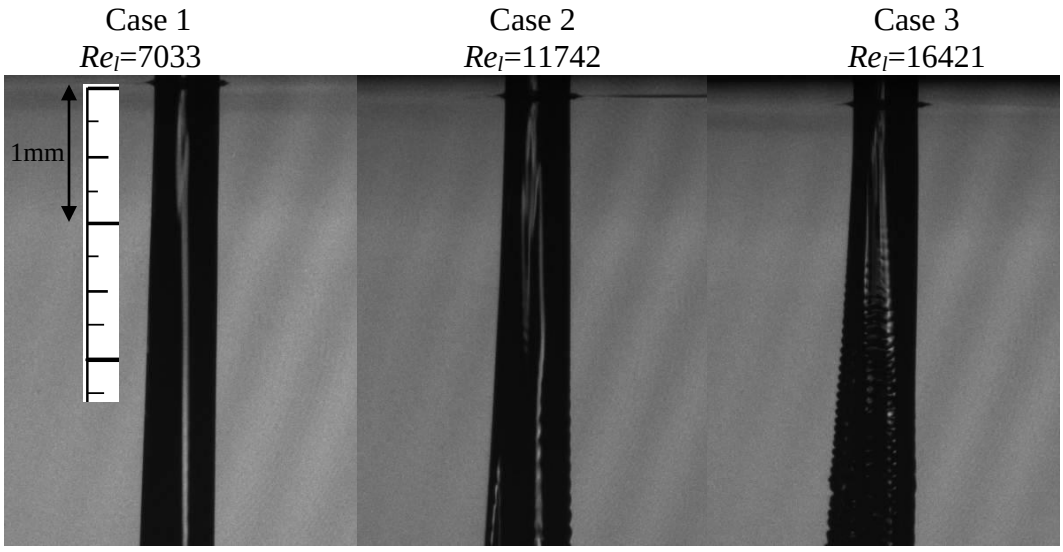

a) Round Edged Orifice

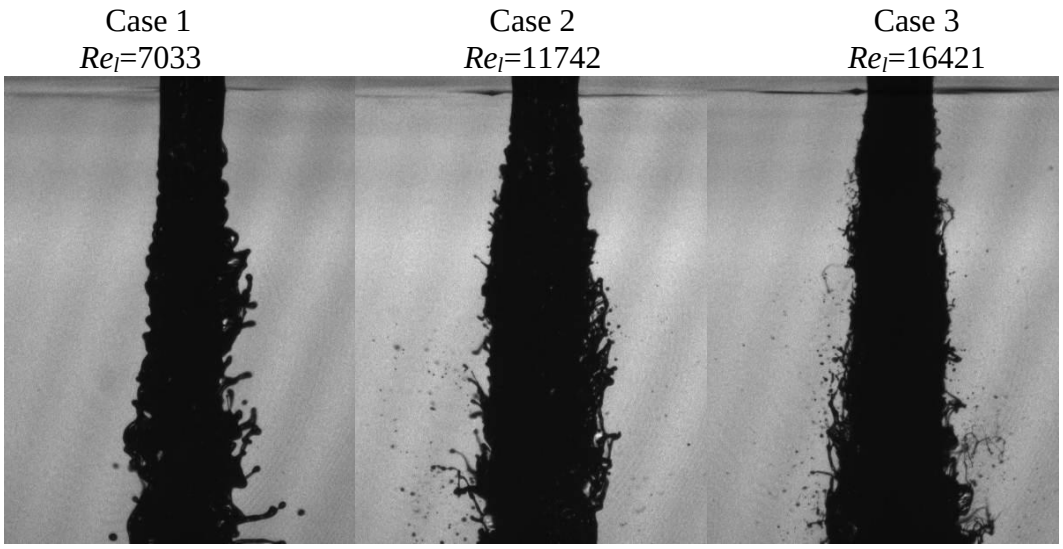

b) Sharp Edged Orifice

Figure 4-6. Micro-images of the liquid column in the absence of crossflow at various flow rates close to the injector. These sprays were generated using a) Round edged orifice and b) Sharp edged orifice

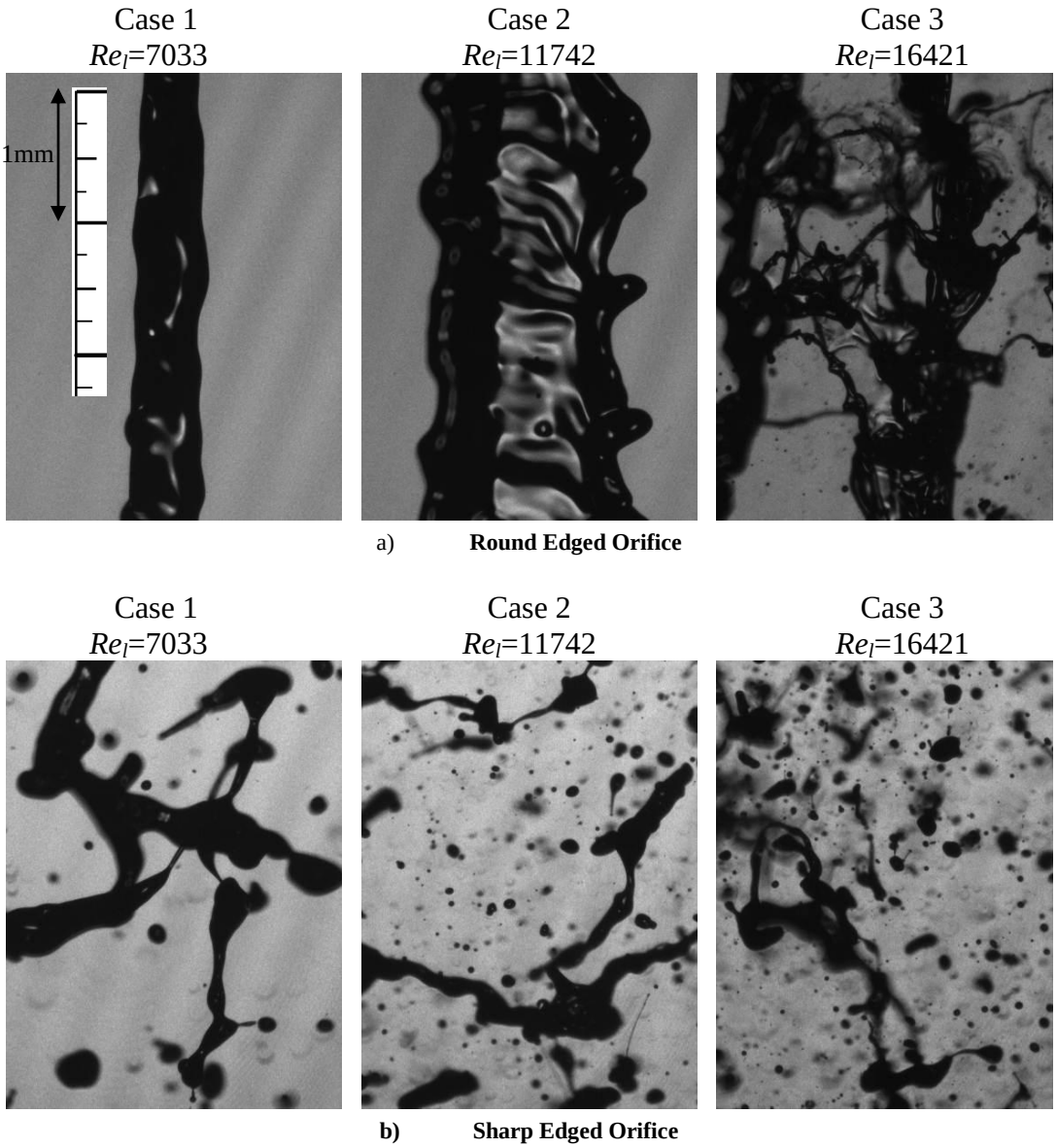

Figure 4-7. Micro-images of the liquid column in the absence of crossflow at various flow rates at a downstream distance of 90 diameters of the orifice. These sprays were generated using a) Round edged orifice and b) Sharp edged orifice

4.3 Structures on the Surface of a Liquid Jet in Crossflow

This section makes observations of the structures formed on the surface a liquid jet in the presence of a crossflow. Past studies have noted that generally, hydrodynamic

instabilities develop and distort the liquid jet column. Such instabilities produce waves or disturbances that increase in magnitude as they propagate downstream along the jet. These disturbances grow, forming ligaments that break off the liquid column and subsequently break up into droplets. These surface waves have been linked to the classical Rayleigh Taylor instabilities. Figure 4-8(a) shows a micro-image of the spray created using the round edged orifice at We=500 and q=10. It shows that the wave crests form on the windward side (i.e., the upper surface of the liquid column facing the airflow) of the liquid column. These wave crests are not symmetric about a normal drawn to the trajectory of the liquid column. Close to the orifice, they experience aerodynamic drag due to their velocity in the direction of liquid injection and tend to lean towards the orifice. Further downstream, the liquid column bends and the drag forces experienced because of the crossflowing air become significant. This leads to the surface waves tilting away from the orifice. This eventually can lead to the liquid mass contained in the wave crest pinching off of the column. These waves cause the flattened liquid column to break off at the wave nodes. Figure 4-8(b) shows a micro-image of the spray created using the sharp edged orifice at the same operating conditions. A comparison of the two images reveals a significant difference in the surface structures formed on the liquid column for the two injectors. The sharp edged orifice creates a liquid column with larger structures that are highly irregular and non-periodic. The images also show that the flow around these structures is not continuous but a dispersed spray region.

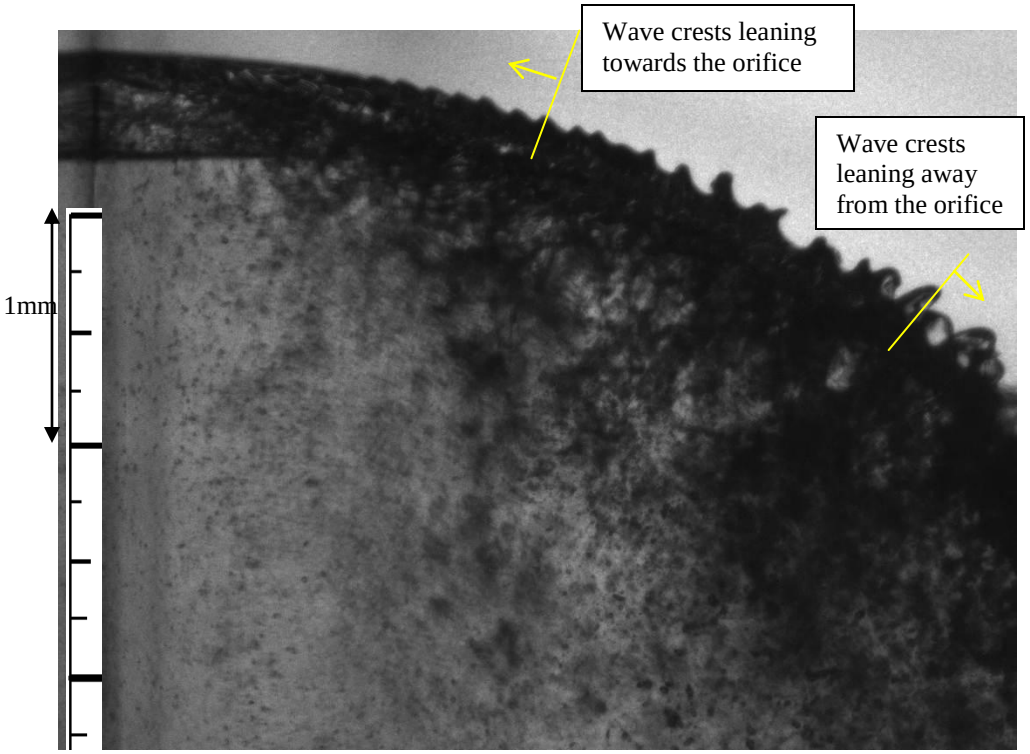

a) Round Edged Orifice

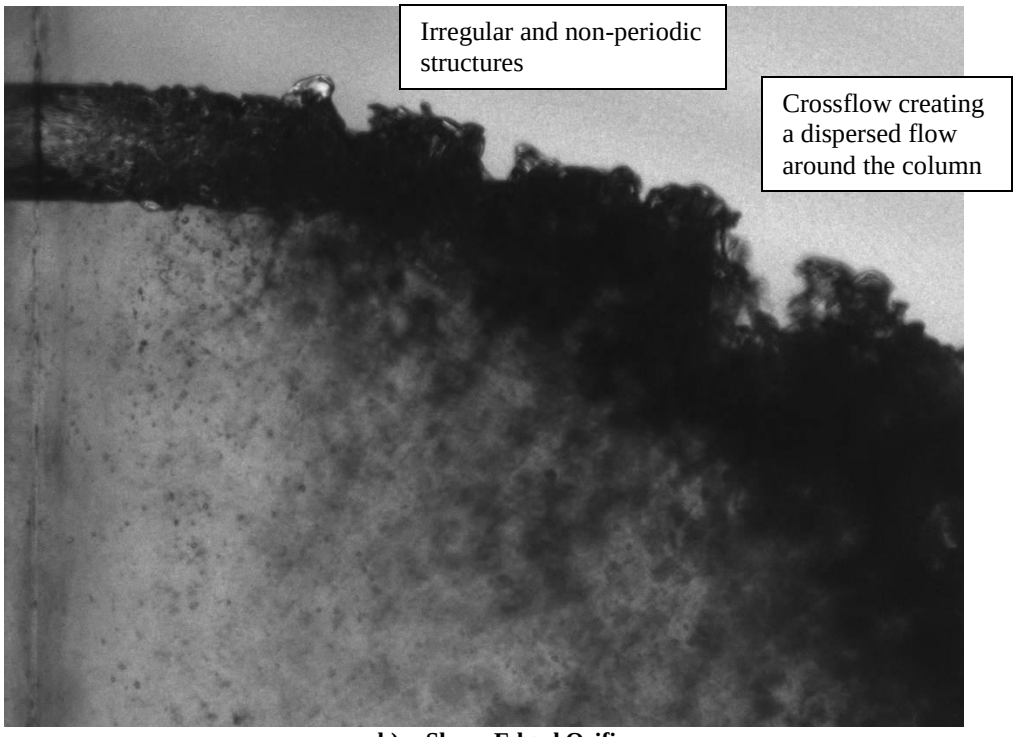

b) Sharp Edged Orifice

Figure 4-8. Micro-images of sprays showing the structures on their surface. They were created at *We*=500 and *q*=10 with a) Round Edged Orifice and b) Sharp Edged Orifice

Figure 4-9 shows the macro-images of the sprays created by the two injectors at the *We*=1500 and *q*=40. An observation of these images shows that the sharp edged orifice generates a spray with large irregular structures. These irregular structures are generated by shear breakup of very large droplets that penetrate further compared to the other droplets in the vicinity. The occurrence of these large structures was quantified with the following procedure

1. The spray penetration trajectories for 20,000 instantaneous images were obtained with the method described in Section 2.2.6.
2. Two narrow bands of thickness 0.2d at Z/d=20 and Z/d=40 were chosen to investigate the occurrence of the large structures.
3. If a large structure exists in an image at these locations, the trajectory showed more than one value of penetration for the same Z value. The maximum difference between these values of penetration was chosen as a measure of the size of the irregular structure
4. The process was repeated for all the images and the number of occurrences of the structures were obtained and segregated by their size.

Figure 4-10 shows the occurrence of the structures for sprays created by the two injectors at *We*=1000 and *q*=40. It shows that the sharp edged orifice creates a spray with a larger number of these structures and also larger in size.

a) Round Edged Orifice

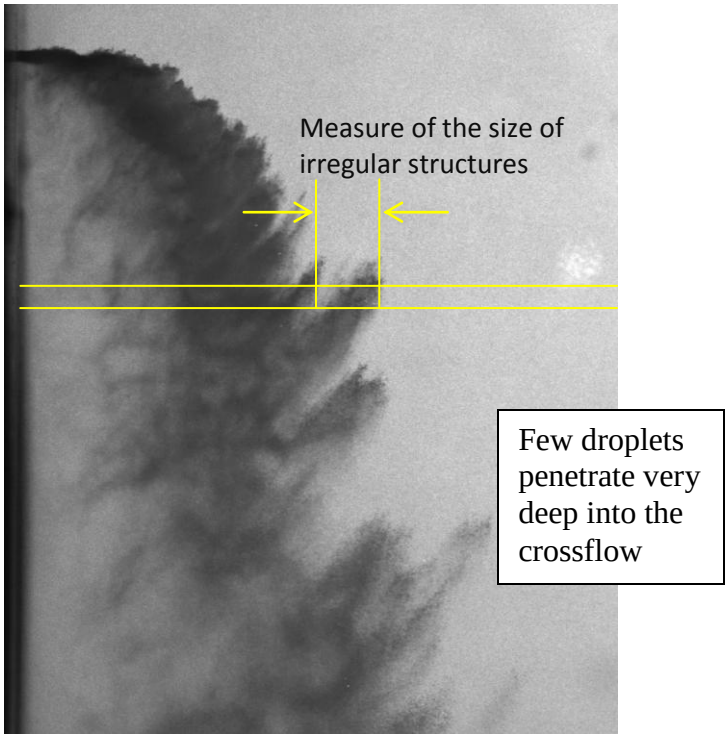

b) Sharp Edged Orifice

Figure 4-9. Macro-images of sprays showing the structures on their surface. They were created at *We*=1500 and *q*=40 with a) Round Edged Orifice and b) Sharp Edged Orifice

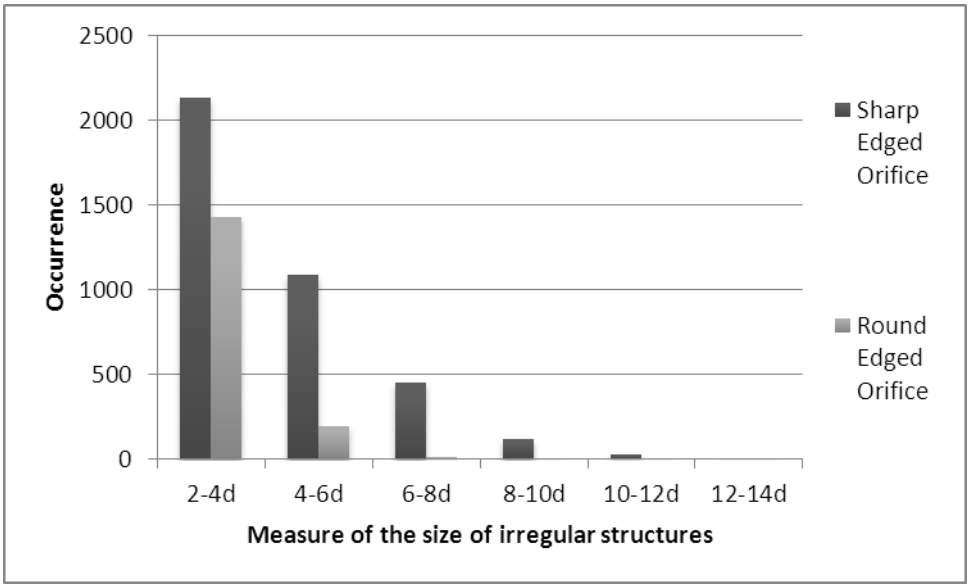

a) Z/d=20

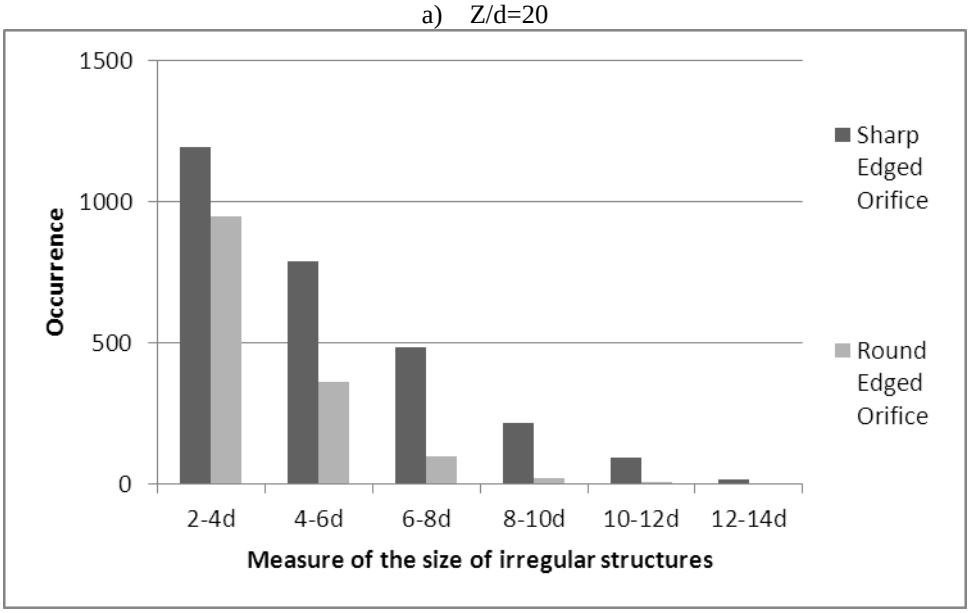

b) Z/d=40

Figure 4-10. Occurrence of the irregular structures in the spray field for the sharp and round edged injectors segregated by the size of the structures at a) Z/d=20 and b) Z/d=40

4.4 Location of the CBP

The liquid jet light guiding technique (LJLGT), described in section 2.2.3, was used to locate the CBP for the two injectors. The results for the round edged orifice have

been presented in section 3.1. This section focuses on the comparison of the results of the location of the CBP of the sprays produced by the two injectors to gain an insight on the effect of the injector geometry on the breakup of the liquid column. This study was carried out with Jet A. The crossflowing air was pre-heated to 555K. Two sets of experiments were carried out to investigate this effect. In one set, the *We* was varied between 300 and 1500 by changing the velocity of the airflow while the momentum ratio was maintained at a constant value of 20. In the other set of experiments, the *We* was maintained at a constant value of 1000 and the momentum ratio was varied in the range of 2.5-180 by changing the mass flow rate of the liquid. These were the same operating conditions for the measurements made with the round edged orifice discussed in Section 3.1.

Figure 4-11 shows the dependence of the mean location of the CBP upon *We* for the two injectors. It shows that the liquid column from the sharp edged orifice breaks up into ligaments and droplets comparitively closer to the orifice (~1-2 diameters in the direction of liquid injection and ~1 diameter in the direction of airflow). Another interesting phenomenon occurrs when the flow rate of the liquid is increased beyond a value corresponding to Re_l=16,000. The jet disintegrates immediately after issuing out of the orifice. This phenomenon was made very clear by the second set of experiments with varying *q*. Figure 4-12 shows the coordinates of the CBP at different values of *q* and *We*=1000. It can be seen that the Z_b/d location falls below the value of 1. Beyond *q*=30 (Re_l~16,000), measurements could not be made since the laser light ceased to come out of the orifice. This strongly supports the presence of cavitation bubbles in the injector, which attenuates the light intensity. It should be noted that when cavitation bubbles begin

to form, they are formed in a region close to the wall where the flow separates and they implode quickly [64]. Thus, the attenuation of light, which strongly suggests the presence of cavitation bubbles, does not necessarily indicate the onset of cavitation. Another factor to consider in the presence of dissolved nitrogen in the liquid. Compressed nitrogen gas that is used to pressurize the liquid, dissolves in it. The dissolved nitrogen can separate from the liquid and form bubbles when the pressure is low. Unlike cavitation bubbles that implode quickly, the nitrogen bubbles result in a two phase flow inside the injector. The solubility of a gas in a liquid is measured with Ostwalds coefficient. It gives an estimate of the volume of gas that can dissolve in a liquid per unit volume of the liquid. The Ostwalds coefficient of Jet A is 0.2 at room temperature [83] meaning 0.2 mm^3 of nitrogen gas dissolves in 1 mm^3 of liquid Jet A. Together with cavitation of Jet A, the presence of nitrogen bubbles, could enhance the atomization process.

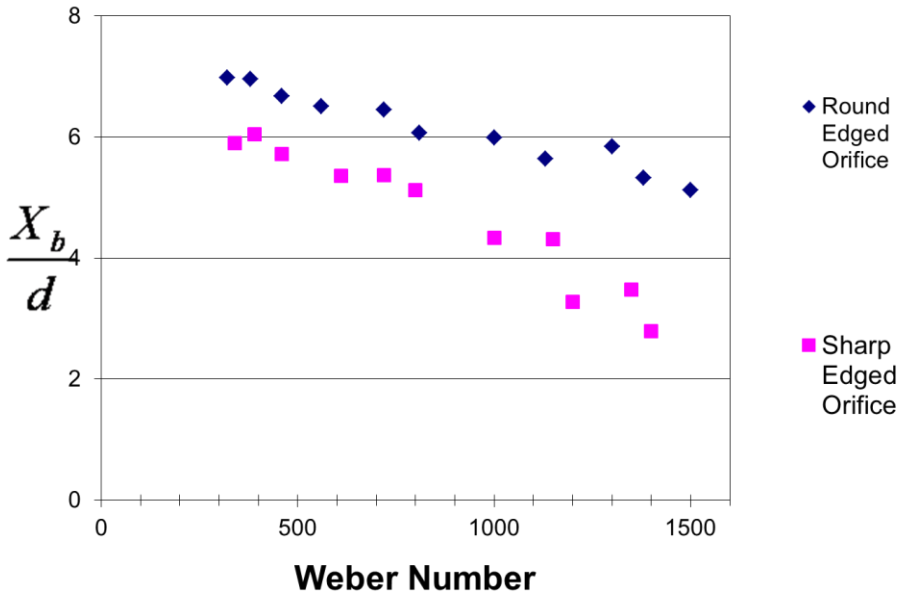

a)

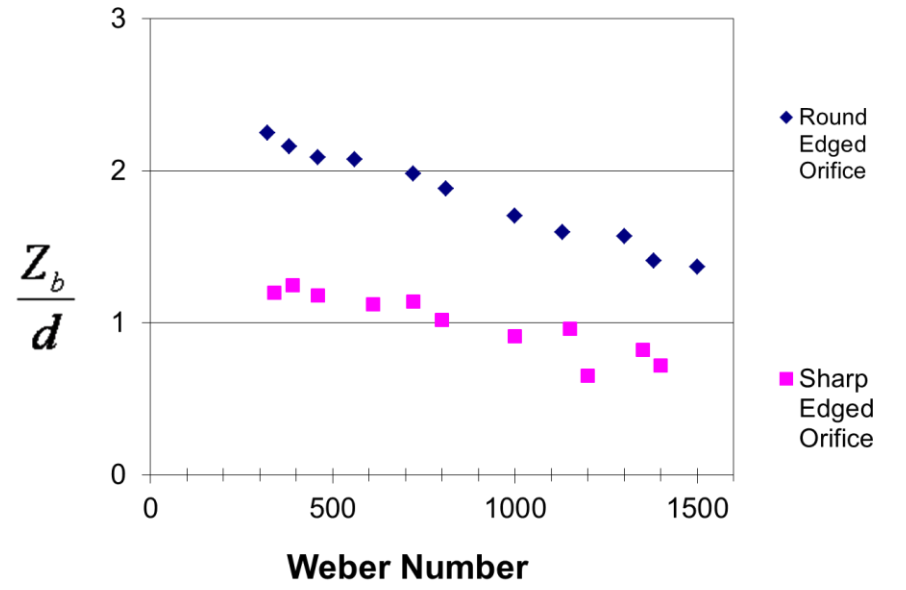

b)

Figure 4-11. The coordinates of the mean location of the column breakup point as different values of We. The q was maintained at a constant value of 20. a) X coordinate (in the direction of liquid injection and b) Z coordinate (in the direction of airflow)

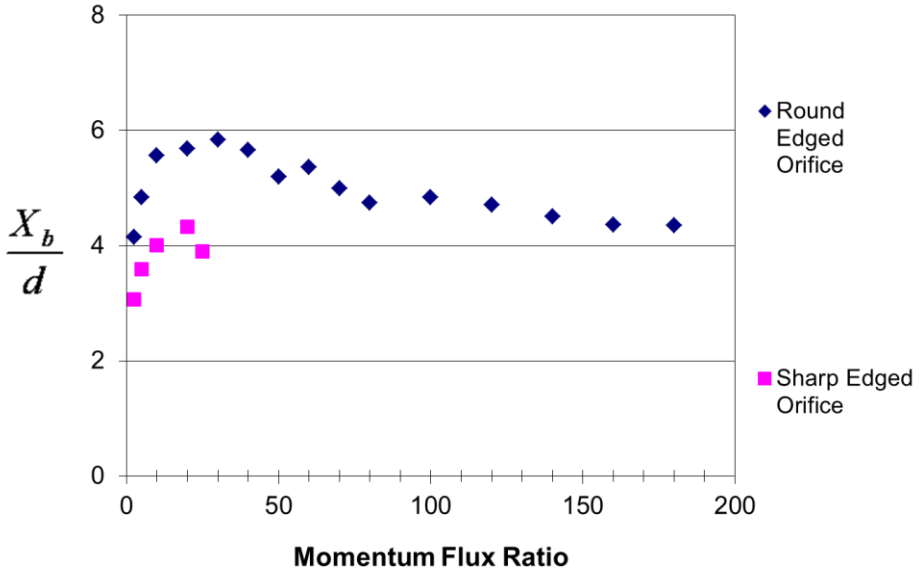

a)

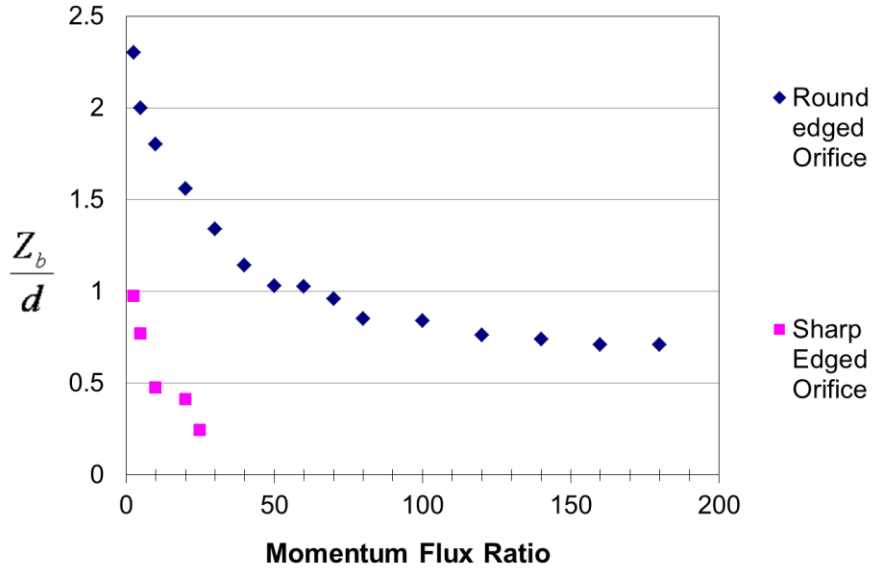

b)

Figure 4-12. The coordinates of the mean location of the column breakup point as different values of *q*. The *We* was maintained at a constant value of 1000. a) X coordinate (in the direction of liquid injection and b) Z coordinate (in the direction of airflow)

The primary breakup time was evaluated for the flows under Re_l=16,000, from the measurements shown above. These data are compared with the correlation for the primary breakup time obtained in Seciton 3.1 as shown in Figure 4-13. It shows that the sharp edged orifice follows the correlation with a slightly lower value upto a Reynolds number of about 16,000. Beyond that, as mentioned earlier, the light ceased to come out of the orifice and no measurements of the loction of the CBP could be made. The results obtained with the sharp edged orifice further supports the findings that the primary breakup time scale is governed by the liquid jet properties

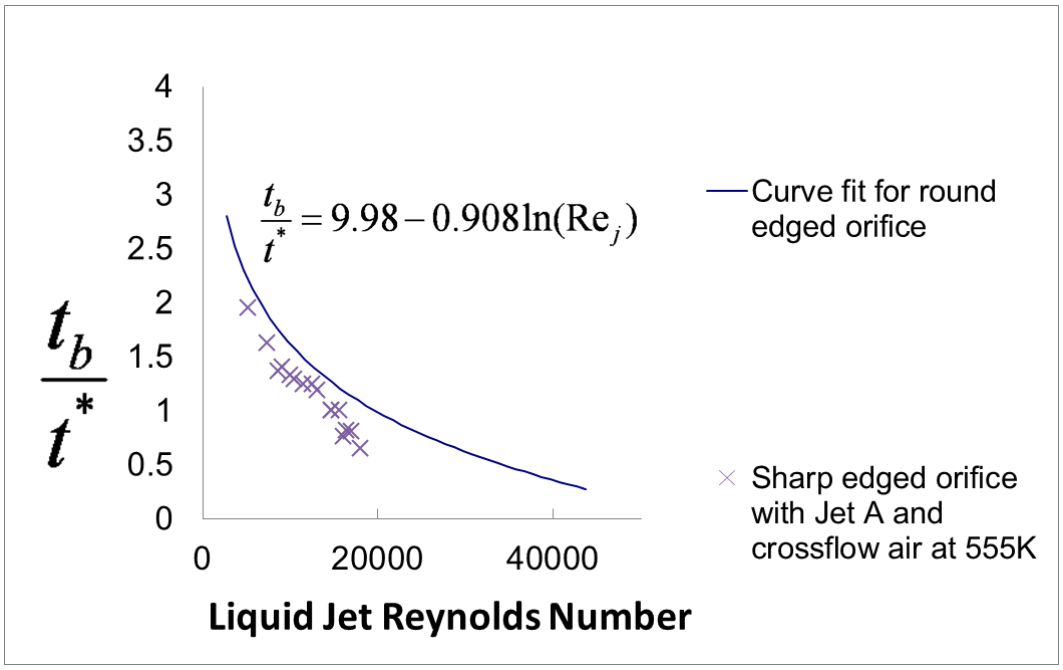

Figure 4-13. Comparison of correlation of the primary breakup time obtained for the round edged orifice with the results of primary breakup time for the sharp edged orifice

4.5 Droplet Sizes and Velocities

Representative measurements of droplet sizes and velocities measurements in an X-Y plane corresponding to a Z/d location of 60 at *We*=1000 and *q*=20 are used to illustrate the effect of injector geometry on droplet sizes and velocities.

Table 4-2. Operating conditions for the comparison of droplets' sizes and their velocities

lists the operating conditions at which these measurements were made. Figure 4-14 shows a sample flowfield measurement of the spray in the X-Y plane. In this study, the spray region is demarcated into the core region, the lateral periphery and the outer periphery as shown in the figure.

Figure 4-15 shows the planar colormap of Sauter mean diameters (SMD) of the droplets in the X-Y plane created by the two injectors. It can be seen that the sharp edged orifice creates a spray with larger droplets, especially in the outer periphery region of the spray. The droplet velocities in the direction of the air flow (Z velocities) were normalized with the velocity of the incoming airflow and are shown in Figure 4-16. It can be seen that the droplets in the spray created by the round edged orifice accelerated comparatively faster. This can be attributed to the smaller sizes of the droplets created by the round edged orifice, which follow the airflow better. Figure 4-17 and Figure 4-4 show the comparison of the velocity profiles in X and Y directions, respectively. The data indicates that these velocity profiles are very similar to each other in magnitude. Thus, it can be said that sharp edged orifice creates a spray with larger droplets that accelerate slower in the direction of airflow, while the other two velocity components are not significantly different for the two injectors.

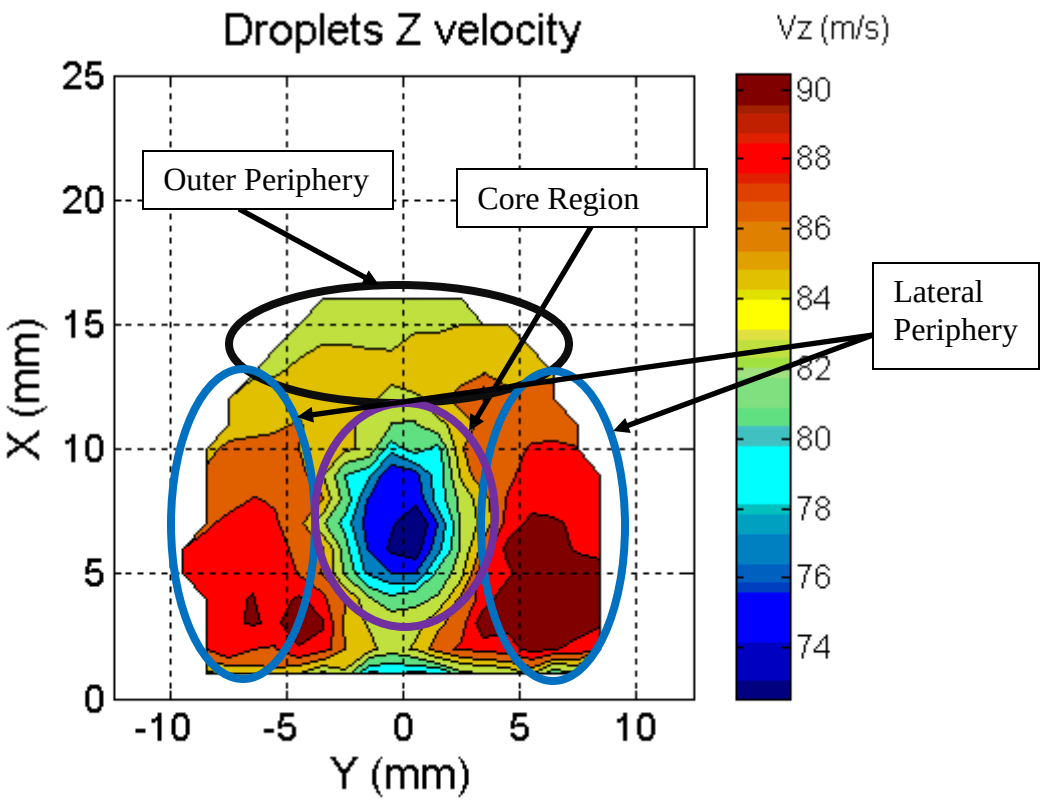

Figure 4-14. Sample flow field measurements of the spray with a nomenclature for the different regions for the spray

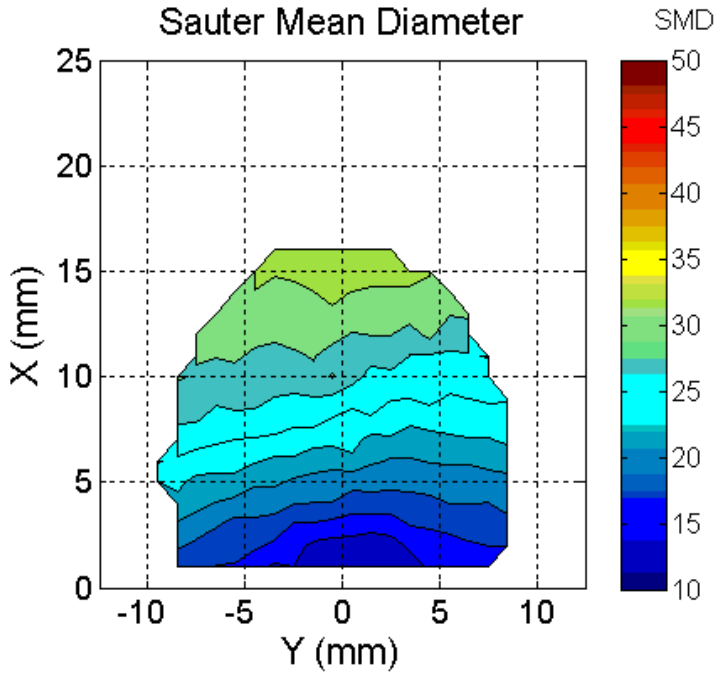

a) Round Edged Orifice

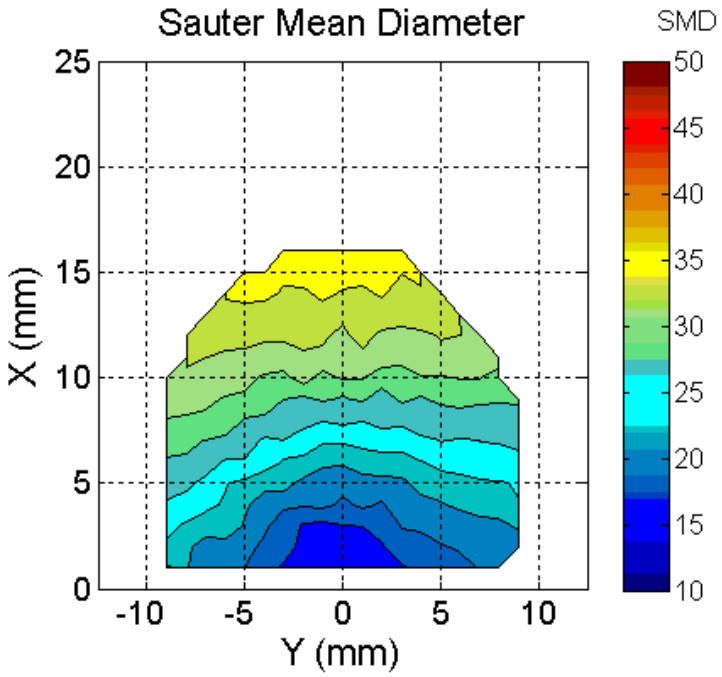

b) Sharp Edged Orifice

Figure 4-15. Sauter Mean Diameters of the droplets (in μm) in a X-Y plane corresponding to a Z/d location of 60 at *We*=1000 and *q*=20

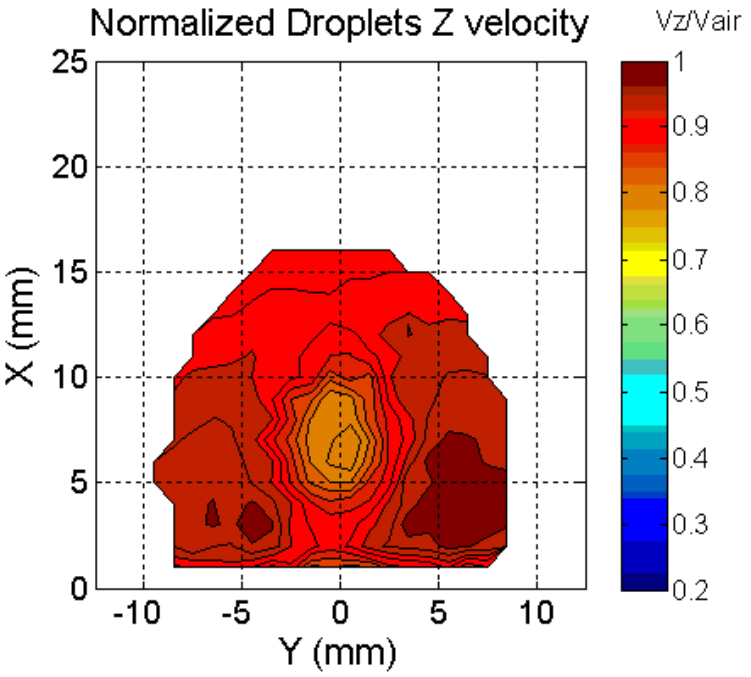

a) Round Edged Orifice

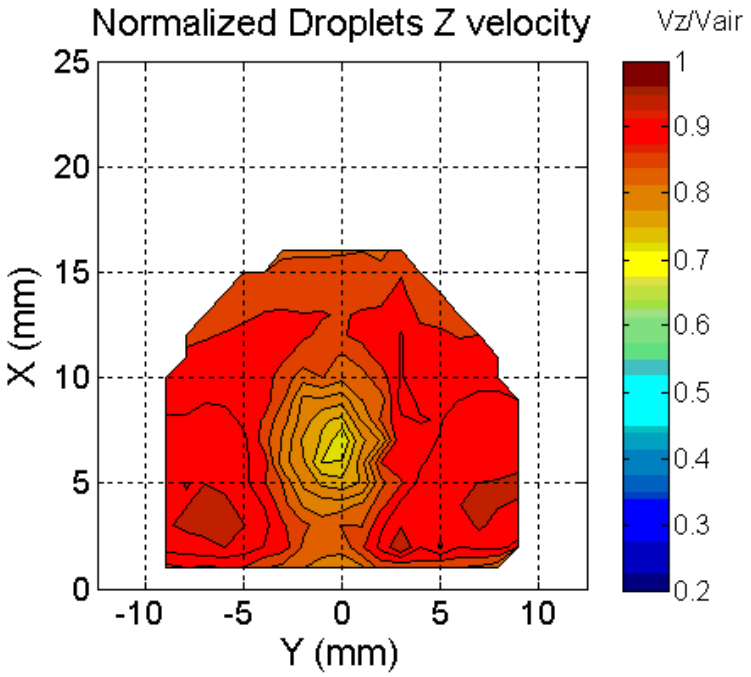

b) Sharp Edged Orifice

Figure 4-16. Velocities of the droplets in the direction of airflow normalized with the velocity of the freestream airflow in a X-Y plane corresponding to a Z/d location of 60 at *We*=1000 and *q*=20

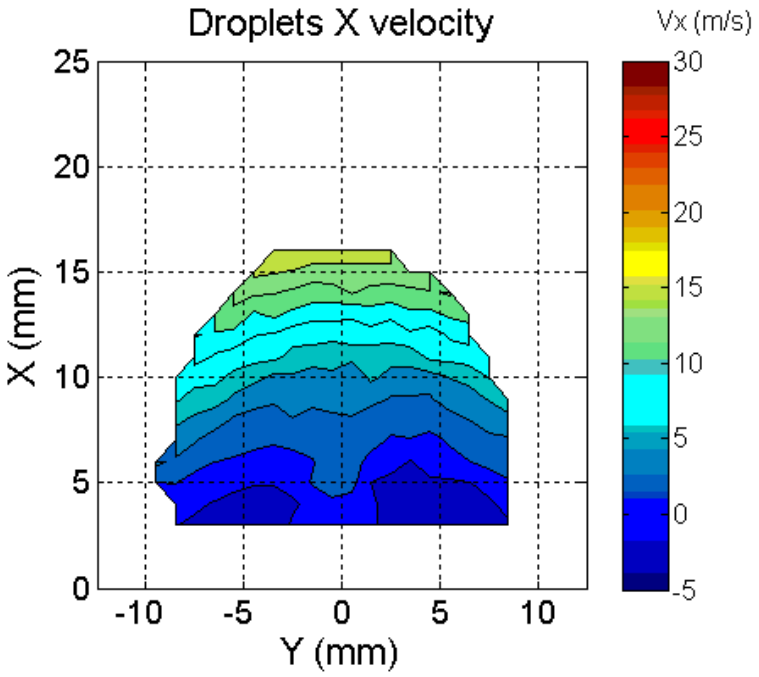

a) Round Edged Orifice

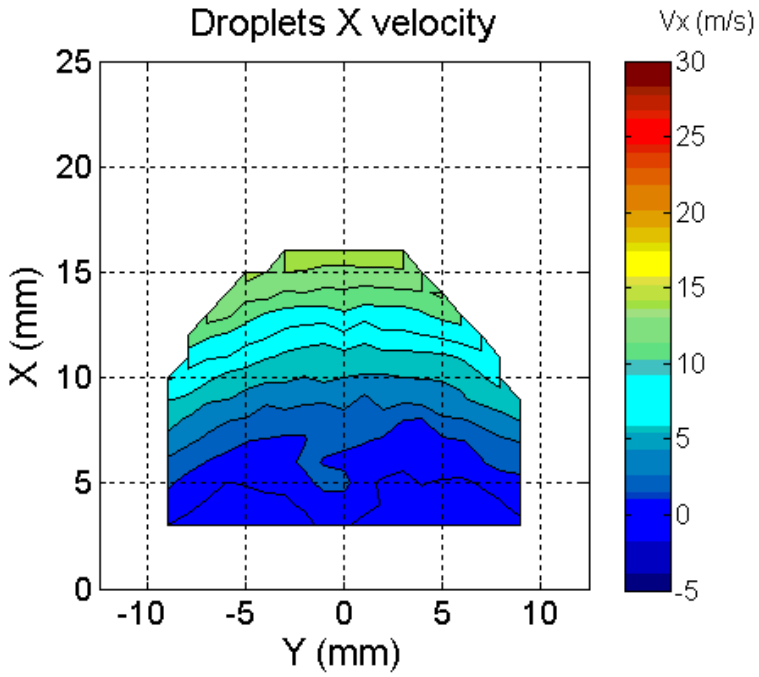

b) Sharp Edged Orifice

Figure 4-17. Velocities of the droplets (in m/s) in the direction of liquid injection in a X-Y plane corresponding to a Z/d location of 60 at *We*=1000 and *q*=20

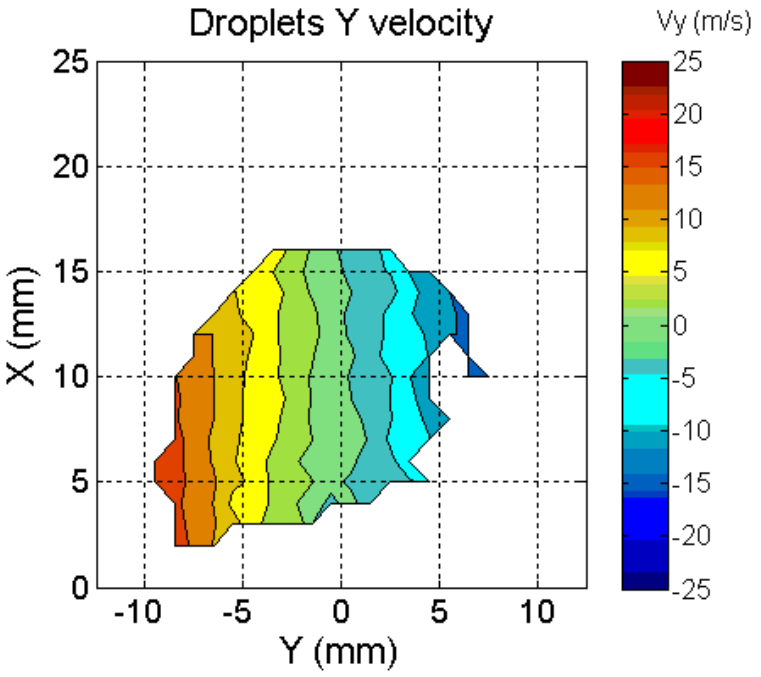

a) Round Edged Orifice

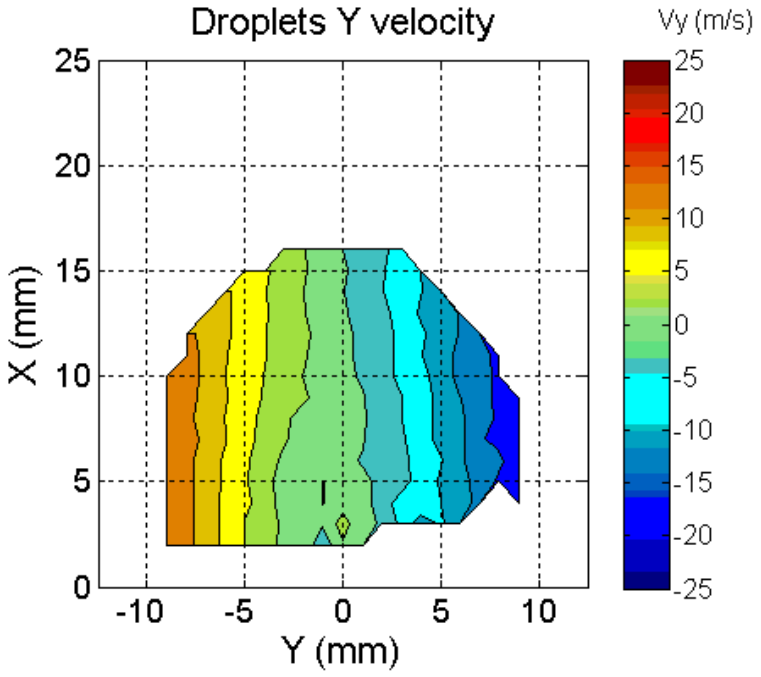

b) Sharp Edged Orifice

Figure 4-18. Velocities of the droplets (in m/s) in the Y-direction in a X-Y plane corresponding to a Z/d location of 60 at *We*=1000 and *q*=20

4.6 Spray Penetration Trajectories

Spray images were obtained by employing the back illumination technique described in section 2.2.5. These images were used to evaluate the spray penetration trajectories – the outermost edge, the median edge and the innermost edge using the methodology described in section 2.2.6. These trajectories were obtained for nine different operating conditions with variation in both *We* and *q* as listed in Table 4-3.

Table 4-3. Operating conditions for measurements of Spray Penetration Trajectories

We	500			1000			1500		
q	10	20	40	10	20	40	10	20	40
Air Velocity (m/s)	66.4			93.9			115		
Liquid Jet Exit Velocity (m/s)	18.5	26.1	37	26.1	37	52.3	32	45.3	64

The trajectories thus obtained were used to develop correlations as a function of z/d location and q as shown below for the two injectors. The outermost edge and the median edge trajectories were described with the logarithmic equation while the trajectory for the innermost edge was described with the multizone equation, which gave a better fit. The R^2 value gives an estimate of the fit. The closer its value is to one, the better the fit is.

Round edged Orifice

Outermost edge: $\frac{x}{d} = 1.89 q^{0.437} \log\left(1 + 1.123 \frac{z}{d}\right)$ R^2=0.9929

Median edge: $\frac{x}{d} = 1.187 q^{0.468} \log\left(1 + 1.579 \frac{z}{d}\right)$ R^2=0.9939

Innermost edge: $\frac{x}{d} = 4.1 q^{0.478} \left(1 - e^{-0.054 z/d}\right)\left(1 + 1.555 e^{0.105 z/d}\right)\left(1 + 1.147 e^{-0.448 z/d}\right)$

R^2=0.9898

Sharp edged Orifice

Outermost edge: $\frac{x}{d} = 1.914 q^{0.415} \log\left(1 + 2.238 \frac{z}{d}\right)$ R^2=0.9769

Median edge: $\frac{x}{d} = 1.393 q^{0.482} \log\left(1 + 1.267 \frac{z}{d}\right)$ R^2=0.9971

Innermost edge: $\frac{x}{d} = 4.98 q^{0.483} \left(1 - e^{-0.045 z/d}\right)\left(1 + 1.484 e^{0.01 z/d}\right)\left(1 + 0.939 e^{-0.385 z/d}\right)$

R^2=0.9981

These equations were used to compare the spray trajectories between the two injectors. For example, Figure 4-19 shows a comparison of the spray trajectories for q=20. It can be seen that the sharp edged orifice produces sprays with deeper penetration. This can be attributed to two factors namely

1. The velocity profile of the liquid jet issuing out of the orifice is different for the two injectors. The sharp edged orifice has a longer internal flow of 10 orifice diameters, as opposed to 1 orifice diameter for the round edged orifice. Since the mass flow rate was the same for the two injectors, the average jet exit velocity was the same. However, with a longer length of the orifice, the boundary layer in the sharp edged orifice can be expected to be more

developed resulting in a higher velocity at the center of the orifice. This higher velocity increases the overall penetration of the spray.

2. The sharp edged orifice produced larger droplets as seen in section 4.6. The acceleration (or deceleration) of any body is proportional to the applied force and inversely proportional to the mass. (i.e., Acceleration = Force / Mass). In the context of droplets, the aerodynamic drag force on them is proportional to the projected area, which is proportional to d^2. The mass is proportional to d^3. Thus, the deceleration of the droplets is inversely proportional to the diameter of the droplet. This results higher penetration of larger droplets.

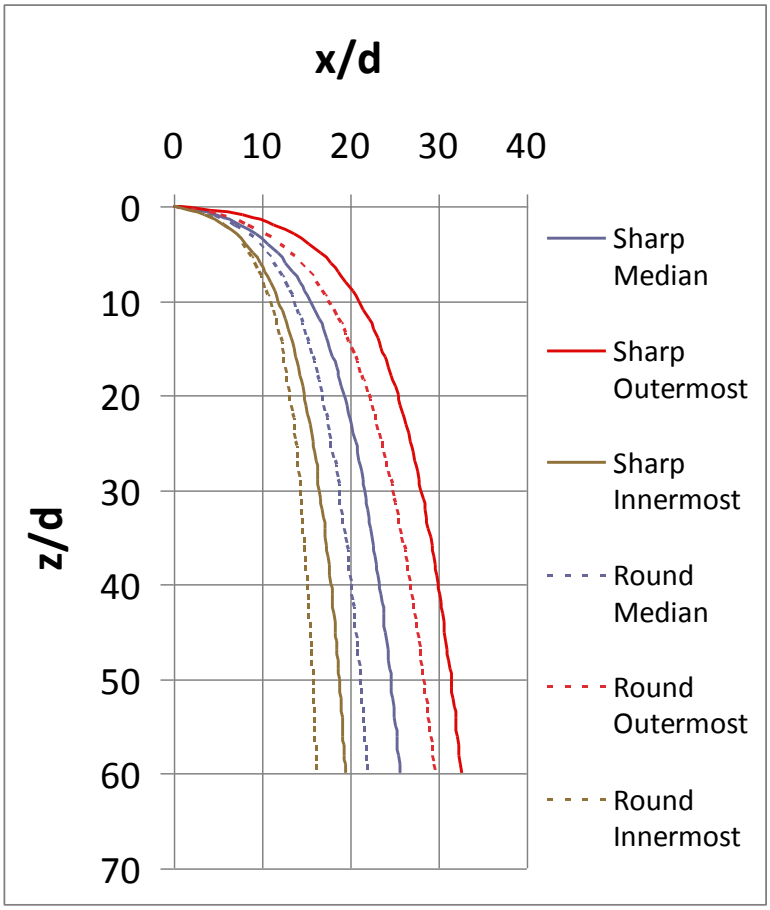

Figure 4-19. Comparison of the Spray Penetration Trajectories between the two Injectors. These trajectories are plotted for *q*=20

To back up the hypothesis of the reasons for greater penetration of the spray created by the sharp edged orifice, a simple program was used calculate the trajectory of a droplet in crossflow and evaluate the effect of the size of a droplet on its penetration. Consider a droplet with radius r, injected at the origin with an initial velocity of u_i in the X-direction into a free stream of air with a velocity of u_a in the Z direction as shown in Figure 4-20.

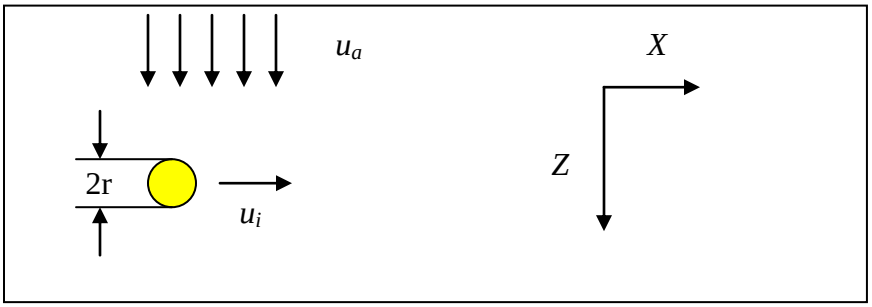

Figure 4-20. Schematic for the reduced order model

The droplet was assumed to be spherical in shape. The aerodynamic drag on a sphere is given by

$$\frac{1}{2}\rho_a v_{rel}^2 C_D A$$

where, v_{rel} is the relative velocity between the droplet and the airflow, C_D is the drag coefficient (0.1 for a sphere in turbulent flow) and A is the projected area of the droplet ($=\pi r^2$). This drag force was decomposed into X and Z components. The equations of motion were solved independently in the two directions following the steps mentioned below.

1. The instantaneous acceleration components of the droplet were obtained by dividing the respective force components by its mass ($=\frac{4}{3}\pi r^3 \rho_l$)
2. Using the acceleration components obtained in Step 1, the velocity components of the droplet after a time step of Δt were computed as $u_{t+\Delta t} = u_t + a_t \Delta t$. In this exercise, a time step of 10 microseconds was used. It should be noted that the results did not change with a larger time step of 100 microseconds.
3. The coordinates of the droplet after the time step were computed as $x_{t+\Delta t} = x_t + (u_t)_x \Delta t$ and $z_{t+\Delta t} = z_t + (u_t)_z \Delta t$
4. Steps 1-3 were repeated with the new coordinates until the desired Z location was reached (60 diameters of the orifice, which covers the field of view of the test section).

The locus of the X and Z coordinates gives the trajectory followed by the droplet in the crossflow. The trajectories were thus obtained for droplets with diameters of 20, 25, 30 and 35 microns. In this exercise, the velocity of the air was set to 91 m/s and the air density to 6.02 kg/m^3. These are the flow conditions that correspond to *We*=1000. The evaluated trajectories are plotted in Figure 4-21. It shows that the droplets with a larger size penetrate deeper into the crossflow. On an average, an increase in droplet size by 5 microns results in an increase of penetration by 2 diameters of the orifice at a Z/d location of 60.

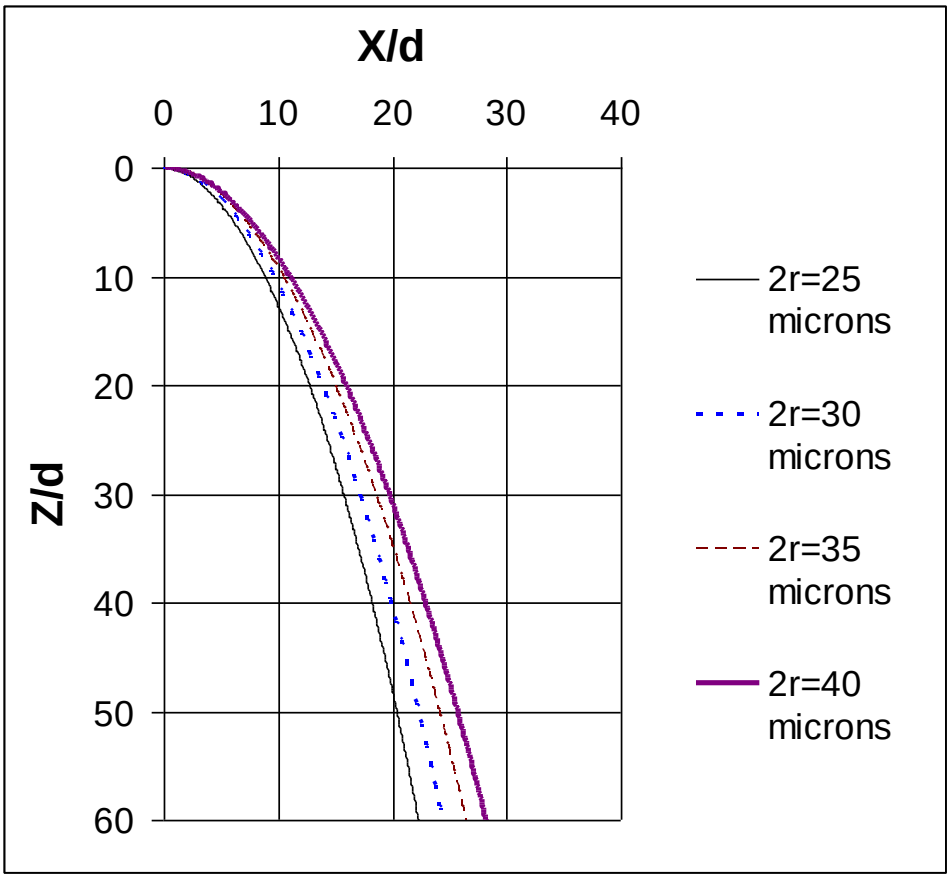

Figure 4-21. Penetration of droplets of different sizes in a crossflow calculated with equations of motion

The same model was used to evaluate the effect of droplet initial velocity, u_i on droplet penetration into the crossflow. The penetration trajectories of a droplet, 35 microns in diameter were evaluated for initial velocities of 20, 25, 30 and 35 m/s and are plotted in Figure 4-22. The plots show that the penetration increases with increasing initial velocity. At a Z/d location of 60, an increase in initial velocity by 5 m/s results in an increased penetration by about 3 diameters of the orifice.

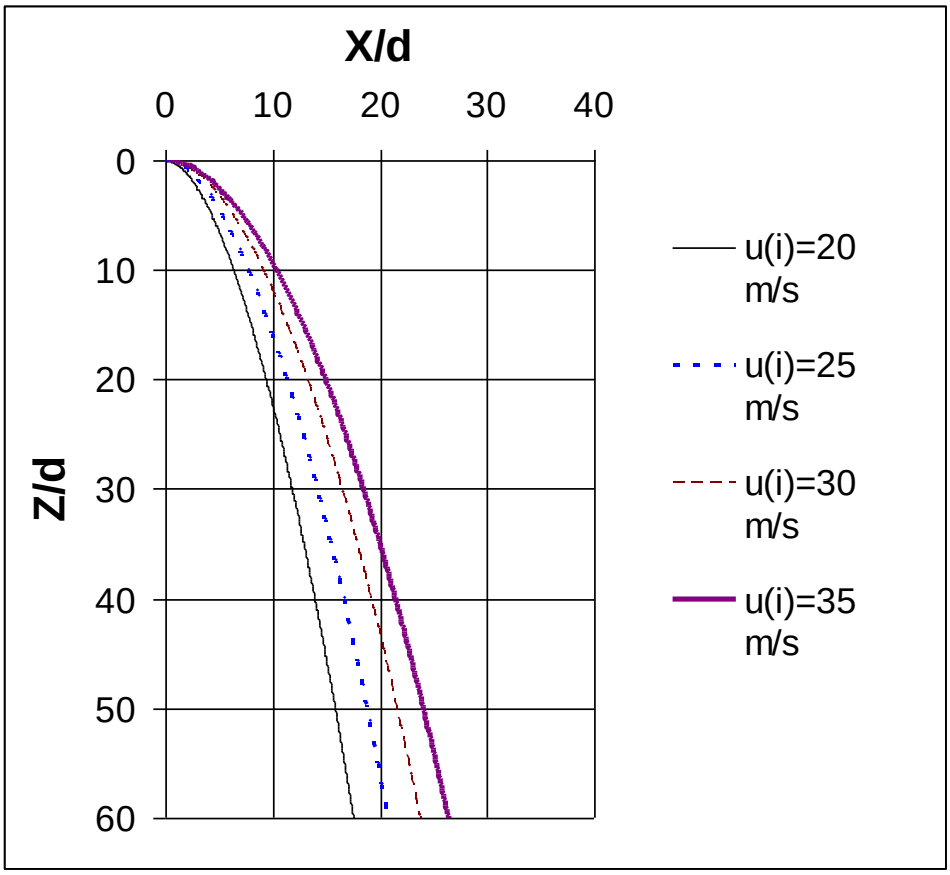

Figure 4-22. Penetration of droplets with different initial velocities in a crossflow calculated with equations of motion

4.7 Summary of Differences in spray properties between the injectors

This chapter discussed the differences in the properties of sprays created by the two injectors and identified the possible causes for the observed differences. They are listed as follows:

1. The pressure difference across the sharp edged orifice indicates the presence of cavitation in the orifice internal flow. Comparing the flow characteristics to similar injectors in literature, cavitation occurred in the sharp edged orifice beyond a liquid jet Reynolds number of 8000.
2. In the absence of crossflow, the round edged orifice creates a jet with a

smooth surface that does not disintegrate within the operating conditions of interest. In contrast, the sharp edged orifice creates a jet that expands in diameter creating a dispersed flow around the column and disintegrates completely further downstream, typical of flows undergoing cavitation.

3. A jet in crossflow created by the round edged orifice develops surface instabilities that grow in amplitude downstream and pinch off of the liquid column. In contrast, the sharp edged orifice creates a jet that has large irregular structures and shows some droplets penetrating deeper into the flow compared to the rest of the liquid mass.
4. The round edged orifice exhibits the phenomenon of jet splitting while the sharp edged orifice does not.
5. The liquid column created by the sharp edged orifice breaks up faster than that of the round edged orifice owing to increased jet turbulence induced by the sharp transition. Beyong a Reynolds number of 16,000, the laser light illuminating the liquid jet from the back of the injector did not come out of the injector indicating a dense two phase flow inside the injector.
6. The round edged orifice creates a spray with smaller droplets in the far field compared to the sharp edged orifice. These smaller droplets follow the airflow more closely and attain a higher velocity in the direction of airflow. The other two velocity components remain largely the same for the two injectors.
7. The spray created by the sharp edged orifice penetrates deeper into the crossflow because of the higher jet exit velocity in the core of the jet and larger droplets that have lower deceleration.

CHAPTER V

CONCLUSIONS AND RECOMMENDATIONS FOR FUTURE RESEARCH

This chapter highlights the principal findings of this thesis and concludes with recommendations for further research.

A review of the literature on liquid jet in crossflow identified the key areas in which the research so far is inadequate. The time scales for the primary breakup of the liquid column was identified as one of the parameter that needed improvement. The existing model for the primary breakup time did not take into account the parameters such as the liquid jet exit velocity, which is known to affect the breakup of the liquid column. Another important area where the requirement for further research was identified is the effect of injector geometry on the spray formation processes and properties of the spray such as the spray penetration, the droplet sizes and velocities and the location of the CBP.

Prior to this study, the primary breakup time was thought to be a function of the density ratio of the liquid and the gas, the diameter of the orifice and the air velocity. These parameters were arrived at from experiments of a single droplet breaking up in supersonic flow. The mechanism for this process involves the effect of the aerodynamic forces on the droplet. However, a liquid jet can break up due to its own turbulence and with no interaction with the surrounding air. In the past, the breakup length of a turbulent liquid in quiescent medium, where the turbulence of the liquid causes its atomization, has

been linked to the Reynolds number of the liquid jet. The studies of the primary breakup time scale in the past were limited because of the difficulty in locating the breakup point because of the large number of droplets surrounding the liquid column, especially in the shear breakup regime. This thesis employed the liquid jet light guiding technique to accurately determine the primary breakup location. The results showed that the primary breakup time scale, t_b/t^*, defined in Equation 1-4, is not a constant. It was found to depend on liquid jet properties. This study showed that the Reynolds number of the liquid jet had the best correlation with the primary breakup time scale. It suggests that the breakup of a turbulent liquid jet is influenced by both the aerodynamic breakup processes and the turbulent breakup processes. It also provided a correlation for the primary beakup location as a function of the liquid jet Reynolds number (see Equation 3-1) that can be used for validation of detailed numerical simulations and as a parameter for numerical models. The liquid jet light guiding technique also enabled the visualization of the phenomenon of jet splitting into two or more streams before atomizing.

Sprays created by two injectors of different geometries were investigated to understand the differences between the sprays formation processes and spray properties. One injector was a round edged orifice with a length to diameter ratio of 1 and a discharge coefficient of 0.95 at the operating conditions of interest. The other injector was a sharp edged orifice with a length to diameter ratio of 10 and a discharge coefficient of 0.74. It was shown that the sharp edged orifice was likely to develop cavitation bubbles beyond a flow Reynolds number of 8,000. The spray created by injecting liquid into a quiescent medium was imaged for the two injectors. It showed that in the absence of a crossflow, the round edged orifice creates a liquid jet that has a smooth surface and

does not disintegrate readily while the sharp edged orifice created a liquid jet with irregular structures on its surface and disintegrates within a few diameters downstream of the orifice. The images of a liquid jet in a crossflow revealed that the classical Rayleigh Taylor instabilities that are usually seen with a smooth transition in the injector were not seen in the presence of a sharp transition. The CBP of a spray created by the sharp edged injector was comparatively closer to the orifice showing that the distortion of the liquid jet plays an important role in the primary breakup of the jet. The results followed the correlation of the primary breakup time developed for the round edged orifice closely, with a lower value. Beyond a liquid jet Reynolds number of 16,000, the light illuminated from the back of the injector did not come out of the orifice indicating two phase flow in the orifice. The droplets produced with the sharp edged orifice were found to be larger in size. These larger droplets accelerate slower comparatively and consequently, move with lower velocities in the direction of airflow compared to the droplets created by the round edged orifice. The other two components of the velocity were similar for both the injectors. The spray created by the sharp edged orifice penetrated deeper into the crossflow. This was attributed to higher jet exit velocity in the core of the jet and larger droplets formed.

This study has also provided motivation for future research in some areas. One of them is the investigation of the phenomenon of jet splitting. Experimental evidence of the occurrence of this phenomenon has been shown. Computational studies in the past have demonstrated the existence of the counter-rotating vortex pair in the flow field of a liquid jet in crossflow. However, this flow feature, which has been studied extensively for a gas jet in crossflow, is seldom mentioned in literature of liquid jets in crossflow. Numerical

studies of the presence of CVP and its effect on the liquid column would be an interesting problem for future studies.

Another area of study recommended for further research is the role of the surface tension of the liquid in the primary breakup of the liquid jet. It can be expected that the surface tension forces that are holding the liquid mass together and opposing the aerodynamic forces from breaking it up, play an important role in the primary breakup. However, the correlation obtained for the primary breakup time in this study does not account for the surface tension. It is possible that at the operating conditions of this study, surface tension did not play an important role. However, it is expected to play a major role at lower values of Weber number, i.e., in the column breakup regime, and a study at these conditions would be of interest.

APPENDICES

Appendix A: Characterization of incoming airflow

This section describes the characteristics of the airflow in the test section. As mentioned in Chapter I, the quality of the airflow affects the properties of the spray and thus, it is important to have knowledge of the characteristics of the airflow. Representative measurements of the mean velocity and the root mean square (RMS) of the airflow were made using the LDV technique and are presented here. The air velocity at the center of the test section for the following measurements was maintained at 100m/s, which corresponds to a Reynolds number of about 5,500. Axial velocities were measured in two X-Y planes (refer to Figure 2-8 for the coordinate system) located at 5mm upstream of the orifice (Z=-5mm) and 20mm downstream of the orifice (Z=20mm). The influence of spray on the incoming air flow characteristics was investigated by comparison of velocity fields measured in the cross sections located at the distance 5mm and 2mm upstream of the injection orifice.

Figure A.1(a) shows the axial velocity profiles measured at 5mm upstream of the orifice with and without spray and at 20mm downstream of the orifice without the spray. As seen in the graph, the velocity profiles for the three cases did not differ from one another by more than 1%. Thickness of the boundary layer near the orifice plate did not exceed 3mm. Figure A.1(b) shows the RMS values normalized with the air velocity. The RMS values were typically around 4% of the mean velocity in the core region. Figure A.2 (a & b) show the axial velocity and its normalized RMS value measured at 5mm upstream of the orifice (Z=-5mm) in the Y-direction (i.e., along the plate) at a distance of

10mm from the orifice plate (X=10mm). The velocities measured showed uniform air flow in the center of the test section, while the velocities near the windows was lower. However, the spray does not spread beyond 10mm on either side of the centerline and thus, the region of interest had uniform airflow with an RMS value of 4%.

Figure A.3 shows the effect of spray on the incoming air flow. Axial velocities of the airflow were measured along the Y-direction (along the plate) at two locations, 2mm and 5mm upstream of the orifice (Z=-2mm and Z=-5mm, respectively) at a distance of 3mm from the orifice plate (X=3mm). It was seen that at a location 2mm upstream of the orifice (Z=-2mm), the velocity of the air decreased by a maximum of 5m/s (around 5% of mean velocity) when the spray was turned on. At a distance of 5mm upstream of the orifice (Z=-5mm), this change in velocity did not exceed 1% of the mean velocity. Combining the above mentioned results, it can be said that the effect of the spray on flow characteristics 5mm upstream of the orifice was not significant. On the contrary, significant effect of the spray on velocity profiles was observed at 2mm upstream of the orifice.

The measured velocity profiles were typical of turbulent flows. The observed RMS velocity was around 4% of the mean velocity and the boundary layer on the plate with the injection orifice was about 3mm thick. Boundary layer near the window was thicker but the spray was completely encompassed in the core region of the flow. The characteristics of the incoming air flow at a plane located 5mm upstream of the orifice were independent of the spray and thus, the plane can be treated as a boundary for CFD codes. The flow was uniform and stable in the region of interest.

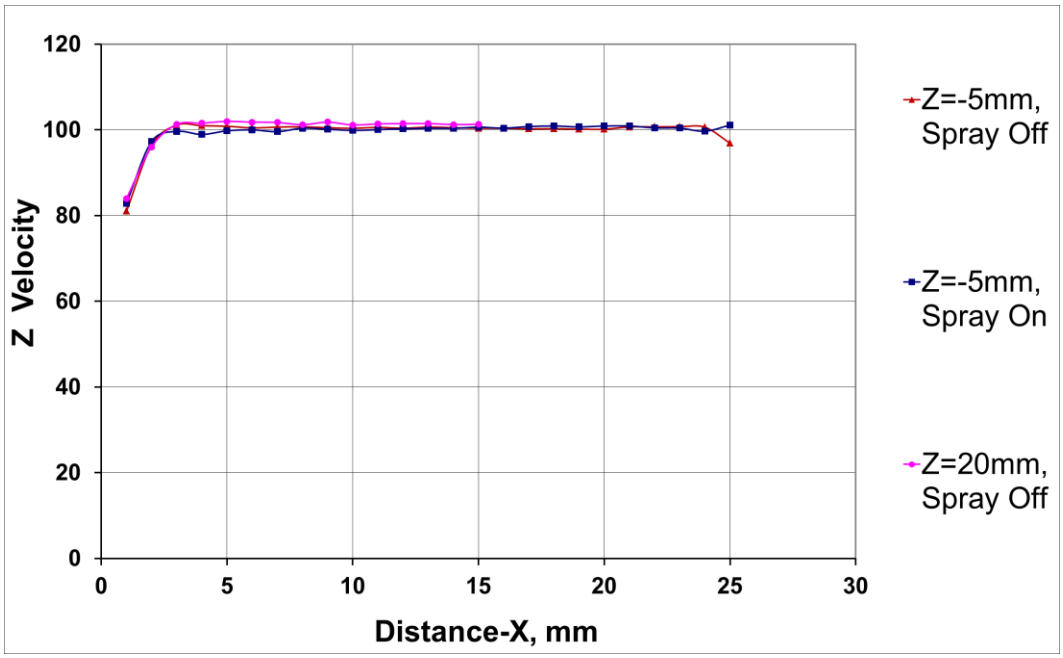

a)

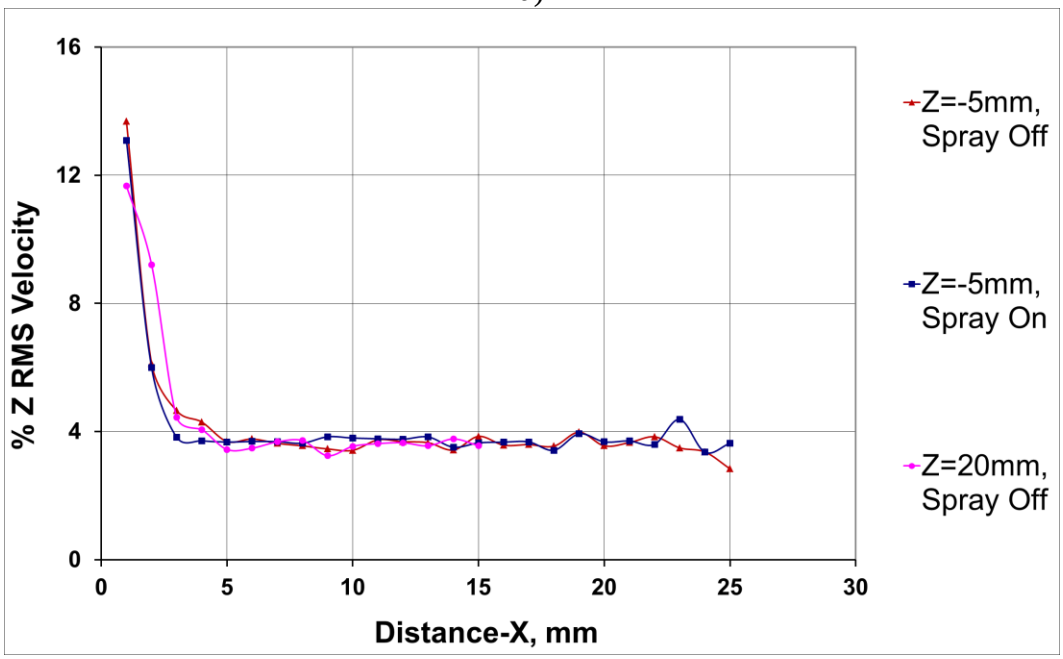

b)

Figure A.1. Flow characteristics of air flow in the test section measured along the X axis a) Mean velocity and b) RMS value normalized with air velocity

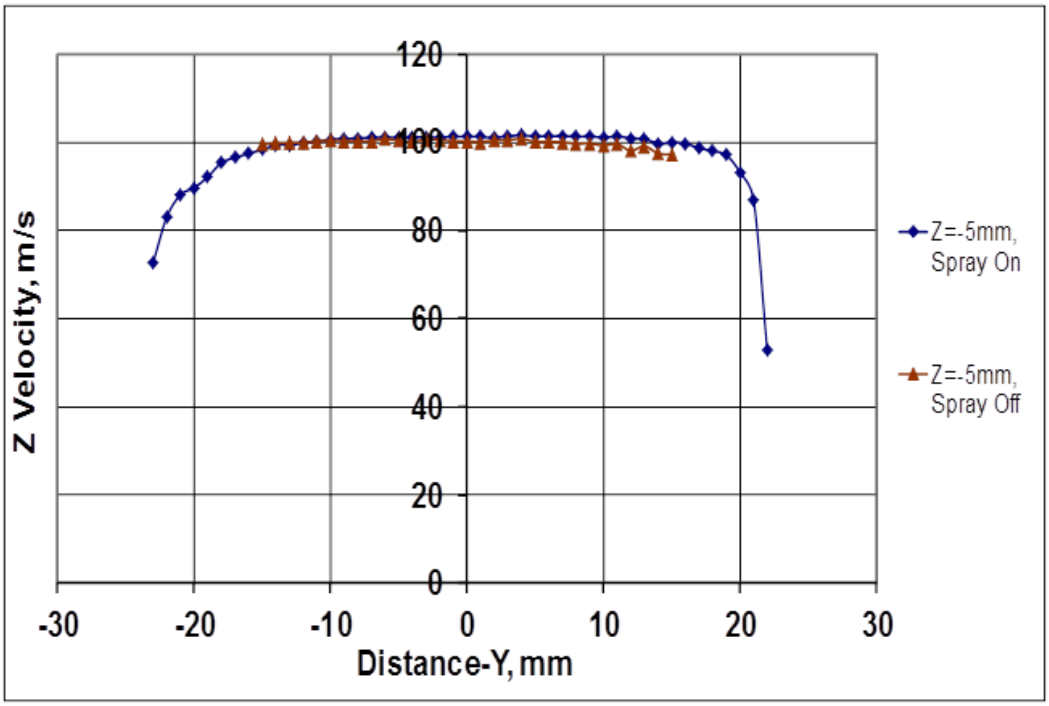

a)

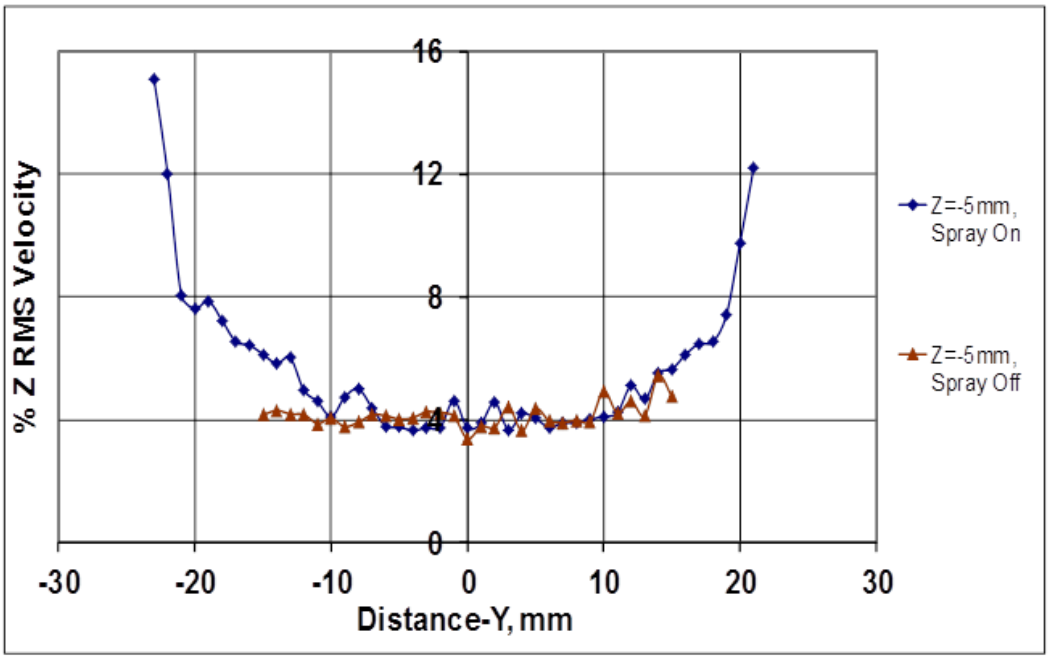

b)

Figure A.2. Flow characteristics of air flow in the test section measured along the X axis a) Mean velocity and b) RMS value normalized with air velocity

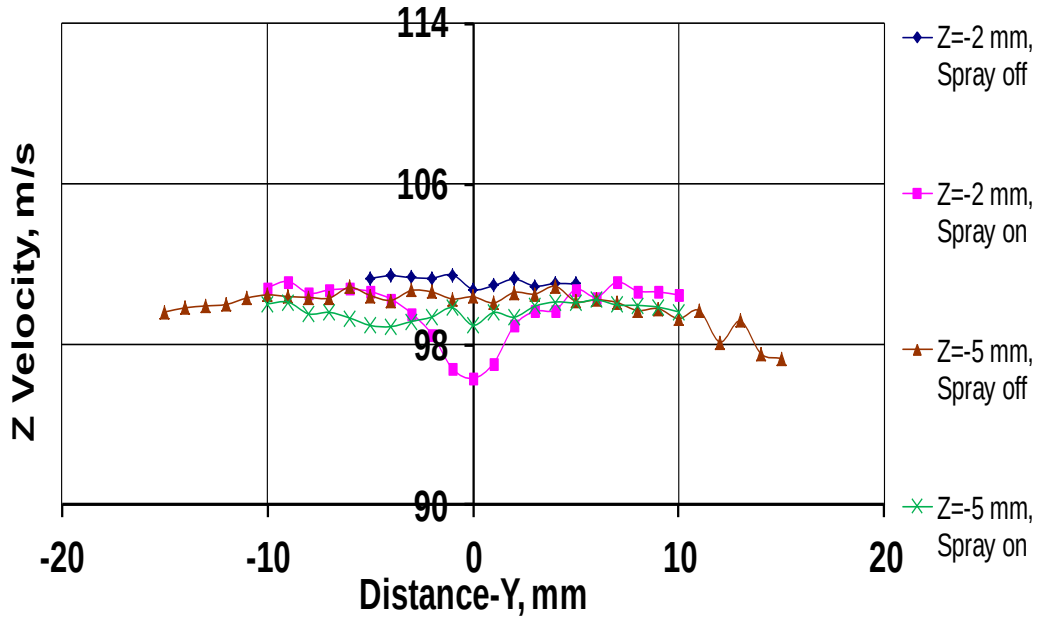

a)

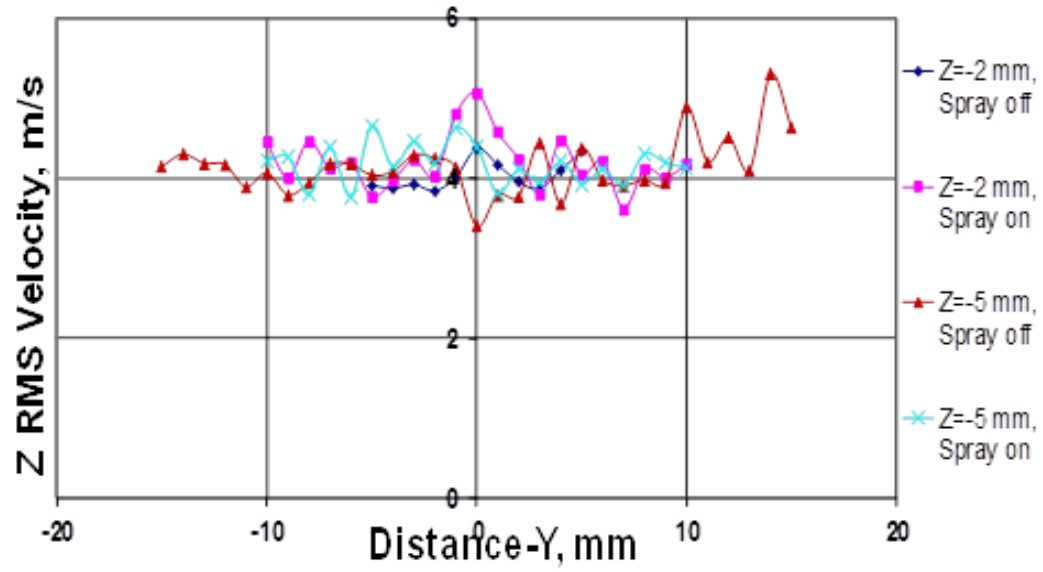

b)

Figure A.3. Effect of spray on the airflow velocity upstream of the spray
a) Mean velocity and b) RMS value normalized with air velocity

Figure A.4 shows the velocity profiles in the boundary layer of the wall at 2mm upstream of the orifice in the presence and absence of the spray. It can be seen that the spray has an effect on the wall boundary layer at 2mm upstream. Figure A.5 shows similar velocity profiles at a distance of 7.5mm upstream of the orifice. It can be seen that the spray does not have an effect on the velocity of the airflow at this distance.

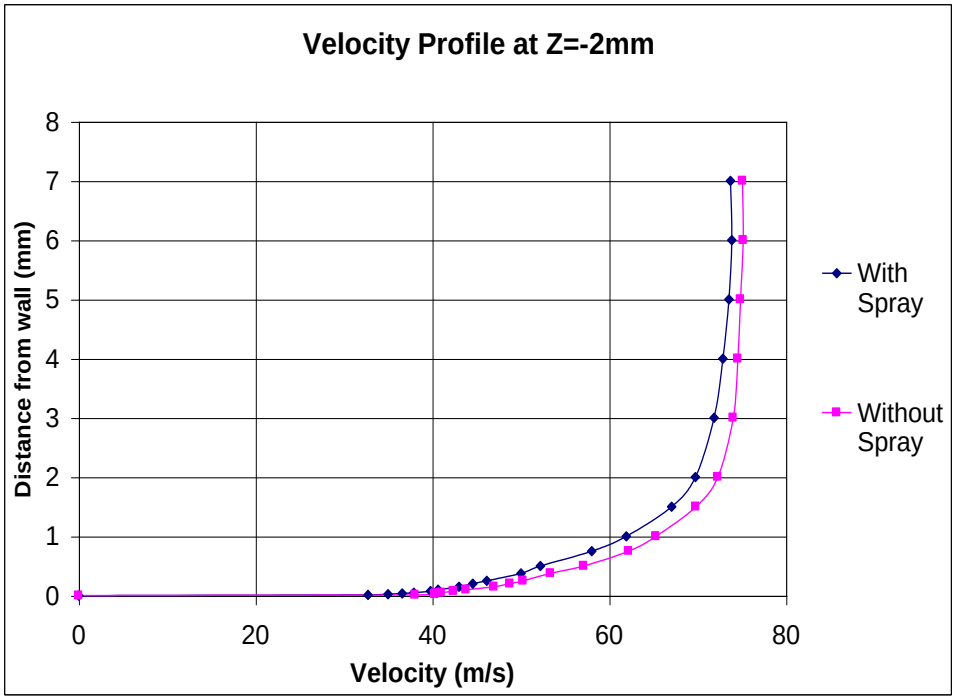

Figure A.4. Velocity profile in the Boundary Layer at 2mm upstream of the orifice in the presence and absence of spray

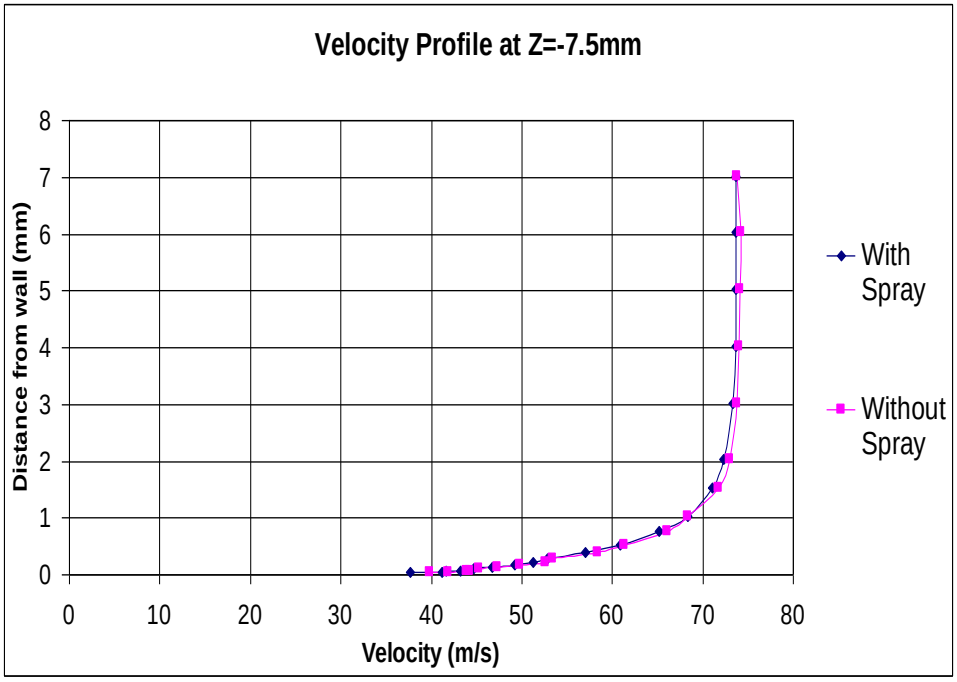

Figure A.5. Velocity profile in the Boundary Layer at 5mm upstream of the orifice in the presence and absence of spray

Appendix B: Injector Characteristics

The characteristics of the two injectors have been plotted in Figure A. 6. It shows the mass flow rate and the discharge coefficient as a function of the pressure drop across the injectors. It is seen that the round edged orifice has a C_d of 0.95 and the sharp edged orifice has a C_d of 0.74

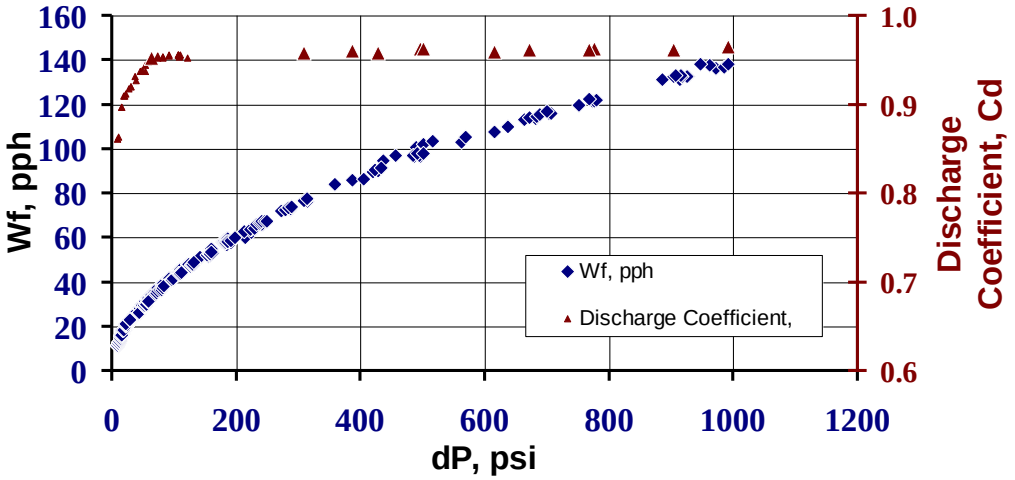

a) Round edged orifice

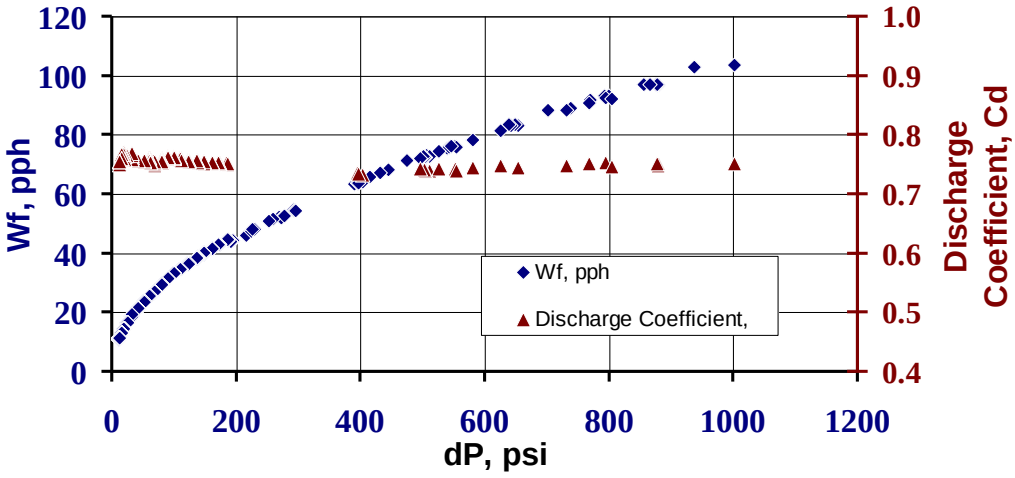

a) **Sharp edged orifice**

Figure A. 6. Characteristics of the two injectors. The graphs show the mass flow rate in pounds per hour and the discharge coefficient as a function of the pressure drop across the injectors

Appendix C: Error Analysis

The analysis indeterminate errors related to the measurements made during the experiments to obtain the operating conditions was carried out with two methods. One is Taylor series expansion method that gives the measure of maximum error in the experiments. The other one is the variance method, which gives an estimate of the average error in the experiments. The propagation of error with these two methods are briefly described with an example of the volume of a cuboid given by $V = L \times B \times H$. The maximum error is given by the Taylor series expansion that adds all the maximum errors possible and gives the following expression

$$\frac{\Delta V}{V} = \frac{\Delta L}{L} + \frac{\Delta B}{B} + \frac{\Delta H}{H}$$

The variance method, on the other hand is the standard deviation of the maximum errors of each parameter and the expression for the mean error becomes

$$\frac{\Delta V}{V} = \left[\left(\frac{\Delta L}{L} \right)^2 + \left(\frac{\Delta B}{B} \right)^2 + \left(\frac{\Delta H}{H} \right)^2 \right]^{\frac{1}{2}}$$

The propagation of error analysis was carried out for all the measured properties of the flow. An example is of the error analysis for the momentum ratio is shown here. The momentum ratio is a function of the following parameters

$$q = f(V_{air}, \rho_{air}, V_{fuel}, \rho_{fuel})$$

It is defined as

$$q = \frac{\rho_{fuel} . V_{fuel}^2}{\rho_{air} . V_{air}^2}$$

The error by Taylor series expansion becomes

$$\frac{dq}{q} = \frac{d\rho_{fuel}}{\rho_{fuel}} + 2\frac{dV_{fuel}}{V_{fuel}} + \frac{d\rho_{air}}{\rho_{air}} + 2\frac{dV_{air}}{V_{air}}$$

The error by Variance method becomes

$$\frac{dq}{q} = \left[\left(\frac{d\rho_{air}}{\rho_{air}}\right)^2 + \left(2\frac{dV_{air}}{V_{air}}\right)^2 + \left(\frac{d\rho_{fuel}}{\rho_{fuel}}\right)^2 + \left(2\frac{dV_{fuel}}{V_{fuel}}\right)^2\right]^{1/2}$$

The errors for the individual measuring equipment components were obtained from the manufacturer's manuals of the instruments used and are listed in Table A.1. Substituting these values in the equations for the error for each parameter, the maximum and mean errors in their measurement were obtained and are listed in Table A.2.

Table A.1 List of error in instruments obtained from the manufacturer

$\frac{dP_s}{P_s}$	0.25%
$\frac{dP_{diff}}{P_{diff}}$	0.25%
$\frac{dT_{air}}{T_{air}}$	0.33%
$\frac{dm_{fuel}}{m_{fuel}}$	0.5%

Table A.2 List of maximum and mean errors evaluated using the Taylor series expansion and variance methods

Parameter	Taylor Series Expansion Method	Variance Method
$\frac{d\rho_{air}}{\rho_{air}}$	0.58%	0.41%
$\frac{dV_{air}}{V_{air}}$	0.25%	0.18%
$\frac{d\rho_{fuel}}{\rho_{fuel}}$	0.51%	0.50%
$\frac{dV_{fuel}}{V_{fuel}}$	1.01%	0.72%
$\frac{dM}{M}$	0.09%	0.06%
$\frac{dq}{q}$	3.61%	1.62%
$\frac{dWe}{We}$	2.78%	1.78%

The measurement of the droplet sizes and velocities were made using a TSI 3 component Phase Doppler Particle Analzer (PDPA). Measurements were made with a resolution of 1mm X 1mm. The main errors associated with the current experiments come with the ability to maintain the operating conditions through the entire duration of the experiment. To assess this error, measurements in one of the planes (Z/d=60) were repeated at the operating conditions corresponding to *We*=1000, *q*=20 to check the repeatability of the experiment. These measurements were made using the sharp edged orifice. The mean differences in the measurements of the droplet sizes and velocities were obtained and are listed below

- AMD – 1.17 μm (2.68% of mean AMD of the two measurements)

- SMD – 1.18 µm (2.27% of mean SMD of the two measurements)
- Z Velocity – 0.88 m/s (0.94% of Crossflow velocity)
- X Velocity – 0.3 m/s (1.17% of Jet exit Velocity)
- Y Velocity – 0.67 m/s

References

[1] Lefebvre, A. H., Atomization and Sprays, (Combustion: An International Series), CRC Press

[2] Sirignano, W. A., Fluid Dynamics and Transport of Droplets and Sprays, Cambridge University Press

[3] Bayvel, L., and Orzechowski, Z., Liquid Atomization, Taylor and Francis

[4] Lefebvre, A. H., and Ballal, D. R., Gas Turbine Combustion: Alternative Fuels and Emission, CRC Press

[5] J.A. Schetz and A. Padhye, "Penetration and Breakup of Liquids in Subsonic Airstreams," AIAA J., vol. 15, pp. 1385 – 1389, 1977.

[6] Wu, P.-K., Kirkendall, K. A., Fuller, R. P., and Nejad, A. S., "Breakup Processes of Liquid Jets in Subsonic Cross-flows," *Journal of Propulsion and Power*, Vol. 13, No. 1, 1997, pp. 64,73.

[7] P. Marmottant and E. Villermaux, "On spray formation", Journal of Fluid Mechanics, 2004, vol 498, pp. 73-111

[8] Taylor, G. I., "Generation of Ripples by wind Blowing over a Viscous Liquid", The Scientific Paoers of Sir Geoffrey Ingrim Taylor, Vol. III, G. K. Batchelor, ed., Cambridge Univ. Press, Cambridge, England, pp. 244-254, 1963

[9] Oda, T., Hiroyasu, H., Nishida, K., and Arai, M., "Characterization of liquid jet atomization across a high-speed airstream," *JSME International Journal, Series B: Fluids & Thermal Engineering*, Vol. 37, No. 4, 1994, pp. 937-944.

[10] Cavaliere, A., Ragucci, R., and Noviello, C., "Bending and break-up of a liquid jet in a high pressure airflow," *Experimental Thermal and Fluid Science*, Vol. 27, No. 4, 2003, pp. 449-454.

[11] Mazallon, J., Dai, Z., and Faeth, G. M., "Primary Breakup of Nonturbulent Round Liquid Jets in Gas Crossflows," Atomization and Sprays, Vol. 9, 1999, pp. 291-311.

[12] Sallam, K. A., Aalburg, C., Faeth, G. M., "Breakup of Round Nonturbulent Liquid Jets in Gaseous Crossflow," AIAA Journal, Vol. 42, No. 12, December 2004.

[13] Wu, P.-K., Hsiang, L.-P., and Faeth, G. M., ‘‘Aerodynamic Effects on Primary and Secondary Breakup,’’ Liquid Rocket Engine Combustion Instability, edited by V. Yang and W. Anderson, Vol. 169, Progress in Astronautics and Aeronautics, AIAA, Washington, DC, 1995, pp.247 – 279.

[14] Julian Becker and Christopher Hassa, “Breakup and atomization of a kerosene jet in crossflow at elevated pressure”, Atomization and Sprays, vol. 11, pp. 49-67, 2002

[15] Tambe, S. B., Jeng, S. M., Mongia, H., and Hsiao, G., "Liquid Jets in Subsonic Crossflow," *43rd AIAA Aerospace Sciences Meeting and Exhibit; Reno*, pp. 2005.

[16] Ghosh, S., and Hunt, J. C. R., “Spray Jets in Cross-Flow,” *J. Fluid Mechanics*, Vol. 365, 1998, pp. 109, 136.

[17] Ragucci, R., Bellofiore, A., Cavaliere, A., “Trajectory and Momentum Coherence Breakdown of a Liquid Jet in High Density Air Cross-flow,” *Atomization and Sprays*, col. 17, pp. 47-70, 2007.

[18] Bellofiore, A., Ragucci, R. & Cavaliere, A. (2007). “Trajectory and momentum coherence breadown of a liquid jet in high-density air cross-flow. *Atomization and Sprays*, 17, 47-70.

[19] Amighi, A., Eslamian, M., & Ashgriz, N. (2009). Trajectory of a liquid jet in high pressure and high temperature subsonic air crossflow. *Proceedings of the ICLASS*. ftp://ftp.mines.edu/pub/tparker/Papers/ICLASS2009-225.pdf

[20] Stenzler, J. N., Lee, J. G., and Santavicca, D. A., “Penetration of Liquid Jets in a Crossflow”, AIAA 2003-1327, 41st Aerospace Science Meeting & Exhibit, , Reno, NV 2003.

[21] Chen, T. H., Smith, C. R., and Schommer, D. G., “Multi-Zone Behavior of Transverse Liquid Jet in High-Speed Flow,” AIAA Paper, 93-0453, 1993

[22] Wu, P. K., Kirkendall, K. A., Fuller, R. P., and Nejad, A. S., "Spray structures of liquid jets atomized in subsonic crossflows," *Journal of Propulsion and Power.Vol.14*, No. 2, 1998, pp. 173-182.

[23] Lin, K.-C., Kennedy, P. J., & Jackson, T.A. (2002). Penetration heights of liquid jets in high-speed crossflows. AIAA 2002-0873, *40th AIAA Aerospace Sciences Meeting and Exhibit*, Reno, NV.

[24] Schetz, J. A., and Padhye, A., “Penetration and Breakup of Liquids in Subsonic Airstreams,” AIAA

Journal, Vol. 15, No. 10, October 1977

[25] Ghenai, C., Sapmaz, H., Lin, C., “Penetration Height Correlations for Non-Aerated and Aerated Transverse Liquid Jets in Supersonic Cross Flow,” *Experiments in Fluids*, 2009, 46, 121-129

[26] Ahn, K., Kim, J., Yoon, Y., “Effects of Orifice Internal Flow on transverse Injection into Subsonic Crossflows: Cavitation and Hydraulic Flip”, *Atomization and Sprays*, vol. 16, pp.15-34, 2006.

[27] Chelko, L. J., “Penetration of Liquid Jets into High-Velocity Airstream”, NACA Research Memo. E50F21, 1950

[28] Tambe, S., “Liquid Jets in Non-uniform Crossflow,” PhD Thesis dissertation, 2010

[29] Ranger, A. A., and Nicholls, J. A., “The Aerodynamic Shattering of Liquid Drops,” AIAA Journal, Vol. 7, No. 2, 1969, pp. 285-290.

[30] Sallam, K. A., Aalburg, C., Faeth, G. M., “Breakup of Round Nonturbulent Liquid Jets in Gaseous Crossflow,” AIAA Journal, Vol. 42, No. 12, December 2004.

[31] Lee, K., Aalburg, C., Diez, F. J., Faeth, G. M., and Sallam, K. A., “Primary Breakup of Turbulent Round Liquid Jets in Uniform Crossflows”, *AIAA Journal*, vol. 45, No. 8, August 2007

[32] Birouk, M., Azzopardi, B. J., Stabler, T., “Primary Break-up of a Viscous Liquid Jet in a Cross Airflow,” *Part. Part. Syst. Charact.*, 2003, 20, 283-289

[33] Birouk, M., Stabler, T., Azzopardi, B. J., “An Experimental Study of Liquid Jets interacting with Cross Airflows,” *Part. Part. Syst. Charact*., 2003, 20, 39-46

[34] NGUYEN, T. T. and Karagozian, A. R., "Liquid fuel jet in subsonic crossflow," *Journal of Propulsion and Power*, Vol. 8, 1992, pp. 21-29

[35] Oda, T., and Hiroyashu, H., “Breakup Model of Liquid Jet across High Speed Air Stream”, *Proc. 9th Annual Conference on Liquid Atomization and Spray Systems, San Francisco*, 1996, pp. 99-103

[36] Rachner, M., Becker, J., Hassa, C., and Doerr, T., "Modeling of the atomization of a plain liquid fuel jet in crossflow at gas turbine conditions," *Aerospace Science and Technology*, Vol. 6, No. 7, 2002, pp. 495-506.

[37] Madabushi, R., “A Model for Numerical Simulation of Breakup of a Liquid Jet in Crossflow”, *Atomization and Sprays*, Vol 13, pp. 413-424, 2003.

[38] Raju, M. S., “Numerical Investigation of Various Atomization Models in the Modeling of a Spray Flame.” *Tech. Rep. NASA/CR - 2005-214033*, NASA, 2005.

[39] Ryan, M. J., "CFD prediction of the trajectory of a liquid jet in a non-uniform air crossflow," *Computers & Fluids*, Vol. 35, 2006, pp. 463-476.

[40] Yi, Y., and Reitz, R. D., “Modeling the Primary Breakup of High-Speed Jets”, *Atomization and Sprays*, Vol. 14, 2004, pp. 53-80

[41] M. Pilch and C. A. Erdman, “Use of Breakup Time Data and Velocity History Data to Predict the Maximum Size of -Stable Fragments for Acceleration-Induced Breakup of a Liquid Drop”, International *Journal of Multiphase Flow*, vol. 13, pp. 741-757, 1987

[42] Reitz., R. D., “Modeling Atomization Processes in High-Pressure Vaporizing sprays”, *Atomization and Spray Technology*, vol. 3, pp. 309-337, 1987

[43] Pai, M. G., Pitsch, H., and Desjardins, O., “Detailed Numerical Simulations of Primary Atomization of Liquid Jets in Crossflow,” AIAA 2009-373, *47th AIAA ASM*, January 2009

[44] Herrmann, M., “Detailed Numerical simulations of the Primary Atomization of a turbulent Liquid Jet in Crossflow,” *Journal of Engineering for Gas Turbines and Power*, vol. 132, June 2010

[45] Juhasz, K.J., Zahn, O.F., Jr., Schweitzer, P.H., “On the formation and dispersion of oil sprays,” Bulletin No.40, 1932, *Engineering Experiment Station*, Pennsylvania State University, University Park, PA

[46] Lee, D.W., Spencer, R.C., “Photomicrographic studies of fuel sprays,” *NACA Tech. Note 454*, Washington,1933.

[47] Schweitzer, P.H., “Mechanism of disintegration of liquid jets,” *Journal of Applied Physics*, 1937.8, 513-521

[48] Grant, R.P., Middleman, S., “Newtonian jet stability,” *AIChE J.* 12, 1966. 669-678

[49] Phinney, R.E., "The breakup of a turbulent jet in a gaseous atmosphere," *Journal of Fluid Mechanics*, 60, 689-701, 1973.

[50] Faeth, G. M., Hsiang, L. P., and Wu, P. K., "Structure and Breakup Properties of Sprays," *International Journal of Multiphase Flow*, vol. 21. Pp. 99-127, 1995

[51] McCarthy, M.J., Malloy, N.A., "Review of stability of liquid jets and the influence of nozzle design," *Chemical. Engineering Journal*, vol. 7, pp. 1-20, 1974

[52] Hoyt, J.W., Taylor, J.J., "Waves on water jets," *Journal of Fluid Mechanics* 88, 119-123. 1977a

[53] Hoyt, J.W., Taylor, J.J., "Turbulence structure in a water jet discharging in air," *Physics of Fluids* 20, S253-S257, 1977

[54] Chehroudi, B., Onuma, Y., Chen, S. H., and Bracco, F. V., "On the Intact Core of Full-Cone Sprays," *SAE Paper* 850126, 1985

[55] Ruff, G.A., Sagar, A.M., Faeth, G.M., 1989. Stucture and mixing properties of pressure-atomized sprays. *AIAA Journal*, 27, 901-908.

[56] Ruff, G.A., Bernal, L.P., Faeth, G.M., "Structure of the near injector region of non-evaporating pressure-atomized sprays," *Journal of Propulsion and Power* 7, 221-230. 1991

[57] Ruff, G.A., Wu, P.-K., Bernal, L.P., Faeth, G.M., 1992. "Continuous and dispersed phase structure of dense non-evaporating pressure atomized sprays," *Journal of Propulsion and Power* 8, 280-289.

[58] Tseng, L.-K., Ruff, G.A., Faeth, G.M.,. "Effects of gas density on the structure of liquid jets in still gases," *AIAA Journal*, 30, pp. 1537-1544, 1992

[59] Wu, P. K., Tseng, L. K., and Faeth, G. M., "Primary Breakup in Gas/Liquid Mising Layers for Turbulent Liquids," *Atomization and Sprays*, vol. 2, pp. 295-317, 1992

[60] Wu, P. K., and Faeth, G. M., "Aerodynamic Effects on Primary Breakup of Turbulent Liquids," *Atomization and Sprays*, vol. 3, pp. 265-289, 1993

[61] Frank M White, "Viscous Fluid Flow," McGraw-Hill Higher Education, 2006

[62] Tamaki, N., Shimizu, M., Nishida, K., and Hiroyasu, H., "Effects of cavitation and internal flow on atomization of liquid jet," *Atomization and Sprays*, Vol. 8, No. 2, 1998, pp. 179-197.

[63] Tamaki, N., Shimizu, M., and Hiroyasu, H., "Enhancement of the atomization of a liquid jet by cavitation in a nozzle hole," *Atomization and Sprays*, Vol. 11, No. 2, 2001, pp. 125-137.

[64] Schmidt, D. P., and Corradini, M. L., "The Internal Flow of Diesel Fuel Injector Nozzles: A Review," International Journal of Engine Research, Vol. 2, No. 1, 2001

[65] Arai, M., Shimizu, M., and Hiroyasu, H., "Similarity between the breakup lengths of a high speed light jet in atmospheric and pressurized conditions," *ICLASS*, 1991

[66] Soteriou, C., Andrews, R., and Smith, M., "Direct injection diesel sprays and the effect of cavitation and hydraulic flip on atomization," *SAE Paper* 950080, 1995

[67] Hiroyasu, H., Arai, M., and Shimizu, M., "Breakup length of a liquid jet and internal flow in a nozzle," *ILASS*, 1991

[68] Kent, J. C., and Brown, G. M., "Nozzle exit flow characteristics for square-edged and rounded inlet geometries," *Combusiton Science and Technology*, 1983, 30, pp. 121-132

[69] Knox-Kelecy, A., "Turbulent flow in scale model of diesel fuel injector nozzle hole," PhD Thesis, University of Wisconsin, 1992

[70] Nurick, W. H., "Orifice cavitation and its effects on spray mixing," *Jounal of Fluids Engineering*, 1976, 98

[71] Reitz, R. D., and Bracco, F. V., "Mechanism of atomization of a liquid jet," *Physics of Fluids*, 1982, 26(10)

[72] Ohrn, T. R., Senser, D. W., and Lefebvre, A. H., "Geometric effects on spray cone angle for plain orifice atomizers," *Atomization and Sprays*, 1991, 1.

[73] Bergwerk, W., "Flow pattern in diesel nozzle spray holes," *Proceedings of Institute of Mechanical Engineers*, 1959, 173.

[74] Gellales, A. G., “Coefficients of discharge of fuel injection nozzles for compression-ignition engines. *NACA Technical Memo* 373, 1931

[75] http://www.tsi.com/en-1033/products/2262/pdpa_system_3-component.aspx

[76] Daniel Colladon, “On the reflections of a ray of light inside a parabolic liquid stream”, *Comptes Rendus* 15, pp. 800-802, 1842.

[77] Charalampous, G., Hardalupas, Y., Taylor, A. M. K. P., “A Novel technique for measurements of the intact liquid jet core in a coaxial air-blast atomizer,” AIAA 2007-1337, *45th Aerospace Science Meeting & Exhibi*t, Reno, NV 2007.

[78] Fawcett, P. A., and Komerath, N. M., “Spatial Correlation Velocimetry in Unsteady Flows,” *AIAA* 91-0271, 1991

[79] Wu, P.-K., and Faeth, G. M., “Onset and End of Drop Formation Along the Surface of Turbulent Liquid Jets in Still Gases,” *Physics of Fluids*, Vol. 7, No. 11, 1995, pp. 2915–2917

[80] Salewski, M., and Fuchs, L., “Dispersion of Circular, Non-Circular and Swirling Spray Jets in Crossflow,” *Proceedings of the Sixth International ERCOFTAC Workshop on Direct and Large-Eddy Simulation*, University of Poitiers, 2005

[81] Fric, T. F., and Roshko, A., “Vortical Structure in the wake of a Transverse Jet,” *Jounal of Fluid Mechanics*, vol. 279, pp. 1-47, 1994

[82] Sedarsky, D., Paciaroni, M., Berrocal, E., Petterson, P., Zelina, J., Gord, J., and Linne, M., “Model Validation image data for Breakup of a Liquid Jet in Crossflow: Part I,” *Experiments in Fluids*, 49, pp. 391-408, 2010

[83] Cavage, W. M., "The Effect of Fuel on an Inert Ullage in a Commercial Transport Airplane Fuel Tank," DOT/FAA/AR-05/25, Office of Aviation Research Washington, D.C. 20591,

VITA

Name:	Yogish Gopala
Address:	635 Strong Street, Atlanta, GA 30318
Email:	yogish@gatech.edu

Education:

Bachelor of Technology in Aerospace Engineering at Indian Institute of Technology Madras, Chennai, India, 2005

Master of Technology in Aerospace Engineering at Indian Institute of Technology Madras, Chennai, India, 2005

Master of Science in Aerospace Engineering at Georgia Institute of Technology, Atlanta, Georgia, USA, 2010

Doctor of Philosophy in Aerospace Engineering at Georgia Institute of Technology, Atlanta, Georgia, USA, 2012